Experimental and Analytical Evaluation of Disproportionate Collapse in Flat-Plate Buildings

---

A Dissertation

Presented to

The Faculty of the Graduate School

at the University of Missouri-Columbia

In Partial Fulfillment

of the Requirements for the Degree

Doctor of Philosophy

---

by

ZHONGHUA PENG

July 2015

[Experimental and Analytical Evaluation of Disproportionate Collapse in Flat-Plate Buildings]

presented by **Zhonghua Peng,**

candidate for the degree of doctor of philosophy

and hereby certify that, in their opinion, it is worthy of acceptance.

[Sarah Orton, Supervisor]

[Zhen Chen]

[Hani Salim]

[Guoliang Huang]

DEDICATION

Dedicating this work to my family for always being there for support.

ACKOWLEGEMENT

The research was conducted under supervision of Dr. Sarah Orton, my ph.D academic advisor. I'd like to express my great gratitude to her for sharing the expertise and knowledge on the project. Her advice and comments were essential to the successful completion of my dissertation. Thanks also go to Dr.Ying Tian from UNLV for involving in this research and sharing his knowledge in the testing and modeling of flat plates. Gratitude also extended to the members of my dissertation committee, Dr. Zhen Chen, Dr. Hani Salim, Dr. P. Frank Pai and Dr. Guoliang Huang.

I would also like to express my gratitude to Rich Oberto and Rex Gish of Engineering Technical Services. Thanks go to all the graduate and undergraduate researchers who worked with me on the project. I could not have finished all the experimental tests without their help and efforts. Special thanks to Zachary Treece for taking the initiative and helping me on the project.

Last-and definitely not least- my gratitude goes to my parents, Xianzhang Peng and Julan Guo, and my sisters Jifang Peng and Jixia Peng for their love and support for my pursuing of higher education.

Zhonghua Peng

CONTENTS

LIST OF FIGURES

LIST OF TABLES

Experimental and Analytical Evaluation of Disproportionate Collapse Flat-Plate Buildings

Zhonghua Peng

Dr. Sarah Orton, Dissertation Supervisor

ABSTRACT

Reinforced concrete flat plate buildings without continuous integrity reinforcement may be vulnerable to disproportionate collapse if a supporting structural member was lost in an abnormal event. This research forces on the evaluation of potential of disproportionate collapse in older flat-plate structures subjected to the loss of a supporting column in extreme loading events. If a supporting column fails, then the load was carried by that column must be redistributed to the surrounding slab-column connections, which in turn may results in a disproportionate collapse over an entire building or a large portion of it. This progression can occur if the punching shear strength of the surrounding connections is not sufficient.

In order to make the most accurate determination of the potential for disproportionate collapse of flat plate structures, this research seeks to accurately evaluation the punching shear capacity of slab-column connections using the conditions present in a potential collapses event. The in-plane lateral restraint provided by the floor slab can enhance the punching shear strength of surrounding slab-column connections and may be significant. In addition, the post-punching capacity of the original failed slab-column connection may reduce the amount of load to be redistributed to the surrounding connections. In order to investigate the effects of lateral restraint and post punching capacity, six restrained and unrestrained static tests was conducted at 1% and 0.64% reinforcement ratios. The static tests showed that the punching shear capacity can be increased 2-8% as lateral restraint stiffness varies from 17 to75.6 kN/mm but the increase is

highly related to the in-plane lateral restraint stiffness. The tests also indicated that the slab without integrity reinforcement can develop 54% of maximum post- punching strength after punching. However, this capacity decreases dramatically as the deflection increases to a large amount after punching failure.

Since isolated slab-column testing cannot fully represent behaviors of an actual building, multi-panel testing was done at a sub-structure system level. The specimens consisted of two 9 column portion of a flat plate building, one tested with an exterior column instantaneous removal and another tested with an interior column instantaneous removal. The tests further investigated the dynamic load redistribution, punching, and post-punching responses in a flat-plate structure.

The multi-panel tests (with interior and exterior column removal) showed that flat-plate slabs are vulnerable to disproportionate collapse at load levels of approximately 50% of their design capacity. The recorded lateral movements on columns in the tests verified the existence of compression membrane forces in continuous slab panel. Compressive membrane forces form after a column removal and gradually transition to tension membrane forces at deflections approaching the slab depth. Punching failure did not happen in compressive membrane phase, but in the tension membrane phase and tests showed that pre-existing damage in flat-plate structures (from prior overloading or shrinkage cracking) may impede the formation of compressive membrane forces in the slab. Dynamic removal of a supporting column resulted in a dynamic load amplification factor (DLAF) of approximately 1.3. Therefore, surrounding connections need to be able to carry at least 30% more than the predicted redistributed static load in a collapse analysis.

CHAPTER 1 STATEMENT OF PROBLEM

1.1 Statement of Problem

Existing flat-plate buildings designed with pre-ACI 1971 building code may be especially vulnerable to disproportionate collapse due to lack of continuous bottom reinforcement through the columns. In order to accurately evaluate the potential for collapse in these buildings the following problems need to be addressed: (1) Better prediction of punching shear capacity will lead to better prediction of collapse. In a flat-plate structure in-plane lateral restraint due to compressive membrane action can increase the capacity of the connection prior to a failure occurring, but due to different sizes, strengths and reinforcement ratios of slabs, the percentage of punching shear capacity increase due to the lateral restraint by the surrounding slab and column is unknown and whether or not this increase can help to arrest the disproportionate collapse is also uncertain. (2) The role of post punching capacity on disproportionate collapse is uncertain. If there is sufficient post punching capacity this may help to arrest the progression of collapse. (3) There is little experimental data regarding the effects of loading rate on flat plate connections. Once a column fails, the load will be redistributed to the surrounding columns in a dynamic manner. Therefore, it's important to know how the connection responds to the dynamic loading and what the amount of dynamic increase in the redistributed load. (4) There is little experimental evidence for characterizing failure propagation over entire structures and for developing or validating analytical models. By considering the structure as a whole and developing validated analytical models, the accurate prediction of collapse load can be achieved.

1.2 Aims and Scope

The overall goal of this research is to evaluate the potential of dynamic disproportionate collapse in older reinforced concrete flat-plate structures subjected to a sudden loss of a supporting column. Specific primary objectives of this research included:

(1) Evaluate effects of in-plane lateral restraint on slab loading-carrying capacity, deformation capacity and dynamic deformation demand at slab-column connections;

(2) Study the post-punching behavior, especially the capacity of developing tensile membrane action, of slab-column connections with discontinuous slab bottom compressive reinforcing bars through columns;

(3) Provide experimental data for characterizing failure propagation over entire structures and for developing or validating analytical models;

(4) Evaluate potential of disproportionate collapse of flat-plate structures subjected to large deformations due to the loss of a supporting column.

1.3 Research Components

In order to address the research aims the following experiments and analyses will be conducted.

(1) Experimental investigation of six isolated slab-column connections at two different reinforcement ratios: 1% and 0.64%. Four tests are conducted with lateral restraint and the other two tested without lateral restraint to investigate the effects of in-plane lateral restraint. Testing continued after initial punching shear failure to evaluate post-punching response.

(2) Dynamic testing of two multi-panel slabs in a loss of supporting exterior and interior columns to determine the load redistribution, dynamic load amplification factor, and the

potential of disproportionate collapse of flat- plate structures without integrity reinforcement.

(3) The finite element simulation of isolated static tests with and without lateral restraint to predict the punching capacity at different lateral restraint stiffness. Finite element simulation of multi-panel specimen to evaluate failure propagation over entire structure including strain rate has been investigated.

CHAPTER 2 LITERATURE REVIEW

2.1 Background

This chapter states the background of disproportionate collapse, design of flat-plate structures, analytical models and code predictions of punching shear capacity in slab-column connections. In addition, previous experimental and analytical tests relevant to the collapse of flat-plate buildings are reviewed.

2.1.1 Disproportionate Collapse

Disproportionate or progressive collapse is defined by the U.S General Services Administration (GSA) as " a situation where local failure of a primary structural component leads to the collapse of adjoining members which, in turn, leads to additional collapse. Hence the total damage is disproportionate" [GSA, 2003]. Also ASCE Standard "7-05" Minimum Design Loads for Buildings and Other Structures describes disproportionate collapse as " the spread of an initial local failure from element to element, eventually resulting in the collapse of an entire structure or a disproportionately large part of it ". A building which is susceptible to the disproportionate collapse is one where the damage to small areas of a structure or failure of single elements could lead to collapse of major parts of the structure.

Abnormal loads such as explosion or impacts are not considered in an ordinary structural design; however their consequences can be severe. Some of the special events that can initiate the disproportionate collapse by causing the loss of one or more primary load-carrying members include gas explosion, blast, foundation failure, vehicle impact, fire and seismic forces.

The partial collapse of the 22-story Ronan Point Apartment Building in London, England in May 1968 as shown in Figure 2-1, is a landmark of disproportionate collapses in recent history

that resulted in British adopting explicit disproportionate collapse design measures into their building codes. The collapse was caused by a gas explosion on the 18th floor. For this building, the exterior cladding panels supported some edges of exterior slab panels. The explosion caused loss of cladding panels leading to the collapse of the slab when edge supports were lost. The debris from the 18th-22nd floors caused the collapse of the lower parts to the ground [Osama 2006].

Figure 2-1 Disproportionate collapse at Ronan point apartments in London England [Osama 2006]

2.1.2 Flat Plate Structures

A flat-plate structure consists of reinforced slabs supported directly on the column without any beams, girders or column capital panels present as shown in Figure 2-2. Flat-plate structures have been widely used due to the flexibility of architectural design, reduced the structural height,

and easy formwork and low construction cost. There is a large inventory of flat-plate buildings used as apartment, hotel, office, hospital etc. in the US that were designed based on pre-1971 building codes and do not have slab integrity reinforcement. However, stress concentrations in the slab-column intersection make the slab-column connections vulnerable to punching shear failure. When one of the connections is overloaded and fails, the load previously carried by that connection will be redistributed to the adjacent connections, which in turn are overloaded causing the failure of those connections, eventually, leading to the disproportionate collapse of the structure.

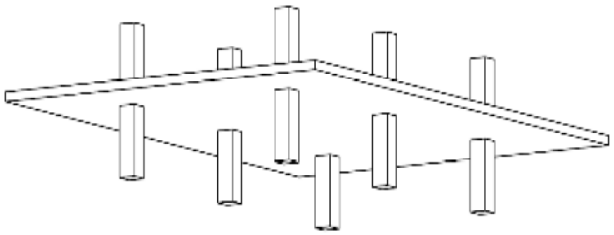

Figure 2-2 Flat plate structures

2.2 Predictions of Punching Shear Capacity

2.2.1 Analytical models

Because punching shear failure is an important mechanism in flat-plate structures significant previous research has been conducted on determining the punching shear capacity of slab-column connections.

2.2.1.1 Kinnunen and Nylander's Model (1960)

Kinnunen and Nylander (1960) proposed a model based on the tests of circular slabs centrally supported on circular columns and loaded on the edges of slabs as shown in Figure 2-3.

The mechanical model of slab is divided into compressed conical strut and rigid segment, the basic idea of the model is to create an equilibrium of forces acting on the rigid segment. The compressed conical shell is separated by the radial cracks; the rigid segment is confined at the front between the column and inclined crack tip and it rotates around an axis located at tip of crack. The failure is assumed to occur when the compressive stress in the strut and the tangential strain at the tip of the crack reaches a certain value. The deflection of the connection and the depth of the neutral axis are calculated by the iteration.

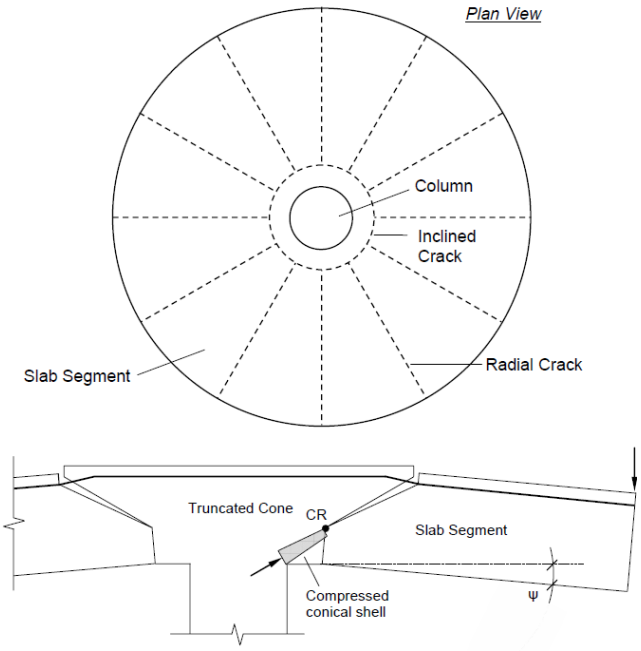

Figure 2-3 Mechanical model of Kinnunen and Nylander [1960]

2.2.1.2 Critical Shear Crack Theory (CSCT)

Muttoni (2008) proposed the critical shear crack theory to predict the punching shear strength of reinforced concrete slabs. According to Muttoni and Schwarts (1991), the width of the critical shear crack (w_c) is proportional to the product of rotation of connection times the

effective depth of the slab (ψd). The theory is based on the rotation of slabs and the maximum size of the aggregates which is related to the roughness of the crack that decides the amount of shear that can be transferred across the critical shear crack.

$$\frac{V_u}{b_0 d\sqrt{f_c'}} = \frac{9}{1+15\frac{\psi_u d}{d_{g0}+d_g}}$$ **(U.S customary units: psi, in)** **Equation 2- 1**

where V_u is connection punching strength, ψ_u is slab rotation relative to column at punching failure, d_g is the maximum size of the aggregate, and d_{g0} is a reference aggregate size equal to 16 mm. Rotation of slab (ψ) is related to the applied load V as given as

$$\psi = 1.5\frac{r_s f_{sy}}{2dE_S}\left(\frac{V}{V_{flex}}\right)^{1.5}$$ **Equation 2- 2**

Where r_s is plastic radius around the column which can be taken as the distance between the center of column to the point of contra-flexure, and V_{flex} can be calculated from yield-line theory. Figure 2-4 shows that the intersection of load- rotation response curve and failure criteria is the predicted punching shear failure point.

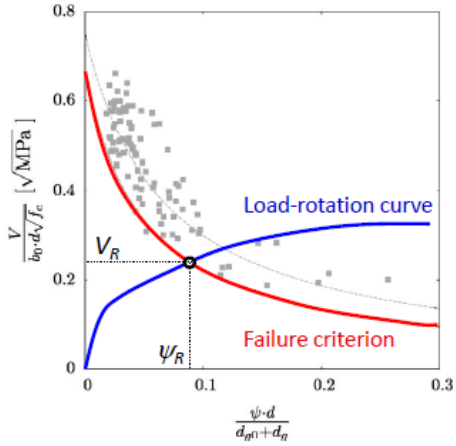

Figure 2-4 Procedure to specify punching shear strength of slab according to Critical Shear Crack Theory [Muttoni , 2008]

2.2.1.3 Broms Model

Broms (1990) proposed a modified model of Kinnuen and Nlander (1960) to incorporate the size-effect. The failure mechanism of the model is that the shear force is assumed to be transferred to the column by an inclined compression strut that squeezes the concrete within the column perimeter and when the compression stress approaches the yield level the compression zone outside the column perimeter collapses due to formation of radial tension strain.

The model further assumes that punching shear failure occurs when the tangential strain or the compressive stress in the radial direction reaches approximately 0.001 with the concrete compressive strength 25 MPa. At a strain exceeding approximately 0.001, it's evident that the almost linearly elastic behavior of the concrete at low strains starts to change. This critical level decreases with increasing concrete strength because high strength concretes are more brittle. The failure is primarily cause by a radial tension strain, a phenomenon that does not exist for continuous one-way slabs and beams. The behavior seems to be so dominant that a tangential flexural compression strain of 0.001 at the column due to the global bending moment is chosen as the failure criterion. The radial strain begins to decrease when the load approaches the punching load and just before the punching failure the radial strain falls to zero. The size effect (decreasing ultimate material strength with increasing structural size) is taken into account by the Equation 2-3

$$\boldsymbol{\varepsilon_{cpu} = 0.001\left(\frac{x_0}{x}\right)^{1/3}\left(\frac{10}{f'_{ck}}\right)^{0.1}} \qquad \textbf{Equation 2- 3}$$

Where ε_{cpu} = critical tangential compression strain due to the bending moment at the column edge; x_o reference size, x_o =0.15 m. x = height of compression zone at linear elastic stress conditions. The punching shear strength based on strain criterion V_ε , can be calculated from Equation:

$$V_{\varepsilon} = m_{\varepsilon} \frac{8\pi}{2In\left(\frac{l}{D}\right)+1-\left(\frac{D}{l}\right)^2}$$ **Equation 2- 4**

where l is the diameter of the test specimen or the distance between points of contra-flexure in the slab, D is the diameter of the column, and m_{ε} is the bending moment at the edge of slab-column connection.

2.2.2 Code predictions

2.2.2.1 ACI 318 (2014)

ACI 318-14 provides equations for checking the punching shear capacity which relates the punching shear strength V_R to the effective depth of the slab d, the control perimeter of a critical section b_o (at a distance $d/2$ from the face of column as shown in Figure 2-5), and the concrete compressive strength f_c. According to the ACI 318-08, the punching shear strength is proportional to the square root of the concrete compressive strength as shown in the Equation 2-5 and 2-6.

$$V_{ACI} = \frac{1}{3} b_0 d \lambda \sqrt{f'_c}$$ **(in SI units; Mpa, mm)** **Equation 2- 5**

$$V_{ACI} = 4 b_0 d \lambda \sqrt{f'_c}$$ **(in U.S. customary units; psi, in)** **Equation 2- 6**

Where λ is the coefficient to account for the light weight concrete, taken as unity for the normal weight concrete. Because the reinforcement ratio is not account for in the design equation, the ACI equation often leads to over-prediction of the punching shear capacity at low reinforcement ratio.

2.2.2.2 Eurocode 2

Eurocode 2 (2004) includes additional parameters such as the flexural reinforcement ratio ρ in the equation 2-7 to predict punching shear capacity.

$$V_{EC2} = 0.18 b_{0,EC2} d \xi (100 \rho f_c^{'})^{1/3} \quad \text{(in SI units; Mpa, mm)} \qquad \textbf{Equation 2- 7}$$

$$V_{EC2} = 5 b_{0,EC2} d \xi (100 \rho f_c^{'})^{1/3} \quad \text{(in U.S. customary units; psi, in)} \qquad \textbf{Equation 2- 8}$$

Where $b_{0,EC2}$ is the control perimeter located at a distance $2d$ from the face of the column as shown in Figure 2-5, ρ is the flexural reinforcement ratio, and ξ is a factor accounting for size effect (decreasing nominal shear strength with increasing size of the member whose value can be obtained as $\xi = 1 + \sqrt{\frac{200mm}{d}} (\xi = 1 + \sqrt{\frac{7.87in.}{d}}) \leq 2.0$

2.2.2.3 Model Code 2010

For the punching shear, the Swiss Model Code 2010 is based on the physical model of the Critical Shear Crack Theory (CSCT). In a general manner MC2010 proposes to calculate the punching strength of members without transverse reinforcement as detailed in Equation 2-9

$$V_E - V_{P,MC} \leq V_{R,MC} = K_{\psi} b_{MC} d \sqrt{f_c} \qquad \textbf{Equation 2- 9}$$

Where $V_{P,MC}$ is evaluated according to the CSCT failure criterion, whose terms are evaluated through the following parameters:

$$K_{\psi} = \frac{1}{1.5 + 0.9 \psi d k_{dg}} \leq 0.6 \qquad \textbf{Equation 2- 10}$$

The vertical component of the tendons $V_{P,MC}$ is calculated at 0.5d from the border of the column as well as for the control perimeter b_{MC} as shown in Figure 2-5.

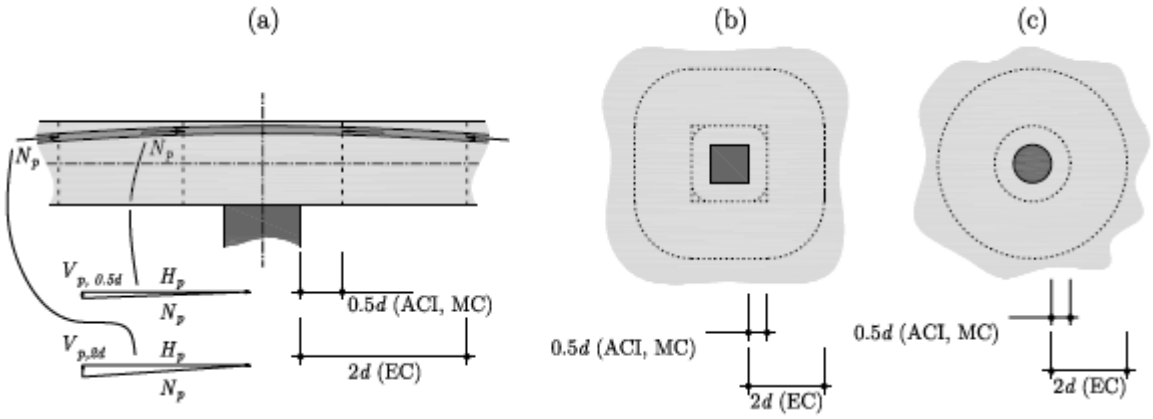

Figure 2-5 Parameters of design codes: (a) vertical component of the tendons according to ACI 318, Eurocode 2 and MC2010; (b) square columns; and (c) circular columns

2.3 Compressive Membrane Force

In order to efficiently design for disproportionate collapse, as much capacity as possible must be calculated for the existing connections. Most of the design code equations are formulated based on the testing of slab-column specimens isolated from the surrounding structure without lateral restraint. In a structure compressive membrane action can help to increase the capacity of the connection prior to a failure occurring. If better predictions of the capacity of slab column connections are made, then analysis for the possibility of disproportionate punching shear failure can be improved.

Ockelston (1955) showed the most dramatic demonstration of membrane action. Lightly reinforced two-way slab panels 135mm thick, 4.9 m by 4.1m in plan and bounded by main and secondary beams in a 10 year-old, three-story reinforced concrete structure were intentionally loaded to destruction. The slabs were designed for a dead load of 3.2 kN/m^2 and a superimposed floor load of 3.4 kN/m^2. The floor didn't collapse until the total load reached 40.4 kN/m^2,

representing a factor of safety 6.1. Ockelston partly attributed this unexpected strength reserve to membrane action.

Vecchio and Tang (1990) showed the strains on the tension face are considerably greater in magnitude than those on the compression face as shown in Figure 2-6. The net tensile strains resulting at the slab mid-depth cause the slab to expand, producing outward horizontal displacements at the slab ends. This outward expansion tendency will be prevented, to some degree, by the lateral restraint of supporting columns, beams, or walls. In a laterally restrained slab, the axial forces induced were several times larger than the applied load. These axial forces serve to increase the flexural stiffness and load-carrying capacity of the slab by about 30%-40% relative to an unrestrained slab. An illustration of enhanced behavior of a restrained slab has shown in Figure 2-7.

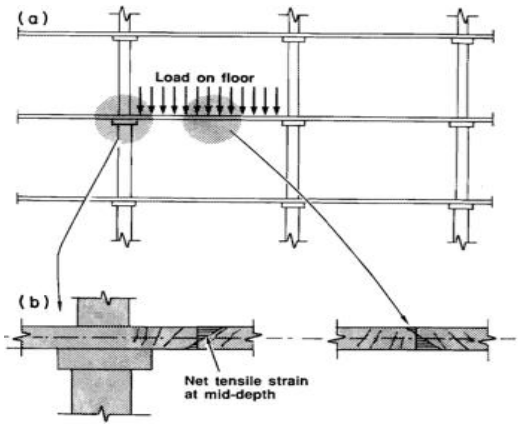

Figure 2-6 Axial forces developed in laterally restrained slab: (a) Slab subjected to transverse loading; (b) slab elongates upon cracking [Vecchio and Tang (1990)]

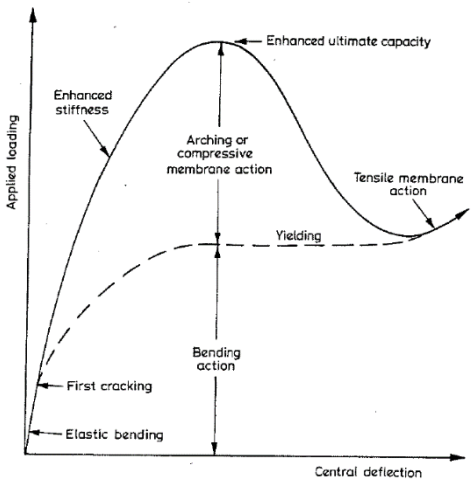

Figure 2-7 Illustration of enhanced behavior of a laterally restrained slab [Leibenberg, 1966]

Compressive membrane action in a beam or a slab is highly sensitive to the degree of lateral restraint at the end supports. A higher degree of lateral restraint may produce a higher load-carrying capacity; on the other hand, a low degree of lateral restraint often produces a disproportionately low load-carrying capacity, together with an outward movement of the end supports. Rankin et al. (1991) showed basic formulations of a simple, rationally based method for predicting the enhanced load capacity of rigidly restrained slabs. The method showed a good correlation with a wide range of test results from various sources.

The method of the prediction is based on the following simplifying assumptions:

(1) A yield-line pattern is assumed to have developed at failure as shown in Figure 2-9

(2) Corner levers can be ignored, i.e. single positive moment yield-lines are assumed to run into each corner of the slab at 45 degree to the slab boundaries

(3) A constant average arching moment of resistance M_{av} is assumed to act at all points along the yield-lines.

The internal work done by bending action is given by

$$I_b = 8(M_b + \overline{M_b}) + 4(M_b + \overline{M_b})(L_y - L_x)/L_x \quad \text{Equation 2- 11}$$

However, arching action causes only positive moment resistance and hence

$$I_a = 8M_{av} + 4M_{av}(L_y - L_x)/L_x \quad \text{Equation 2- 12}$$

The internal work done by arching maybe combined with the internal work done by bending to give the total internal work done along the yield-lines thus:

$$I_w = I_a + I_b \quad \text{Equation 2- 13}$$

Where I_a is the internal work done by the arching action on the slab; I_b is the internal work done by the bending moment; M_{av} is the average arching moment of resistance; L_x is the short span of slab; L_y is the long span of slab; M_b is positive moment of resistance; $\overline{M}_b$ is negative moment of resistance

For a unit virtual displacement, the external work done by a loading N/unit area on the slab is given by

$$E_w = N(3L_y - L_x)\frac{L_x}{6} \quad \text{Equation 2- 14}$$

Equating the internal and external work done gives the following simple expression for the ultimate load capacity of a uniformly loaded laterally restrained slab:

$$N_{ps} = \frac{6I_w}{L_x(3L_y - L_x)} \quad \text{Equation 2- 15}$$

Where N_{ps} is predicted ultimate load by proposed method; I_w is total internal work done at a given unit virtual displacement; E_w is total external work done at a given virtual displacement.

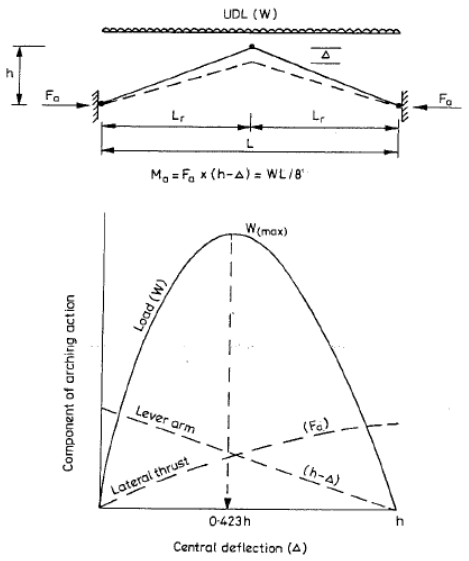

Figure 2-8 Three-hinged arch analogy [Rankin et al. (1991)]

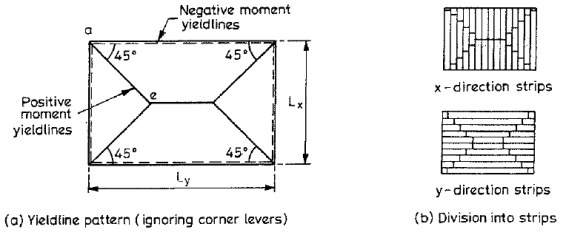

Figure 2-9 Assumed yield-line pattern and division of slab into strips [Rankin et al. (1991)]

Some other research efforts have also been devoted to the study the enhanced effect due to compressive membrane action. Enhancement of punching shear strength with lateral compressive force has been advocated by other researches like Guice and Rhomberg (1988), Salim and Sebastian (2003), and Rankin et al. (1987). They indicate that compressive membrane forces can be developed in the slabs due to the restraint effects and which in turn increases the punching shear capacity of restrained slabs. The tests indicated that, depending on the slab flexural reinforcement ratio and span-to-depth ratio, the in-plane compressive force can enhance the gravity loading capacity by 30 to 100%. The magnitude of the punching shear strength enhancement increases with the degree of edge restraint (Alam et al. 2009).

2.4 Post –punching

The behavior of the slab-column connection after punching shear failure can have a significant impact on the progression of collapse. The post-punching capacity comes from the tensile membrane action of the top reinforcement with the main contribution offered by the continuous bottom reinforcement i.e. integrity reinforcement (Hawkins and Mitchell, 1979; Mitchell and Cook, 1984). Integrity reinforcing bars carry load by developing high tensile stresses can develop nearly 98% of punching shear strength after punching, which can be considered as a way to mitigate the likelihood of the disproportionate collapse (Mirzaei 2010).

The 1971 and earlier editions of ACI codes didn't require bottom reinforcement to be continuous. Therefore, any post-punching resistance had to come from top tensile reinforcement which is continuous through the column. Following punching failure the top reinforcement is often thought not to be efficient due to its tendency to rip out of the concrete cover as shown in Figure 2-10;

On the other hand, the structural integrity reinforcement (continuous bottom reinforcement) can provide robust post punching capacity against collapse by developing the dowel action, offering resistance over large displacements until they either rapture due to high tensile load in the bar, rip out of the concrete, or pull out due to insufficient embedment length as shown in Figure 2-11.

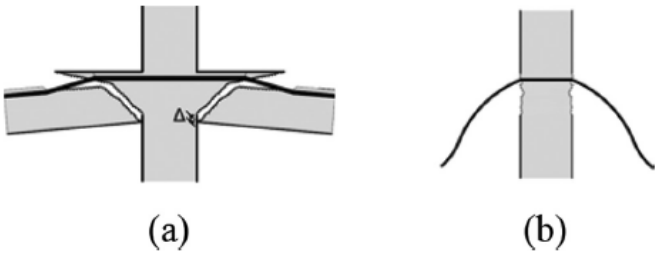

Figure 2-10 Slab-column connection with top bars only: (a) Ripping out of bars after punching shear failure; and (b) loss of support with top bars ineffective. [Habibi et al. 2014]

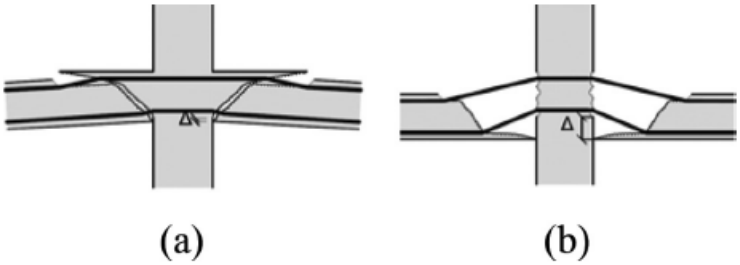

Figure 2-11 (a)Dowel action in structural integrity bars after punching; (b) Post-punching resistance provided by structural integrity reinforcement and ripping out the top reinforcement. [Habibi et al. 2014]

Habibi et al. (2012) found that integrity reinforcement can provide post-punching capacities of 50% to 100% of the punching shear strength. Figure 2-12 shows the effect of length of structural integrity reinforcement. The increase of the develop length of integrity bars resulted in a small increase in the post-punching resistance, but the ultimate deformability increased by 28%. He also concluded that, by the analysis, top bars contributed about 20% of post-punching capacity due to the breakout resistance of concrete cover and pullout of the bars after significant deflections (Habibi et al. 2014).

Tests by Ruiz et al (2013) showed having anchored top reinforcement produced a stable post-punching capacity at about 30% of the punching load. The use of unanchored bars did not produce a stable post-punching response.

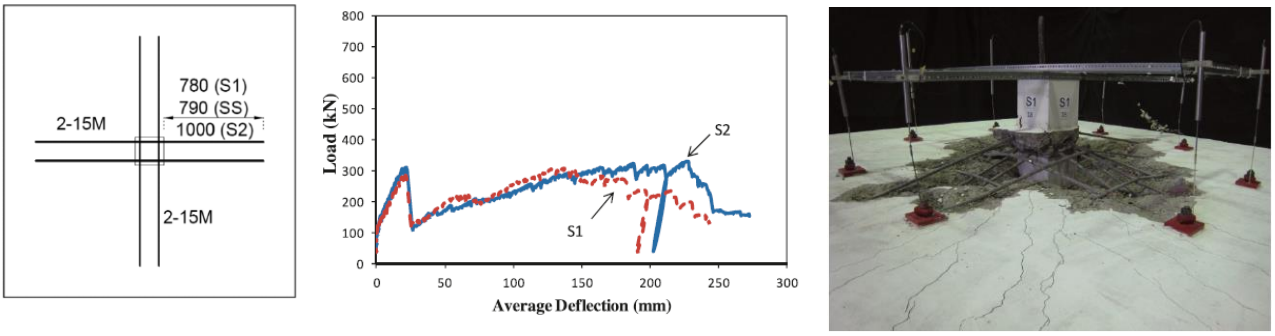

Figure 2-12 Effect of length of structural integrity reinforcement [Habibi, 2012]

Post-punching capacity of the connection also plays a role in improving disproportionate collapse resistance of the slab. If the connection has some residual capacity after punching failure, then that load may not completely be transferred to surrounding connections and lead to their overloading. There are three possible cases following the failure of flat-plate connection in terms of the post punching capacity: Case1: the failed connection has certain amount of post punching capacity, and adjacent connections do not see the full load and therefore have sufficient punching capacity-No collapse; Case 2: the failed connection completely losses the capacity and the adjacent connections have sufficient punching capacity-No Collapse; Case 3: the failed connection losses the capacity and the adjacent connections don't have enough capacity-Collapse, Obviously, Case 1 and 2 are the desirable cases, however the required punching shear capacity of the adjacent connection in Case 2 is very high and may not be achievable in an economic design. On the other hand, the required capacity in Case 1 can be much lower due to the post-punching capacity and may allow for economic design of flat-plate buildings.

2.4.1 Code approaches

Some codes of practice provide explicit formulations to calculate the integrity reinforcement over slab-column connections. Other codes and guidelines provide only some

recommendations to mitigate the likelihood of the disproportionate collapse following a punching shear failure. The Swiss standard SIA 262 requires reinforcement to be provided on the flexural compression side to mitigate the chance of collapse after a local punching shear failure. The reinforcement shall be extended over the supported area and dimensioned as follows:

$$V_d = A_{sb} f_{sd} \sin\psi \qquad \text{Equation 2- 16}$$

Where A_{sb} is the total cross-sectional area of the integrity reinforcement passing through the column, f_{sb} is the dimensioning yield strength of steel reinforcement, V_d is the dimensioning value of the shear transmitted to the column in accidental situation, and ψ is the angle of inclination of the reinforcing bars in the vicinity of the punching shear crack after failure as shown in Figure 2-13.

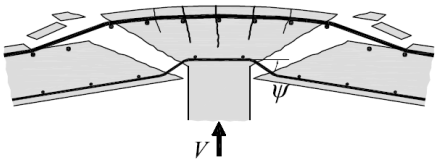

Figure 2-13 Punching failure over a slab-column connection [Mirzaei, 2010].

ACI 318 (2008) does not have explicit formula for post-punching behavior of concrete flat slabs. ACI 318 merely requires that bottom bars be continuous and anchored into the next span and that at least two bottom bars pass through the column. There is no requirement on the size of the bars passing through the column. ACI 352 recommends that continuous integrity bars passing through the column cage in each principal direction at interior connections should have an area at least equal to A_{sm} as shown in Equation 2-17.

$$A_{sm} = \frac{0.5 q_d}{\emptyset f_y} l_1 l_2 \qquad \text{Equation 2- 17}$$

Where A_{sm} is the minimum area of the integrity reinforcement in each principal direction placed cross the column, q_d is the factored uniformly distributed load but not less than twice the slab service dead load, f_y is the yielding strength of steel, ϕ is a shear reduction factor, and l_1 and l_2 is center-to-center span in each principal direction. A_{sm} may be reduced to two thirds of that for edge connections, and one-half of that for corner connections.

Canadian CSA standard A23.3-94 assumes that the structural integrity reinforcement is capable of yielding and forms an angle of 30 degrees from the horizontal. The code adopts an equation proposed by Mitchell (1993) which requires area of bottom reinforcement connecting the slab to the column on all faces to be:

$$A_{sb} \geq \frac{2V_{se}}{f_y} \qquad \textbf{Equation 2- 18}$$

Where V_{se} is the post-punching resistance, is the total area of integrity reinforcement, V_{se} is the post-punching resistance, $\sum A_{sb}$ is the total area of integrity reinforcement, and f_y is the yield strength of the reinforcement.

The New York City Building Code Section 1916.2.3 requires horizontal ties be provided at each level that can develop a tension force equal to the maximum of 1 or 2:

1. Three times the load entering the column at that level, using a load combination of 1.0 * DL (self weight of structure only).
2. One and a half times the load entering the column at that level using the load combinations of (1.2 DL + 1.6 LL) or 1.4 DL.

This beam or slab bottom reinforcement shall be distributed around the column perimeter and shall be extended on all sides of the column into the adjacent slab for at least one-third of the

span length. Where reinforcing bars cannot be extended beyond the column (e.g., at slab edges and openings), they shall be hooked or otherwise developed within the column.

Although most modern codes now require continuous bottom reinforcement, older RC flat-plate buildings in the U.S. were typically designed without using integrity reinforcement needed for developing tensile membrane action. Therefore, these buildings can be highly vulnerable to disproportionate collapse due to the loss of a supporting column in an abnormal event (Liu et al. 2013). However, the effectiveness of well anchored tensile reinforcement in against disproportionate collapse is unknown and there is still a lack of experimental evidence about the post-punching performance of slab-column connection without continuous bottom bars under static and dynamic loading.

2.5 Disproportionate Collapse Analysis and Design

When a primary load bearing element of a flat-plate building fails in an extreme loading event, the gravity load will be redistributed to the surrounding slab-column connections. The structure may fail or survive this abnormal loading condition depending on slab flexural rotation and punching shear capacity. If the surrounding critical slab-column connections fail structure will respond dynamically, causing higher force and deformation demands on the structure than static loading. This action further increases the load to be redistributed and may lead to a propagation of punching failure over a large portion of the structure. Unfortunately, it is often unknown what the initiating cause to the collapse will be. Therefore, different design procedures have been developed to approximate the response of the structure to idealized scenarios.

2.5.1 Design approaches to against disproportionate collapse

The basic principle of progressive collapse prevention is that removal of a primary load-carrying element should not cause collapse. This can be achieved by providing alternate load

paths in case a primary load-carrying element is lost. The overall approach is composed of three methods outlined in UFC 4-023-03(2009): Tie Forces (Indirect Design), Alternate Path (Direct Design), and Specific Local Resistance (Direct Design). The indirect design approach is a prescriptive approach, which is based on providing a minimum connectivity and integrity between various structural elements, the overall robustness of the structure could be improved by incorporating measures typically related to strength, continuity and deformation capacity. The direct design methods are usually based on sophisticated structural analyses such as nonlinear static or dynamic finite element analysis, which are not commonly used in routine design practice.

2.5.1.1 Tie forces

Tie force is an indirect method to resist disproportionate collapse. Key structural elements of a structure must be tied together so that the load redistribution from damaged elements to undamaged elements can occur. The ties consist of internal ties, peripheral ties, and vertical ties as shown in Figure 2-14. Tie forces can be provided by the amount of continuous longitudinal reinforcement in existing structural elements.

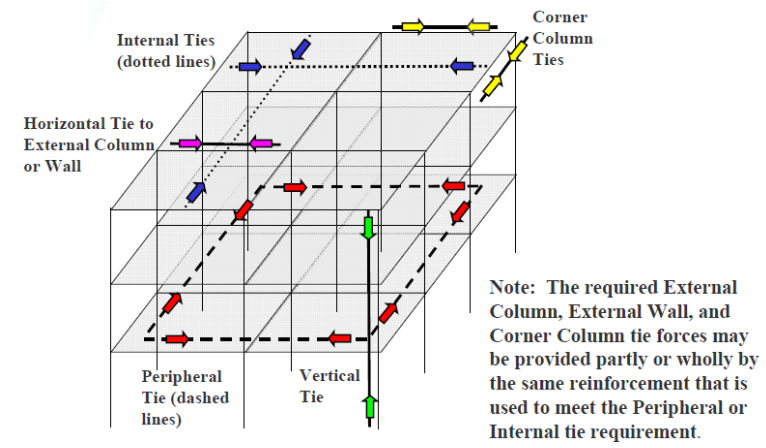

Figure 2-14 System of tie forces [DoD, 2003]

2.5.1.2 Alternate Path Direct Design Approach

In this approach, the structure is designed such that if any one component fails, alternate paths are available for the load that was in that component and a general collapse does not occur. This approach has the benefit of simplicity and directness. This method leads to structures with improved redundancy and continuity. But it neither address the issue of in case of blast more than one member may be damaged nor address explicitly the dynamic effects associated with rapid element removal. [Osama, 2006]

2.5.1.3 Specific Local Resistance

The specific local resistance method provides supplementary strength for key structural elements, which are explicitly designed to withstand a specified level of abnormal loading (ASCE7,2005). Thus, unlike the alternate load path method, this approach provides additional strength at the areas that are believed to be prone to accidental loads or in key elements that are necessary for the load redistribution.

An excellent example of a building avoiding disproportionate collapse through local resistance is the world Trade Center structure in the 1993 terrorist attack (Ramabhushanam 1994). The columns under the building that were exposed to the bomb blast remained standing because of their extreme robustness (the columns were very robust because their need to support a heavy load, not as a deliberate means of avoiding disproportionate collapse). If a similar bomb had been set off to a building with much smaller columns, several of them would have failed, leading to a catastrophic collapse even if the structure had been designed for one-column redundancy.

While local resistance is, clearly, an effective means of resisting disproportionate collapse, an obvious problem this method requires some knowledge of the nature of potential attacks.

This method maybe suitable for accidental events such as a car impact and a small gas explosion, but becomes very costly for a terrorist attack using a large explosion (Dat 2013).

2.6 Code Approaches

Buildings should be designed to have sufficient strength, ductility, and redundancy to resist disproportionate collapse. All the codes and design standards with divisions for disproportionate collapse prevention have either explicit or implicit requirements.

ACI 318 does not provide the direct design provisions against disproportionate collapse, Some of the ACI requirements to enhance continuity and integrity include: (1) continuation of bottom reinforcement of beams and slabs in columns/support zones; (2) use of moment resisting frames and connections; and (3) use of mechanical splices, rather than lap splices, in flexural yield zone in regions where seismic resistance is needed. The American Concrete Institute introduced prescriptive provisions to improve structural integrity against disproportionate collapse for reinforced concrete (RC) structures in 1989 [ACI 318,1989].

ASCE 7 (2005) requires that a safe alternative load transfer path should be ensured if a primary member is damaged locally. Three design alternatives related to disproportionate collapse are suggested as mentioned above: the indirect design approach, the alternate path direct design approach, and the specific local resistance direct design approach.

The General Services Administration (GSA) published guidelines in 2000 and 2003 for the disproportionate collapse analysis and design of structures [GSA, 2003]. The Department of Defense (DoD) has also published criteria to mitigate disproportionate collapse potential of new and existing structures [DoD, 2005]. UFC 4-023-03, “Design of Buildings to Resist Progress Collapse” provides the design guidance necessary to reduce the potential of disproportionate collapse for new and existing DoD facilities that experience localized structural damage through

manmade or natural events. Table 2-1 shows the load combination for design against disproportionate collapse.

Table 2-1 Load combination for design for disproportionate collapse

Codes of practice	Load combination
BS 8110-1:1997	$(1.0D + L/3 + W_n/3)$ (static analysis)
DoD UFC 4-023-03	Ω [1.2D +(0.5L or 0.2 S)] (Nonlinear/linear static analysis) 1.2D +(0.5L or 0.2 S) (nonlinear Dynamic analysis)
GSA 2003	2(D+0.25L) (static analysis) D+0.25L (dynamic analysis)

D, L, S, W_n , L_{LAT} = dead, live, snow, wind and lateral loads; Ω is dynamic increase factor

2.7 Dynamic behavior of structure in disproportionate collapse

When one of connections is overloaded and fails, the load must be redistributed to the surrounding columns. This dynamic redistribution action can amplify the internal forces and lead to increased loading on the structure (Orton et al. 2013). The dynamic load increase may be partially offset by the strain rate effect leading to material strength increase of the steel and concrete materials.

Although most of the work to determine dynamic effects has been done numerically, to date there have been a few experimental tests on structures at both sub assemblage and system levels. Isolated tests conducted by Criswell (1974) indicated that connections in dynamically loaded structures will display increased resistances and larger ductility. The deflection at failure increased 25 to 50 percent with the dynamic loading effects and the strength increased on average 18 percent for the more lightly reinforced slabs and 26 percent for the more heavily reinforced specimens. Similar observations can be made from the dynamic tests of slab-column connections subjected to combined gravity and lateral loading (Ghali et al. 1976).

Some guidelines for collapse-resistant design are provided in Department of Defense (DoD) (2013) and General Services Administration (GSA) (2003). A dynamic amplification factor (DAF) was introduced by DoD (2013) to consider effects of dynamic loading. The factor is a function of ductility, therefore allowing it to be adjusted for members with greater ductility capacity and thus limit the dynamic increase of the load. Dynamic beam tests in a collapse scenario by Tian and Su (2011) showed the dynamic amplification factor ranged from 1.7-1.36 depending on the level of loading. Beams with higher load saw a lower DAF due to decreased stiffness at higher loads. Orton et al. (2014) showed that dynamic tests on the frame with discontinuous reinforcement showed an increase in DIF due to the snap through response.

2.8 Experimental tests on disproportionate collapse

Dat and Hai (2013) presented an experimental study to investigate the static response of double-span beam- slab substructures bridging over a penultimate-internal column. Three 0.25 scaled beam-slab substructures were designed, build and tested by a static loading scheme as shown in Figure 2-15. The boundary of the slabs was rotationally and vertically restrained, but laterally unrestrained. The static response of the test structures was identified with negative bending moments that were greatly affected by T-beam effect, and catenary action replacing positive bending moment in the central area at very early stage. As the deflection increased, the overall load-carrying capacity of test structures increased due to the continuous development of catenary action, and this action was accompanied by partial failures such as fracture of beam bottom bars and compressive failure of beam-to-column connections.

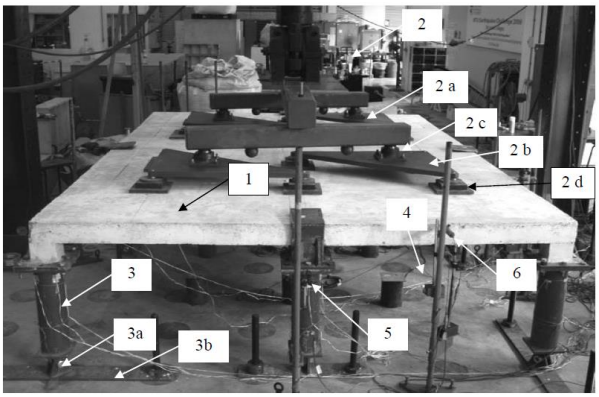

Figure 2-15 Slab in the setup ready to test [Dat and Hai (2013)]

The outward movement of the columns that reached a maximum value of about 10mm at a displacement of 100mm was caused by the elongation of double span beams as shown in Figure 2-16. In test PI-3, continuous inward movement beyond the initial position was a sign of failure of the peripheral compressive ring under catenary tension forces.

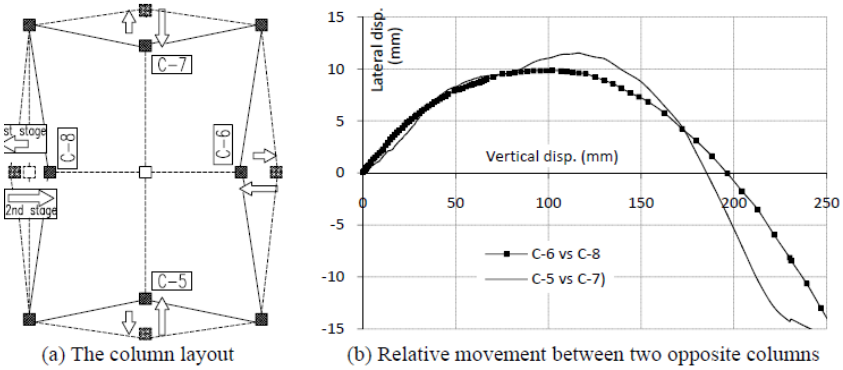

Figure 2-16 Lateral movement among the columns [Pham Xuan Dat (2013)]

Yi et al. (2014) experimentally investigated two identical single –story 2 by 2 reinforced concrete flat slab-column structures by using quasi-static test methods to simulate the effects of the lost column as shown in Figure 2-17, the first model was used to simulate the loss of an interior column and the second model was used to simulate the loss of an exterior and corner column, respectively.

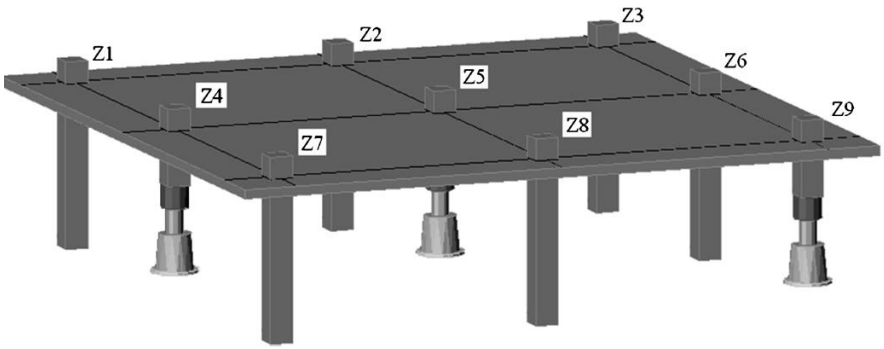

Figure 2-17 Schematic view of test models showing simulation of column removals: (a) model1-interior column loss (Z5); (b) model 2-exterior column loss (Z4) and corner column loss (Z9) [Yi et al. (2014)]

The findings from the testing indicate that the side span and corner span are more vulnerable than the interior span. Compressive and tensile membrane actions are the primary alternate load paths for flat-plate systems following the loss of a load-carrying vertical member. Figure 2-18 shows the relationship between horizontal and vertical displacement during exterior column removal test, this plot indicates that the plate edge first moved outward and then moved inward after a vertical displacement of the exterior column of approximately 76mm (3.0in.), the turning point represents the transition of the load transmission mechanism from compressive to tensile. The study also shows the load-carrying capacity of the side span attributable to compressive membrane action is less than that of the interior span because of the reduced lateral stiffness provided by the exterior cantilevered plate and surrounding column.

Yi et al. (2008) investigated experimentally as well as analytically the disproportionate failure of a four-bay three-story RC planar frame structure using a macro model-based approach. A constant load of 109 kN (24.5kip) was applied to the top of middle column by an actuator to simulate the gravity load of the upper frame. A jack was set up at the bottom of the middle column and was gradually relieved until the final collapse. A load cell was used in the jack to measure the change of the axial force in the removed column. The decrease of axial force N in

the middle column was due to an increase in resistance of catenary action in the beams as shown in Figure 2-19, also it was observed that the development of catenary action resulted in significant inward movement of adjoining columns.

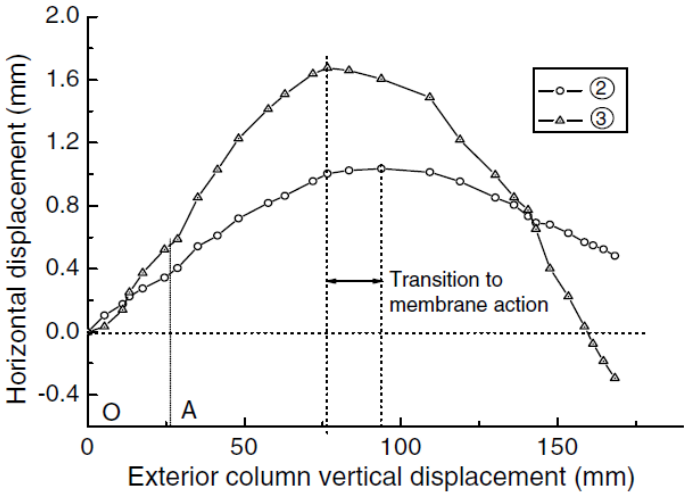

Figure 2-18 Relationship between horizontal and vertical displacement during exterior column test [Yi et al. (2014)]

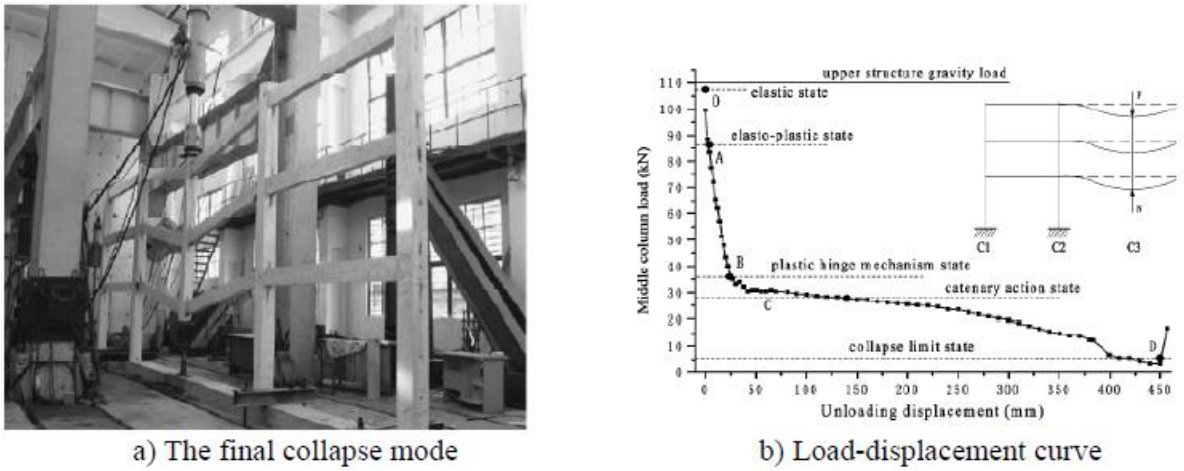

a) The final collapse mode

b) Load-displacement curve

Figure 2-19 A 2-D frame subjected to a column loss [Yi et al. (2008)]

In order to investigate the dynamic response of a building structure subjected to an instantaneous removal of a column, Sasani et al.(2007) conducted experimental and analytical studies following the loss of an exterior column in an actual 10-story reinforced concrete structure. The dynamic response of the affected structure following the instantaneous removal of a first story column can be seen in Figure 2-20. The axial forces in column B5 from the second to the tenth story have been redistributed quickly and approached stable values within a very short time. This redistribution process was caused by the propagation of axial stress wave in column B5 starting from the second story to the roof story. After the axial forces had decreased to steady values, joint B5 at different floors moved downwards almost identically. This study provided two significant insights on the response of building structures following a sudden column removal: (1) the behaviors of all floors above the removed column are identical; (2) uniformly distributed loads, rather than concentrated loads from the column, are the loads which act on the affected floors. Therefore, investigation of disproportionate resistance of building structures can be investigated by considering a typical floor, rather than an entire structure, using uniformly distributed loads.

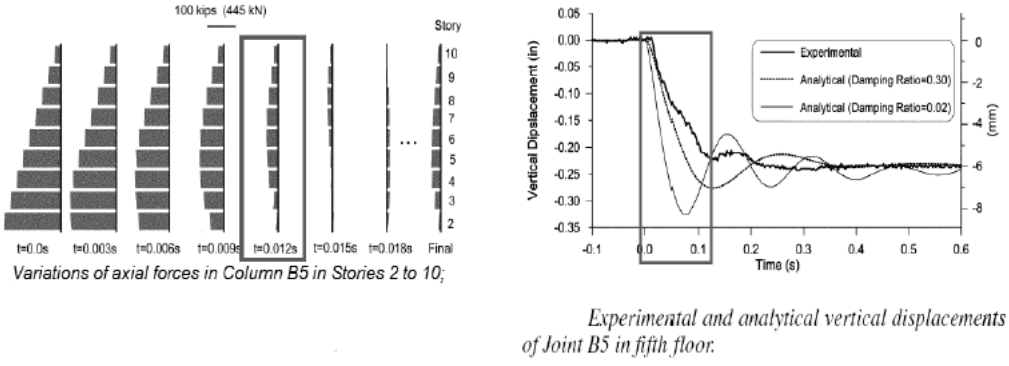

Figure 2-20 Experimental and analysis results [Sasani et al (2007)]

Xiao et al.(2013) experimentally studied a 3-story 3 span half scale RC frame model as a reduced order model of a prototype 10 story building as shown in Figure 2-21. The structure was designed for 1.2 DL+1.6LL of uniformly distributed load.

Figure 2-21 Final failure of test structure after removal of two side columns [Xiao et al. (2013)]

The objective of the study was to generate information on load transfer mechanisms following the loss of one or more lower-story columns to calibrate simulation models for further studies on disproportionate collapse behavior of RC frame structures. Based on the selected removal sequences of the first story columns, the testing programs can be divided into the following phases as shown in Figure 2-22 :

Phase I: removal of the corner column A1, and then removal of the second column B1

Phase II: removal of the side column D2, and then removal of column D3

Phase III: removal of center column B3

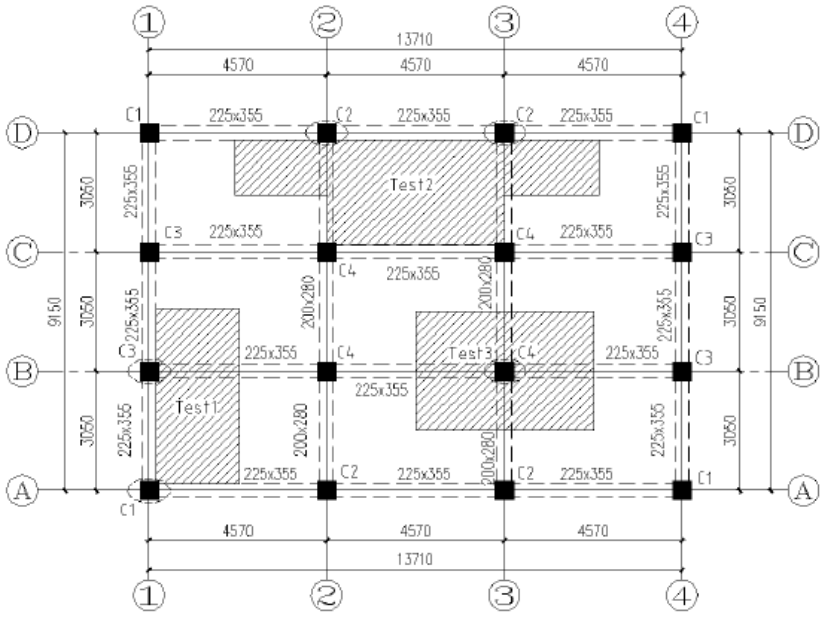

Figure 2-22 Column removal test plan [Xiao et al. (2013)]

After the sudden removal of corner column A1, only fine minor cracks could be observed near the beam ends within span A1-A2 and A1-B2. After the removal of second column B1, more cracks were observed on the beams and slabs near the corner columns that were removed, but the widths of crack were fairly small. Figure 2-23 shows the vertical displacement time histories at the location of the removed columns. After the removal of column D3, the frame at that location only displaced approximately 12mm (0.47in.) vertically, the vertical displacements of the node D2 and D3 were 60.8mm and 35.8mm respectively at the onset of removal of column D2. The side frame continued the downward deformation after the removal of the two columns D3 and D2.

The structure did not collapse during the tests comprising the corner or inner column removal, however, when two side columns in the long direction were removed, the frame experienced transition from moment frame resisting mechanism to catenary mechanism.

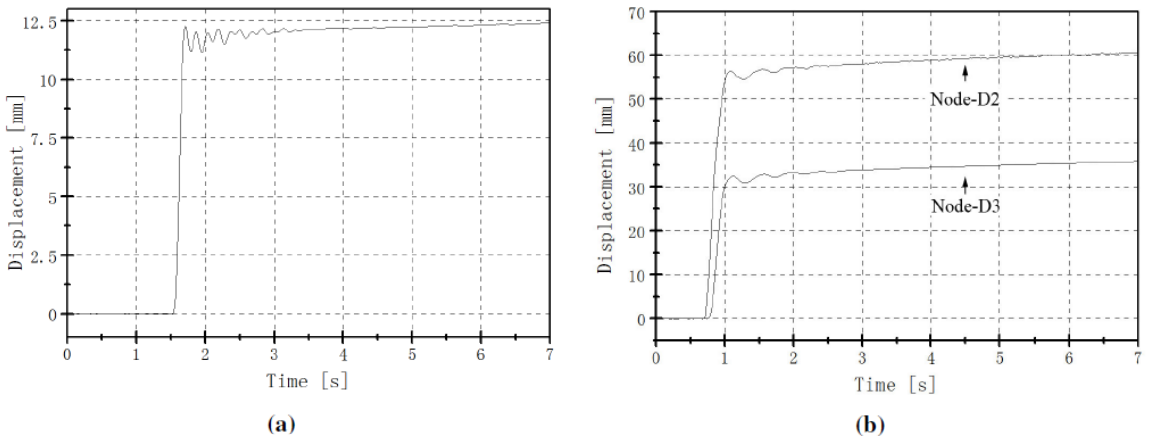

Figure 2-23 Vertical displacement-time histories: (a) after removal of Column D3; (b) after removal of Column D2 [Xiao et al. (2013)]

2.9 Summary

Compressive membrane forces serve to increase the load-carrying capacity of the connection relative to an isolated unrestrained slab-column connection, this increase is highly sensitive to the degree of lateral restraint at the end supports. However, there is no test data verified the existence of compressive membrane action in disproportionate collapse if an interior or exterior is simultaneously removed in an abnormal event. And no test results show the increase of punching capacity due to the compressive membrane action can help to arrest disproportionate collapse in dynamic loadings.

The post punching capacity mainly comes from the contribution offered by the integrity reinforcement. Older RC flat-plate buildings are typically designed without using integrity reinforcement, but the role of post punching capacity without using integrity reinforcement on disproportionate collapse is uncertain if an interior or exterior column is instantaneously removed in an abnormal event. In addition, the effectiveness of well anchored tensile reinforcement in against disproportionate collapse has not been examined in tests.

For the multi-panel test, the test results showed the behaviors of all floors above the removed column are identical. Uniformly distributed loads, rather than concentrated loads from the column, are the loads which act on the affected floors. Therefore, investigation of disproportionate resistance of building structures can be investigated by considering a typical floor, rather than an entire structure, using uniformly distributed loads.

The static experiments results show compressive and tensile membrane actions are the primary alternative load paths for flat-plate systems following the loss of a load-carrying vertical member. Since most of multi-panel slabs were tested statically to investigate the potential of disproportionate collapse, the existence of compressive membrane action in flat-plate systems needs to be verified in a dynamic column removal manner. In addition, there is little experimental evidence for characterizing failure propagation over entire floor either in a static or dynamic loading condition.

CHAPTER 3 ISOLATED STATIC TESTS

3.1 Introduction

The goals for the isolated static tests were to investigate the effects of compressive membrane action on the punching shear capacity of isolated reinforced concrete slab-column connections and the post punching behavior of older reinforced concrete flat-plate structures.

3.2 Prototype Design

The prototype structure that the test specimens are based on is an older flat-plate concrete reinforced structure designed following the ACI 318-71 concrete design provisions (1971). This four floor building has a 3.05 m (10 ft) story height and four bays with an equal length of 6.09 m (20 ft) span in each direction as shown in Figure 3-1 . The slab thickness was designed as 190 mm (7.5 in.) and the column was chosen to be a square section with sides measuring 381 mm (15 in.) The assumed service loadings on the structure were a live load of 2.4 kN/m² (50 psf). and a superimposed dead load of 1.2 kN/m² (25 psf) and the self-weight of slab with a load combination of 1.4DL+1.7LL dominating the design of floor slabs. Grade 0.413 kN/mm² (60 ksi) reinforcing bars and a compressive strength of 4000 psi (27600 kN/m²) concrete were assumed to be used for all the structural members. The maximum size of aggregate was assumed as 19.1 mm (0.75 in.).

It was determined from design that a reinforcement ratio of 0.64% was needed to resist the applied moment in the column strip in the negative direction and 0.23% in the positive direction. Therefore, for an interior span column strip, #4 bars spaced at 127 mm (5 in.) were chosen for the tension reinforcement and #4 bars spaced at 229 mm (9 in.) were chosen for the compression reinforcement. The reinforcement layout of prototype structure is shown in Figure 3-2.

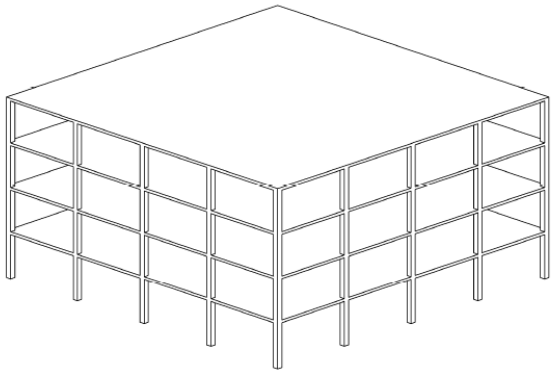

Figure 3-1 3D View of prototype structure

The concrete cover was designed to be 9.1 mm (0.75 in.), the effective thickness of the slab was calculated to be 152mm (6 in.). The older flat plate buildings followed ACI318-71(1971) which didn't require the integrity bars though columns, thus the slab bottom bars are imbedded into column 114mm (4.5 in.) in this prototype design.

3.3 Experimental Program

Six isolated square reinforced concrete flat-plate slab specimens were constructed at 0.73 scale and tested with two different reinforcement ratios 0.64% and 1.0%. The thickness of the slabs was 140 mm (5.5 in) and the effective depth (d) 114 mm (4.5 in). Eleven in. square columns extended 200 mm (8 in.) above and below the slab to accurately reflect the stress state at the slab column intersection. The design of slab column specimens followed the provisions ACI318-71. Dimensions and construction details of the specimens are shown in Figure 3-3.
In the prototype design the top reinforcement should extend 530 mm (21 in.) beyond the edge of the test structure. To simulate the anchorage of the top bars provided by the additional development length four specimens were constructed with hooked bars at the edge of the slab as

seen in Figure 3-3. However, the hooked bars are over-conservative as they do not allow the top bars to rip out of the slab during post-punching. Therefore, two specimens (0.64 RE NH, 0.64RE NH2) were constructed without hooked bars and tested in order to specifically investigate the post punching response.

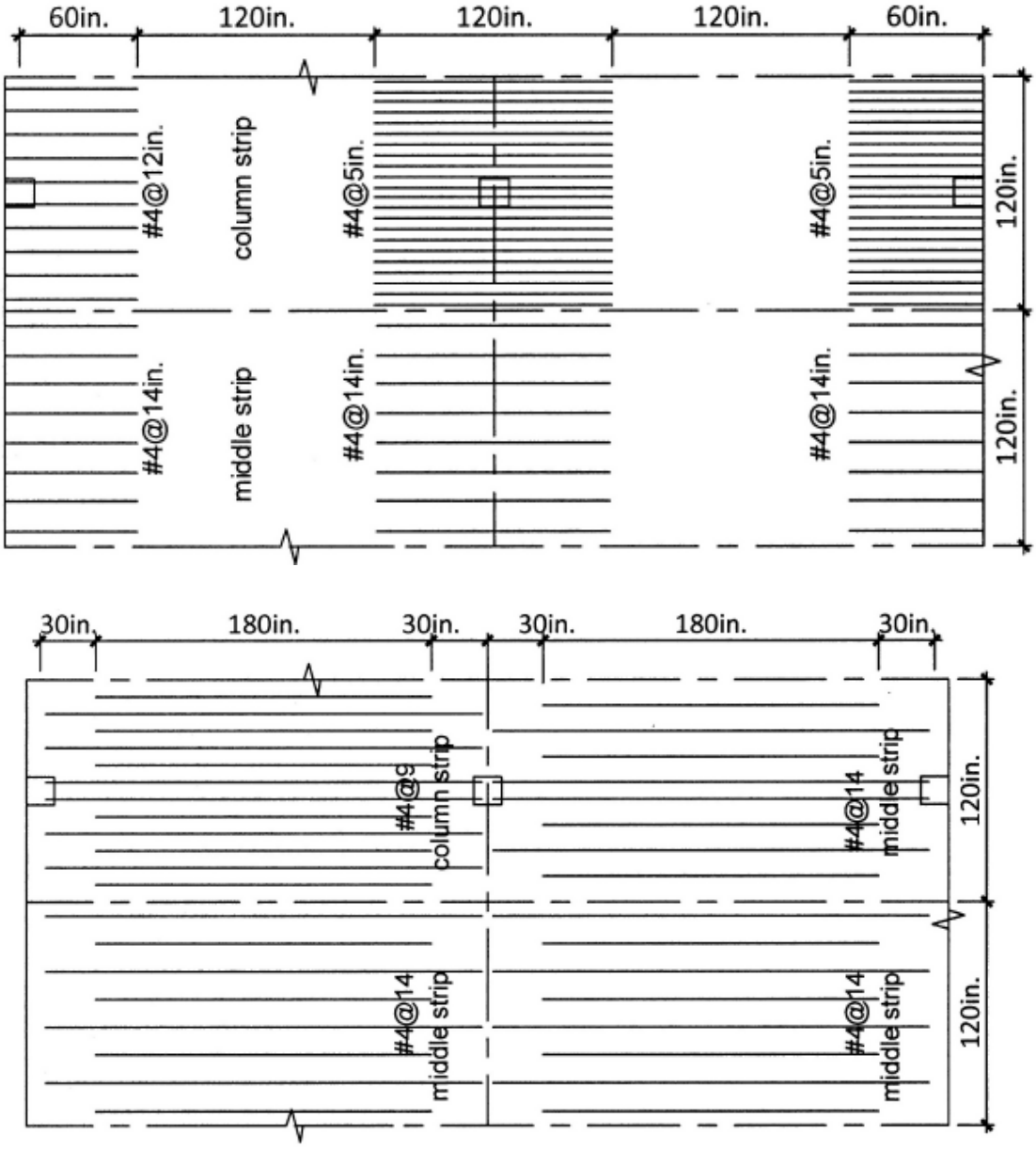

Figure 3-2 Reinforcement layout of prototype structure

The formwork was made by a grid of 2x4's and 2x6's to ensure the slab has a solid base. In order to connect the slab specimens to the test setup threaded rods were imbedded to the slab prior to the pouring of concrete, the top column studs were suspended 140mm (5.5 in). above the formwork by two 2x6's cross the formwork. The completed formwork as shown in Figure 3-4.

3.3.1 Material properties

A local commercial concrete with maximum aggregates size 9.5mm (3/8 in.) from a ready mix company was used for all specimens. Each of the slab specimens were cast at different times from different concrete batches therefore there was some variance in the measured concrete compressive strength at the time of testing. On the day that each specimen was tested, a minimum of four concrete cylinders were also tested for compressive strength (fc). The cylinders that were used were 102 mm (4 in.) in diameter with a height of 203 mm (8 in.).

The flexural reinforcement that was used in the construction of the slab specimens was also tested in a uniaxial tensile test setup to determine its the exact material properties. The steel was ordered on two separate occasions so samples from each delivery were tested to ensure that there was little difference between them. The area of the #3 rebar samples is taken as 71 mm^2 (0.11 in^2), the area of the #4 rebar samples is taken as 123 mm^2 (0.19 in^2) and the gage length of the samples for the uniaxial tension test was 203mm (8 in.).

The properties of the steel from both shipments were very similar. For the #3 rebar samples the yield stress was just over 0.413kN/mm^2 (60,000 psi) with the corresponding yield strain of about 0.0022 in/in and the ultimate stress was about 0.696kN/mm^2 (100,900 psi). All six samples tested were very consistent when looking at yield stress and strain as well as ultimate stress, however the rupture strain varied fairly significantly (from 0.14 – 0.26 in/in). For the #4 rebar samples the yield stress was slightly higher, about 0.427kN/mm^2 (62,000 psi) with a

corresponding yield strain of about 0.0025 in/in. The #4 rebar samples however had a slightly lower ultimate stress of about 0.682 kN/mm² (98,900 psi) but failed at a more consistent rupture strain (0.18 – 0.24 mm/mm).

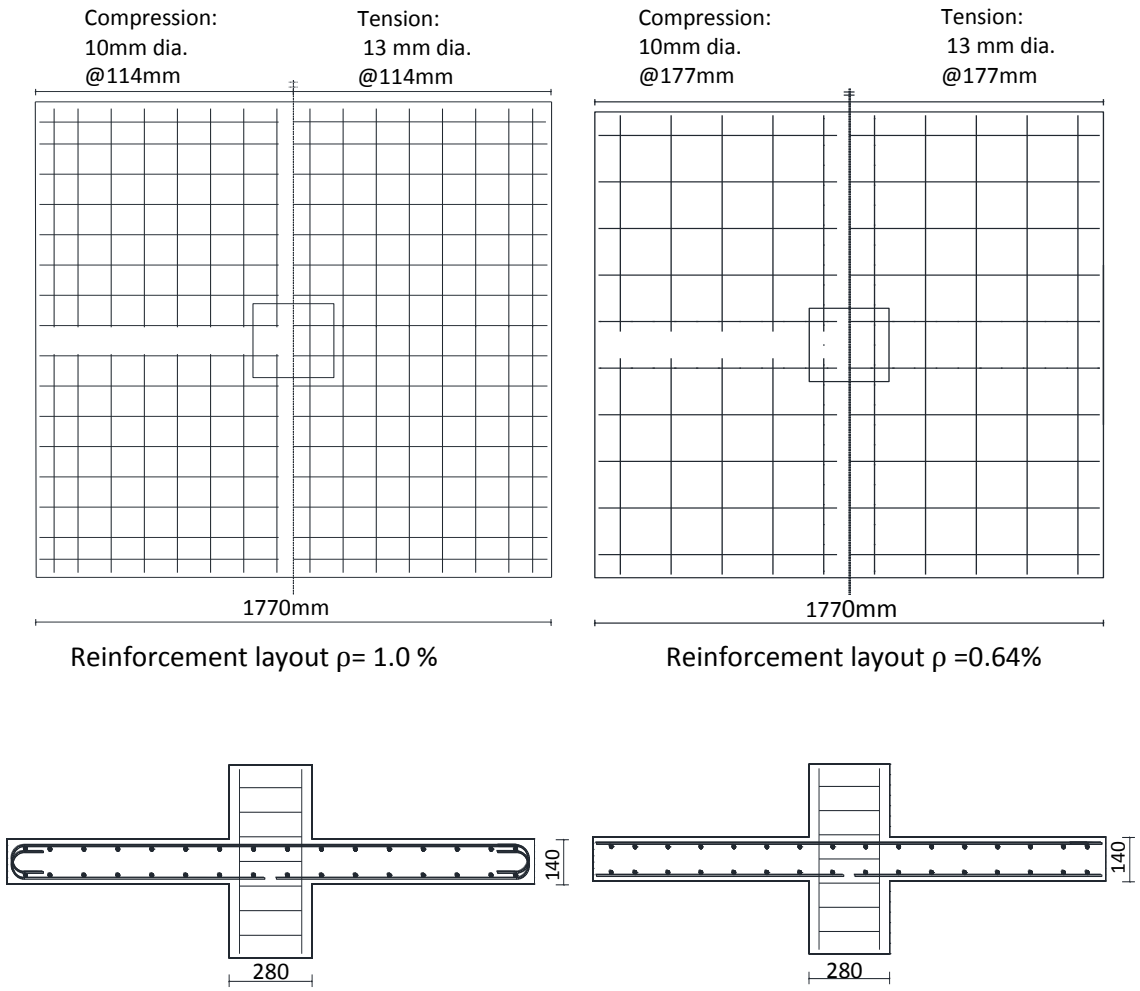

Figure 3-3 Dimensions of specimens

Figure 3-4 Specimen ready to pour concrete

3.3.2 Experimental setup

Four specimens were tested with in-plane forces, and the other two without in-plane forces to be used as references. The slabs are connected to a steel reaction frame using clevises to ensure vertical and horizontal (for restrained tests) restraint as well as zero-moment at that location as seen in Figure 3-5. The location of the clevis corresponds to the location of contra-flexural point in the prototype structure (a distance of $0.2l_n$ (35in.) from the column). The clevises were placed to support the slab at 8 points (2 per side) around the perimeter of the slab. Load was applied the slab at the column using a hydraulic actuator.

The supports provided horizontal (for laterally restrained slabs) and vertical support but allow for rotation of the slab. As detailed in Figure 3-5, the laterally restrained slab was bolted to the steel angle which was bolted to a steel clevis. A 38 mm (1.5 in.) diameter threaded stud connected the clevis to a steel section welded to steel columns. For the unrestrained tests, the horizontal restraint portion of the support was removed as seen in Figure 3-5. Each slab was

subjected to concentrated loading at the column using a hydraulic ram. Overall views of unstrained and restrained tests in position ready for testing are shown in Figure 3-5.

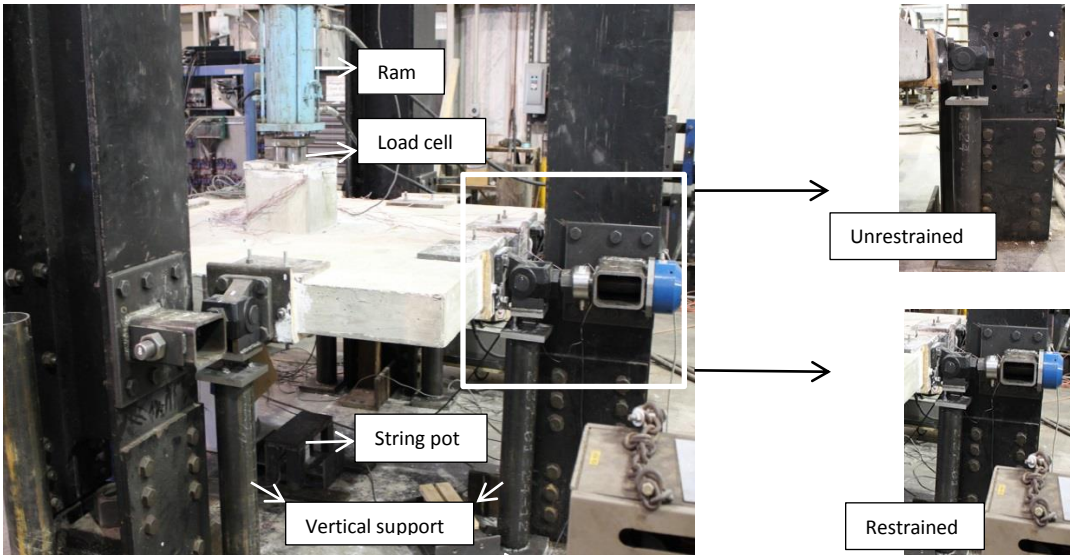

Figure 3-5 Specimens in test setup ready to test

3.3.3 Instrumentation

Measurement of strain profiles prior to punching were made by electrical resistance strain gages were bonded to the reinforcement as shown in Figure 3-6 and Figure 3-7 for 1% and 0.64% reinforcement ratio slabs, respectively. In addition, four concrete strain gages were applied near the column stud on two sides in both perpendicular and parallel to the column. Linear variable displacement transducers (LVDT's) and string pots were used to record the slab lateral and vertical deflection. Horizontal load measurements were determined through a system of four strain gages applied to the threaded rod connecting the clevis to the steel reaction frame and load cells.

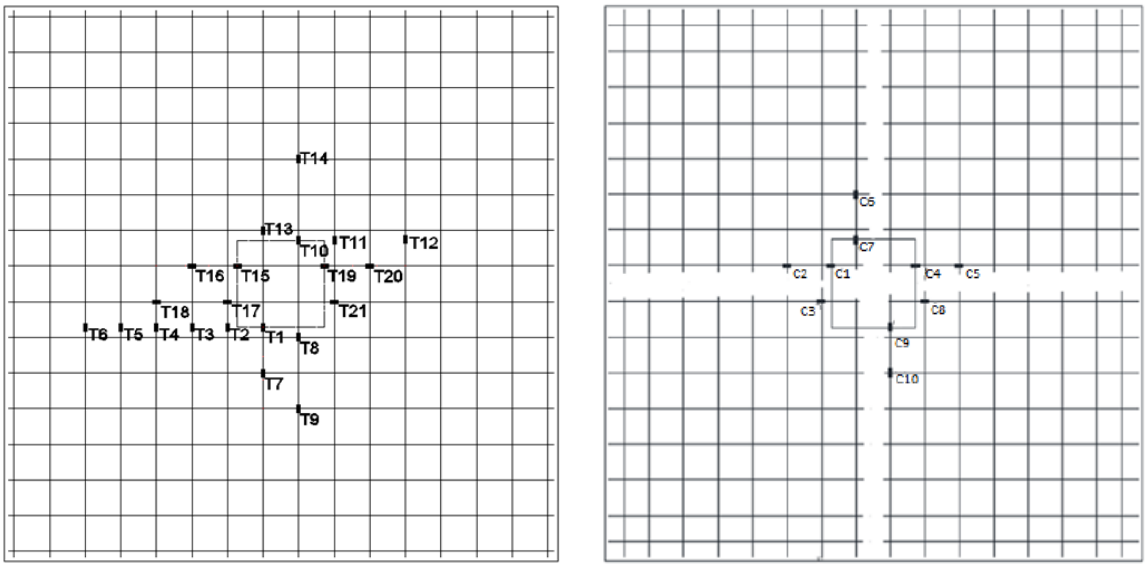

(a)Tension reinforcement strain gage layout **(b)Compression reinforcement strain gage layout**

Figure 3-6 Layout of strain gages for 1% reinforcement ratio

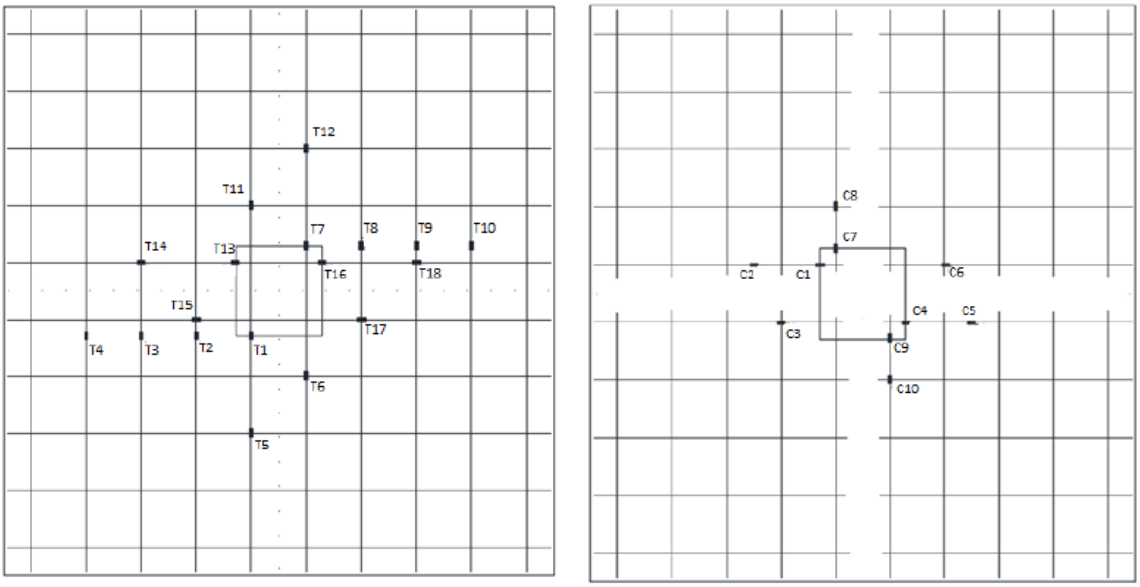

(a)Tension reinforcement strain gage layout **(b)Compression reinforcement strain gage layout**

Figure 3-7 Layout of strain gages for 0.64% reinforcement ratio

3.4 Experimental Results

3.4.1 Overall performance

Figure 3-8 shows typical punching shear failure stages of flat-plate connection. For the pre-punching stage, the slab is pretty constantly stiff until the first crack at about 0.068kN/mm² (10 kips) of loading, then the stiffness of slab changed significantly as can be seen in Figure 3-9. As the load kept increasing, the punching shear failure happened in instant manner without warning. After the punching shear failure occurred the loading of slab column specimens was continued in order to determine the residual capacity of the connection as shown in Figure 3-8(c).

\ (a) Pre-punching (b) Punching failure

(c) Post punching

Figure 3-8 Punching of flat plate connection

3.4.2 Effects of slab tensile reinforcement ratio on punching resistance

Figure 3-9 displays the load versus center deflection response for all specimens up to the occurrence of punching failure. Table 3-1 summaries the peak load (P_E) prior to punching failure and other key measurements at punching failure including center deflection, slab lateral expansion, in-plane restraining force, and lateral stiffness provided by the supports. The post-punching load-carrying capacity (P_R) and the ratio of P_R to P_E are also given in this table. The specimens with higher slab tensile reinforcement ratio (ρ = 1.0%) demonstrated in average 30% more punching capacity and reached this capacity at less deflection than those with lower reinforcement ratio (ρ = 0.64%). This observation was consistent with the findings from previous studies [Elstner and Hognestad 1956; Criswell 1974; Guandalini et al. 2009; Tian et al. 2008]. Reinforcement ratio is a key factor for punching strength and deformation capacity of slab-column connections. For all specimens, the measured punching strength was less than that predicted using the two-way shear strength formulations in ACI 318-14 (2014), which neglects the effects of slab reinforcement ratio. For instance, the measured strength for restrained specimens 1.0RE and 0.64RE was 10% and 39% lower than predictions, respectively.

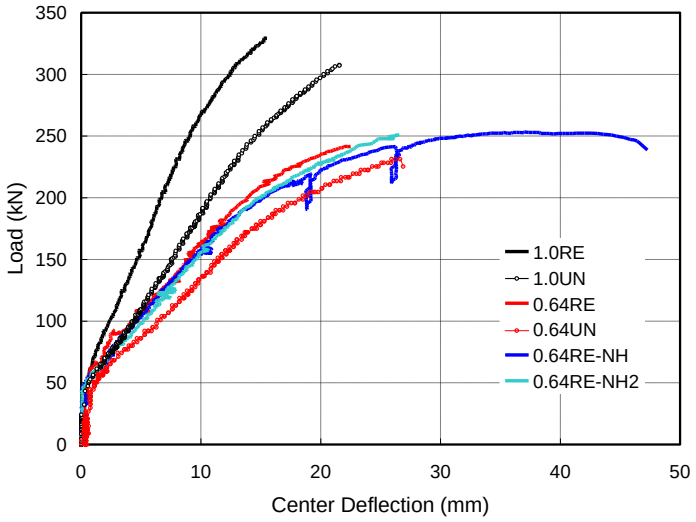

Figure 3-9 Load-center deflection behavior before punching failure.

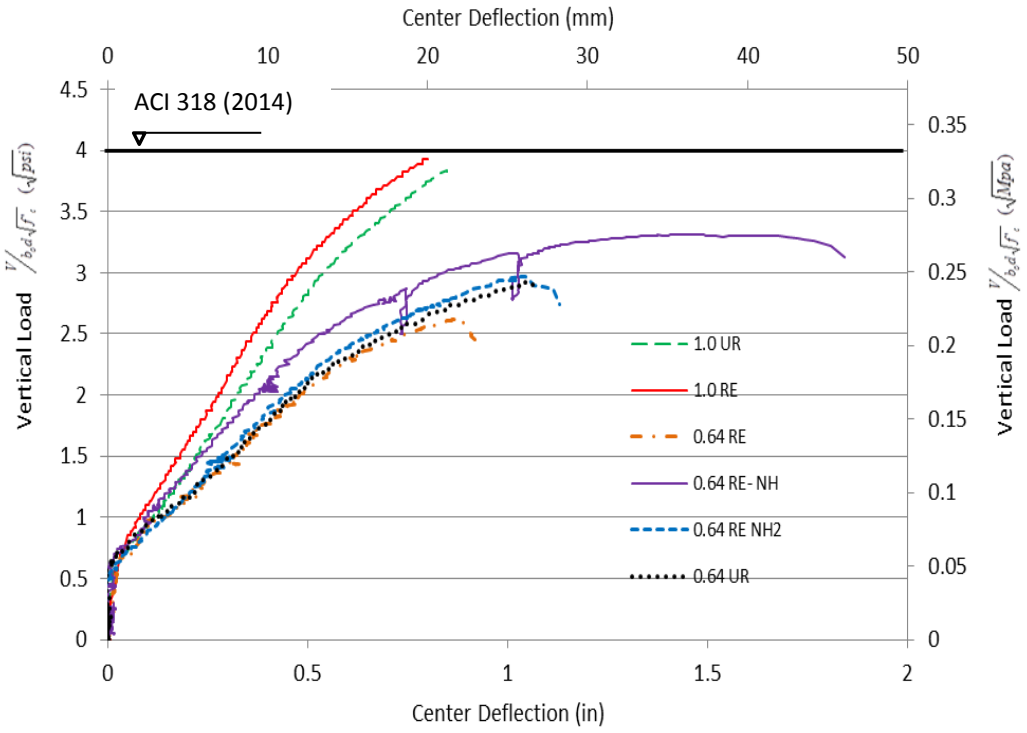

Figure 3-10 Load deflection behavior before punching failure

Table 3-1 Specimen properties and test results at punching failure

Specimens	*Concrete*	*Lateral*	*Lateral*	*Lateral*	P_E	*Deflection*	P_R *(kN)*	P_R/P_E
1.0UN	*33.38*	---	*0.53*	---	*307.5*	*21.6*	*256.2*	*83.3%*
0.64UN	*32.44*	---	*1.22*	---	*231.3*	*26.6*	*183.7*	*79.4%*
1.0RE	*37.79*	*55.2*	*0.38*	*72.6*	*329.2*	*15.5*	*246.0*	*74.7%*
0.64RE	*44.25*	*51.2*	*1.50*	*17.0*	*241.7*	*22.5*	*213.5*	*88.3%*
0.64RE-NH	*29.34*	*104.1*	*0.69*	*75.4*	*253.3*	*43.6*	*140.6*	*55.5%*
0.64RE-NH2	*36.94*	*60.7*	*1.4*	*21.7*	*250.9*	*26.6*	*121.4*	*48.4%*

Note: Slabs: 1.0, 0.64 – Reinforcement ratio; RE, UN – Restrained and unrestrained; NH – No hook for tensile bars

Additionally, reinforcement ratio also affected the slab expansion at punching failure because increased amount of reinforcement impeded crack growth, which resulted in reduced lateral expansion in slab. For instance, the total slab expansion of 1.0UN was 0.53 mm (0.021 in.),

whereas the lateral expansion in 0.64UN was 1.22 mm (0.048 in.), almost twice as much. Similar observations can be made for the two specimens 1.0RE and 0.64RE-NH2 experiencing in-plane restraints, where both the concrete strength and restraining force were comparable.

3.4.3 Effects of slab in-plane restraint on punching resistance

At $\rho = 1.0\%$, the punching strength of restrained specimen 1.0RE was 7.1% higher than the unrestrained specimen 1.0UN. At $\rho = 0.64\%$, the restrained specimens 0.64RE, 0.64RE-NH, and 0.64RE-NH2 had a punching strength 4.5%, 9.5% and 8.5% higher than the unrestrained specimen 0.64UN, respectively. Note that concrete strength may also affect the strength difference between the restrained and unrestrained specimens. However, the in-plane restraint is believed to be a dominating factor; even though the concrete strength of specimen 0.64RE-NH was about 10% lower than that of specimen 0.64UN, 0.64RE-NH obtained greater strength. For specimens 1.0UN and 1.0RE with $\rho = 1.0\%$, failure occurred at a deflection of 21.6 mm (0.85 in.) and 15.5 mm (0.61 in.), respectively. For the specimens with $\rho = 0.64\%$, 0.64RE experienced 15% less deflection at punching failure than 0.64UN.

The behavior of specimen 0.64RE-NH was unusual. As seen in Figure 3-10, the slope of the load-deflection curve became nearly flat prior to punching failure, an obvious flexure-dominating response. The failure deflection of this specimen was 43.6 mm (1.72 in.), which was much higher than in any other test. Given that anchoring slab tensile reinforcement affected only post-punching behavior, the primary cause of this ductile behavior was compressive membrane action that can enhance aggregate interlocking at inclined shear cracks and thus increase the shear resistance of concrete. Figure 3-11 shows the slab lateral restraining force at one clevis versus lateral expansion at two perpendicular sides of specimen 0.64RE-NH. The average restraining force at punching failure in this specimen was 104.1 kN (23.4 kips), which was at

least 70% greater than any other specimen, as shown in Table 1. Even if specimen 0.64RE-NH specimen had the lowest concrete strength, the higher level of lateral restraints enabled it to build up greater in-plane compressive force, punching resistance, and ductility.

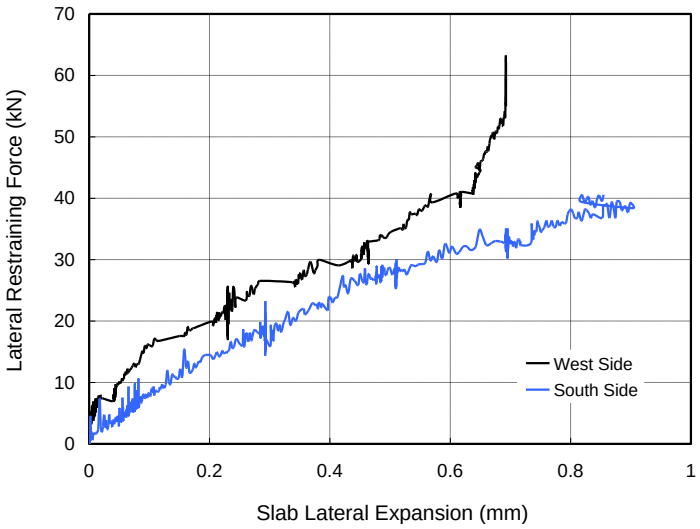

Figure 3-11 Lateral restraining force vs lateral displacement of specimen 0.64 RE-NH.

Figure 3-12 shows the strain profiles of slab tensile bars before punching failure for the four specimens having anchorage at slab edges. Most measured strains have exceeded the yield strain of 0.0025. However, strain distribution was significantly affected by reinforcement ratio. For specimens with $\rho = 0.64\%$, the strain was more evenly distributed across the slab, indicating yielding has spread over a large area of slab. In contrast, the yielding in specimens with $\rho = 1.0\%$ was concentrated in the direct vicinity of column. The in-plane restraint also played a role in the strain profile. Even though the strain in 1.0RE was only slightly higher than in 1.0UN, 0.64RE in general presented much larger strain than its counterpart 0.64UN.

Figure 3-13 shows strain development in slab tensile reinforcement at six load levels for three laterally restrained specimens with $\rho = 0.64\%$. The specimens without hooked bars, 0.64RE-NH and 0.64RE-NH2, generally showed lower strains than 0.64RE due to the greater in-

plane restraining forces. Compared with 0.64RE, the significantly increased in-plane restraint on 0.64RE-NH reduced more than 50% of the steel tensile strain. Thus, the opening of shear cracks in this specimen was delayed and a fairly ductile load-deformation behavior was achieved.

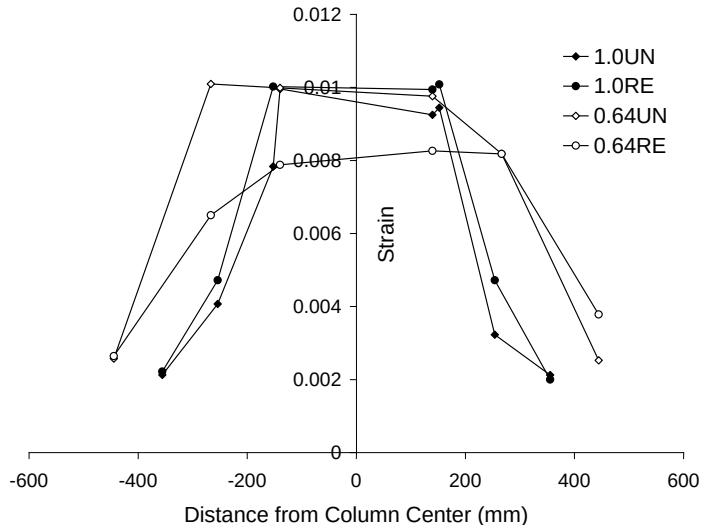

Figure 3-12 Strain profiles for slab tension mat prior to punching failure.

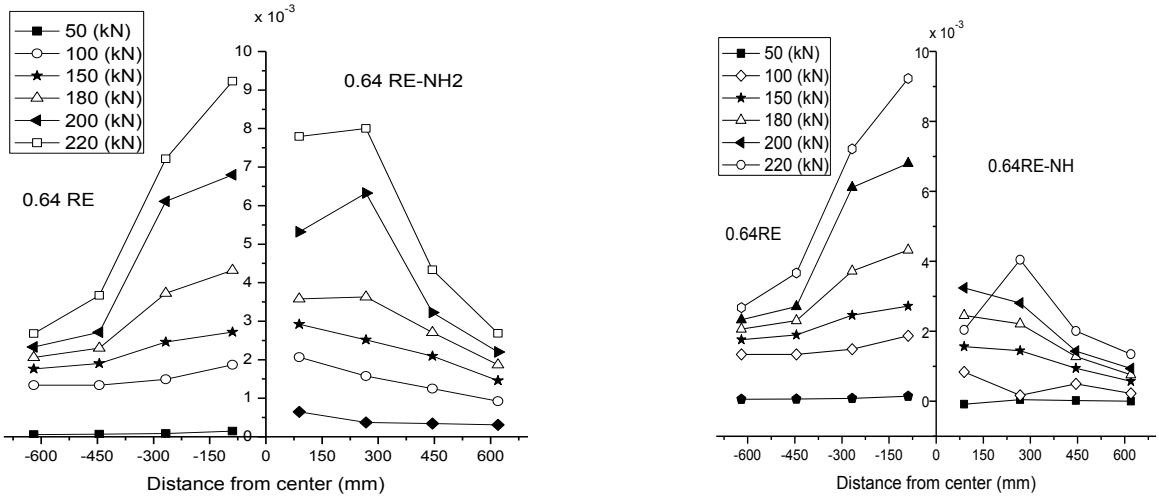

Figure 3-13 Comparison of strain in tensile reinforcement for three restrained specimens with ρ = 0.64%.

The tangential and radial strains of concrete in compression obtained from the average measurements at two sides of the column prior to punching failure are shown in Table 3-2 and Figure 3-14. As expected, the radial strain in specimens with ρ = 0.64% developed faster than those with ρ = 1.0%. All the radial strains dropped sharply when the punching load was approached. This was likely because the shear cracking became unstable and the neutral axis for bending shifted quickly toward the compressive face of slab. Broms (2005) used the tangential strain of slab concrete around the column as an indicator of punching failure. It was assumed that, if the tangential strain exceeds 0.001 for concrete having a strength of 25 MPa (3626 psi), macro cracks begin to form, causing the inclined shear crack to propagate to the column face. It was further assumed that this critical strain decreases with increasing concrete strength. The critical tangential compression strain, ε_{cpu}, is defined by Broms (2005) using Equation 3-1 As shown in Figure 3-14 and Table 3-2, all the measured tangential strains were less than 0.001 and generally much smaller than ε_{cpu}, implying that the test results were inconsistent with the failure criterion suggested by Broms (2005).

$$\varepsilon_{cpu} = 0.001 \left(\frac{x_0}{x}\right)^{\frac{1}{3}} . \left(\frac{10}{f_c'}\right)^{0.1} \qquad \text{Equation 3-1}$$

where x_0 = reference size = 150 mm (6 in.); x = height of compression zone at linear elastic stress conditions; f_c' = concrete cylinder compression strength

3.4.4 Post-punching capacity

The post-punching capacity is defined in this study as the maximum load carried by a slab-column connection after punching failure. Immediately following a punching failure, the load is carried by dowel action provided by the slab compressive reinforcement. As shown in

Figure 3-15 that displays the complete load versus deflection response, the load resisted by dowel action was very similar among the different specimens because there were identically two compressive bars crossing the slab-column interface. Under further loading, the discontinuous slab compressive bars were pulled out of column at large deformations, contributing little to tensile membrane action. The remaining capacity comes from the continuous top reinforcement as it is ripped out of the concrete. For specimen with unanchored reinforcement (no hooks) this strength is temporary and quickly diminishes with increased column deflection. The specimens 0.64RE-NH and 0.64RE-NH2 without hooked bars at slab edges obtained a post-punching capacity of 59% and 48% of the punching failure load, respectively. However, the residual capacity decreased drastically as the deflection increased and bars through the column were ripped out of concrete (Figure 3-15). It can therefore be expected that, in older flat-plate buildings, the quick loss of loading capacity after punching failure of slab-column connections may inhibit their ability to limit failure propagation in a flat-plate structure.

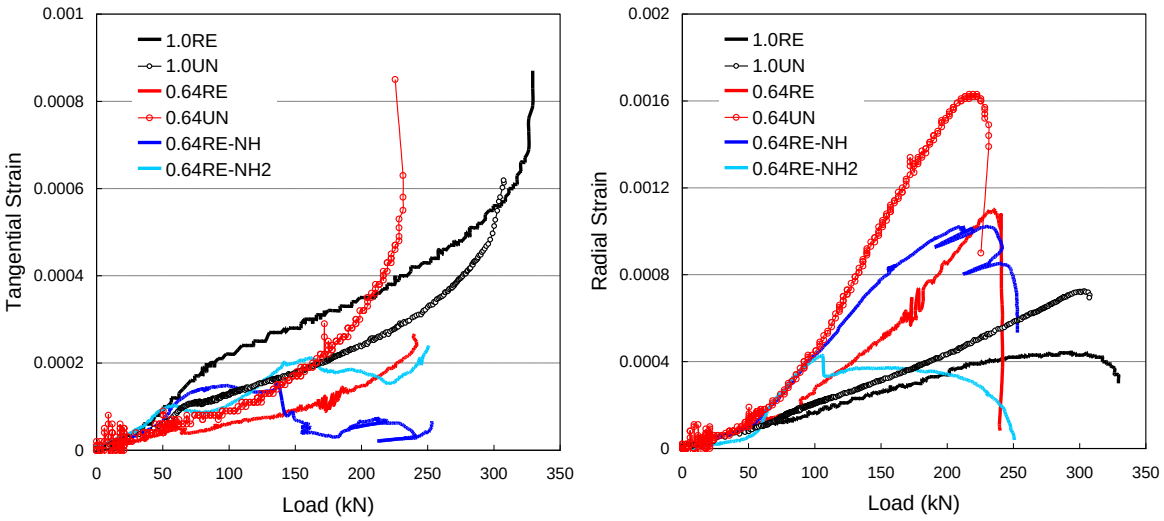

Figure 3-14 Average concrete tangential and radial strains before punching shear failure.

Table 3-2 Concrete strain near the column prior to punching failure

	Average radial strain	Average Tangential strain	ε_{cpu}
1.0UN	0.00070	0.00062	0.0019
0.64UN	0.00163	0.00090	0.0024
1.0RE	0.00044	0.00088	0.0019
0.64RE	0.00108	0.00024	0.0025
0.64RE-NH	0.00101	0.00013	0.0023
0.64RE-NH2	0.00042	0.00024	0.0024

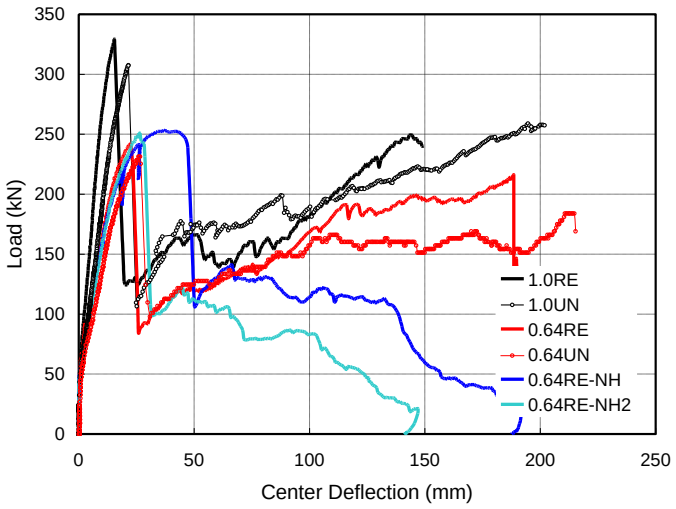

Figure 3-15 Complete load-center deflection response of specimens.

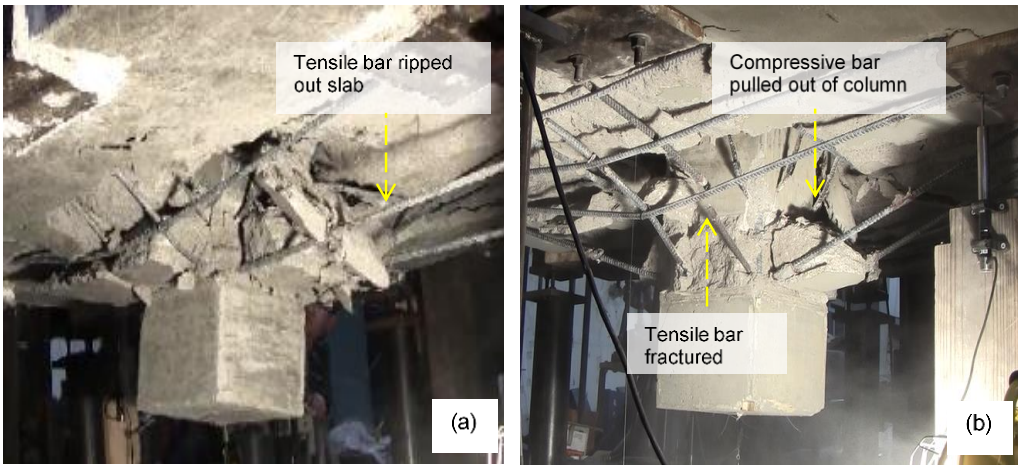

Figure 3-16 Post-punching failure modes: (a) specimen 0.64RE-NH2 without hooked bars, and (b) specimen0.64UN with hooked bars.

In contrast, specimens 1.0RE, 1.0UN, 0.64RE, and 0.64UN having anchored tensile reinforcement showed an average post-punching capacity of 80% of the punching failure load. Given that the discontinuous slab compressive bars were pulled out of column (Figure 3-16) and provided little help to the post-punching strength at large deformations, this strength was contributed mainly by tensile bars because the anchorage allowed them to carry load as a tensile membrane until fractured as shown in Figure 3-16. Thus, although the past studies have focused on developing sufficient post-punching loading capacity from continuous slab compressive bars (Mirzaei (2010), Elstner and Hognestad (1956)), the tests carried out in this study indicated that anchoring slab tensile reinforcement provides an alternative yet practical approach for mitigating failure propagation.

Figure 3-15 suggests that the post-punching load resistance of specimens with hooked bars was a function of slab tensile reinforcement ratio ρ. For specimens 1.0RE and 1.0UN, the post-punching strength was almost identical at 250 kN (56.2 kips); for 0.64RE and 0.64UN, the post-punching strength was about 200 kN (45.0 kips). As ρ increased, the angle of inclined crack relative slab was reduced. Consequently, the punching perimeter at slab tension surface were larger and thus engaged more reinforcing bars in developing tensile membrane action. It is noted that the cover depth, concrete breakout strength, and reinforcement strength and development length may also affect this capacity. Additionally, as shown in Figure 3-15, even though no slab lateral restraints were applied to specimens 1.0UN and 0.64UN, the post-punching capacity was similar to that of their unrestrained counterparts 1.0RE and 0.64RE. Such an observation provided experimental evidence that the self-equilibrium due to slab spatial continuity is enough to permit developing tensile membrane action in the slab near column.

3.5 Numerical Simulations

3.5.1 Nonlinear finite element model

To further investigate the effects of slab in-plane restraint, finite element (FE) simulations were performed on isolated and continuous slab-column substructures. The FE analyses adopted the macromodel proposed by Liu et al. (2015) for simulating the system level performance of flat plates. The model has been validated by more than twenty large-scale tests conducted on slab-column connection specimens subjected to different loading conditions. The FE analysis package Abaqus (2011) was used as analysis platform. As shown in Figure 3-17, the macro-model jointly used shell and connector elements to simulate the nonlinear behavior of slab. Consistent with the ACI 318-14 (2014) provisions for two-way shear, a punching perimeter was assumed at half slab effective depth away from slab-column joint. The slab outside the punching perimeter was simulated by thin shell elements defined with rebar layers. Concrete was modeled by Concrete Damage Plasticity (Lubliner et al.(1989), Lee and Fenves (1998)) and tension stiffening behavior was considered. The shell elements defined with the nonlinear material properties can capture the compressive membrane effects on slab through in-plane force and flexural capacity interaction. The slab-column joint area was simulated by rigid shell elements. The FE model of specimen is shown in Figure 3-18.

The short segment of slab between joint and punching perimeter was modeled by two connector beam elements at each side. The connectors transfer forces associated with six degrees of freedom from the slab to the column, in which primary bending moment and torsion were defined with nonlinear behaviors and shear with linear behaviors. The use of connector elements enabled simulating the separation of slab from column upon a punching failure. Equation (2)

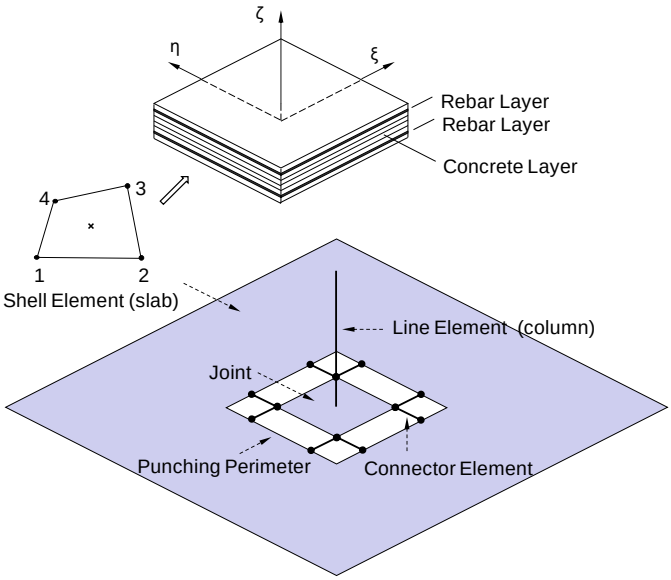

Figure 3-17 Macromodel for flat plates Liu et al. (2015)

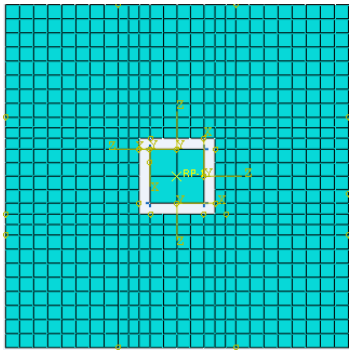

Figure 3-18 Finite element model of specimen

proposed by Muttoni (2008) for punching strength, which correlated the punching resistance of a slab-column connection with slab local rotation angle, was used to define the failure criterion of the connector elements. Since Equation (2) was developed for the total resistance of an interior slab-column connection under concentric gravity loading and two connector elements were used at each side of a slab-column connection in the macro-model, the shear capacity of a connector was defined as 1/8 of V_u in Equation 3-2. More details of the macro-model can be found elsewhere (Liu et al. (2015))

$$\frac{V_u}{b_0 d\sqrt{f_c'}} = \frac{3/4}{1+15\frac{\psi_u d}{d_{g0}+d_g}}$$ (in SI units: N, mm) Equation 3-2

where V_u is connection punching strength, ψ_u is slab rotation relative to column at punching failure, d_g is the maximum size of aggregate, f_c' is concrete cylinder compressive strength, and d_{g0} is a reference aggregate size equal to 16 mm. In the FE simulations, ψ_u was determined based on the rotation of slab immediately outside the assumed punching perimeter.

3.5.2 FE simulations of experiments

The six tests carried out in this study were simulated using the macromodel described previously. The calculated load versus center deflection responses are shown in Figure 3-19 and compared with the experimental results. Good agreement was achieved between the calculated and measured responses even though the relatively large deformation capacity of specimen 0.64RE-NH was underestimated. The mean value of the ratio of predicted to measured strength was 0.97 with a standard deviation of 0.031. To further indicate the effectiveness of the macromodel, the code formulations in ACI 318-14 (2014) and Eurocode 2 (2004), the empirical model proposed by Tian et al.(2008), and the analytical model proposed by Broms (2009) were applied to these specimens. Figure 3-20 compares the strengths predicted using different approaches. It is seen that, compared with Brom's formulation (2009), the macromodel is equally effective in predicting the punching strength of the specimens, whereas all other methods lead to overestimated the strength.

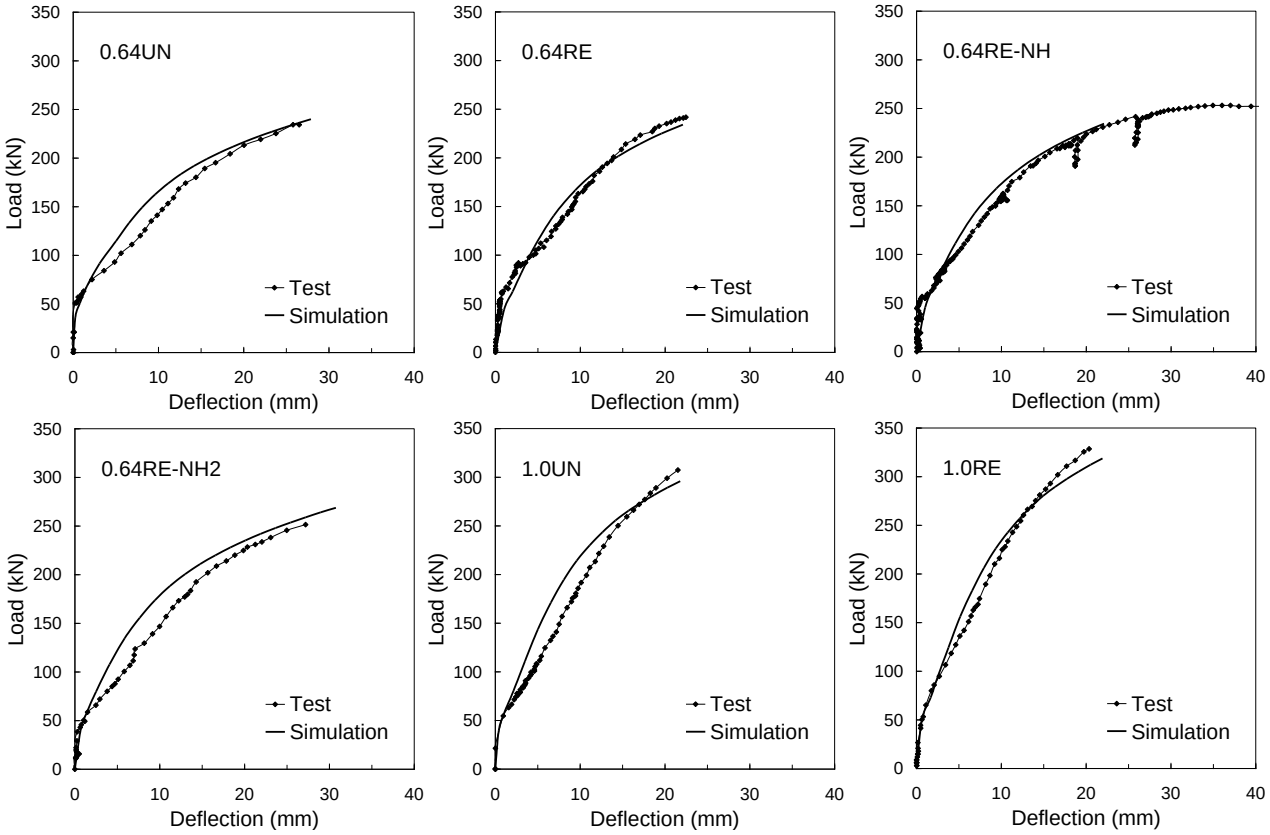

Figure 3-19 Load-deflection response predicted by macromodel versus test results in this study.

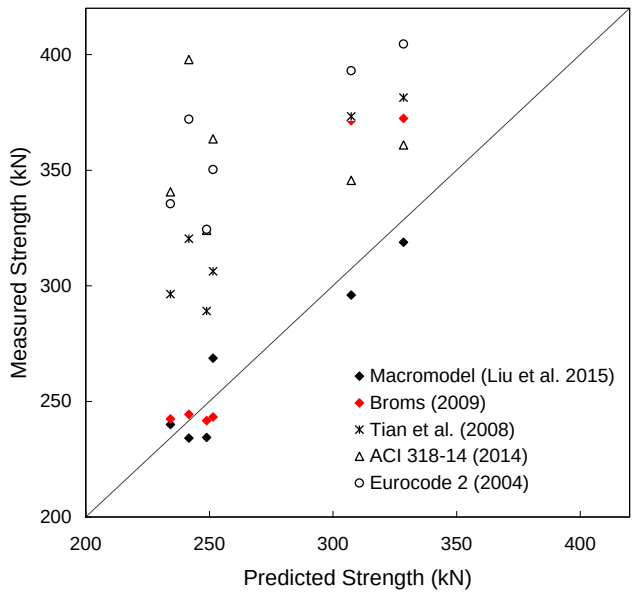

Figure 3-20 Predicted punching strengths using different approaches versus experimental results.

3.5.3 Simulation of other experiments using macromodel

To further examine the effectiveness of the macromodel, other tests of slab-column connections with in-plane restraints were simulated. Extremely few tests incorporating slab restraints exist and were conducted on small scales. Rankin and Long (1987) carried out experiments on "full panel" slab-column specimens. The vertical supports of slabs still simulated the inflection points; however, the slab extended beyond the supports and provided in-plane restraint to the inner portion of slab. The key specimen properties and the results from tests and simulations are given in Table 3-3, where f_{cu} is cube concrete strength, f_y is steel yield strength, c is size of square column, P_E is the measured punching load, and P_P is the simulated punching load. In the simulations, f_{cu} is concerted into cylinder concrete strength f_c' by assuming $f_c' = 0.8 f_{cu}$. Table 3-3 indicates that the macromodel well captured the failure loads in the tests by Rankin and Long (1987). The average ratio of P_E to P_P is 1.10 with a standard deviation of 0.10. The underestimated loading capacity from the simulations may be caused by the size effect. The failure criterion adopted in the macromodel was developed by Muttoni (2008) based on the experiments of slabs with effective depths d greater than 98 mm. However, d was no more than 53.5 mm in the tests by Rankin and Long (1987).

3.5.4 Effects of in-plane stiffness of restraint

The theoretical formulations for one-way RC slabs (Park and Gamble (2000)) indicated that the effects of compressive membrane on slab flexural capacity is a function of both reinforcement ratio and in-plane stiffness of supports. A parametric study was performed to examine the effects of lateral stiffness on the punching resistance of slab-column connections with two levels of reinforcement ratios. FE analyses were conducted first on specimens

Table 3-3 Simulation of experiments conducted by Rankin and Long [23]

Specimen	f_{cu} (MPa)	f_y (MPa)	d (mm)	ρ (%)	c (mm)	P_E (kN)	P_P (kN)	P_E/P_P
R5-08	53.8	530	40.5	0.802	100	77.84	82.32	0.94
R5-11	38.9	530	40.5	1.107	100	87.89	75.65	1.16
R5-05	38.5	530	40.5	0.517	100	62.51	63.01	0.99
R5A-08	39.6	530	46.5	0.800	100	95.34	82.19	1.16
R5B-08	39.4	530	35.0	0.799	100	60.34	55.31	1.09
R5C-08	44.1	530	53.5	0.800	100	126.3	101.5	1.24

0.64RE-NH2 and 1.0RE subjected to five levels of in-plane stiffness of the supports. Figure 3-21 shows that the load-carrying capacity of a slab increased significantly with the increase in lateral restraint stiffness. When the lateral stiffness changed from 0 to 393.9 kN /mm (2250 kip/in), the punching strength increased 25% and 14.4% for 0.64RE-NH2 and 1.0RE, respectively. The analyses also indicated that the lateral restraining effects are more pronounced in slabs with lower reinforcement ratio. In addition to strength, the load redistribution during the disproportionate collapse in a structure is also affected by the stiffness properties of components. It is seen from Figure 3-21 that in-plane restraint can significantly increase the slab flexural stiffness by delaying concrete cracking, which is consistent with test observations shown in Figure 3-9.

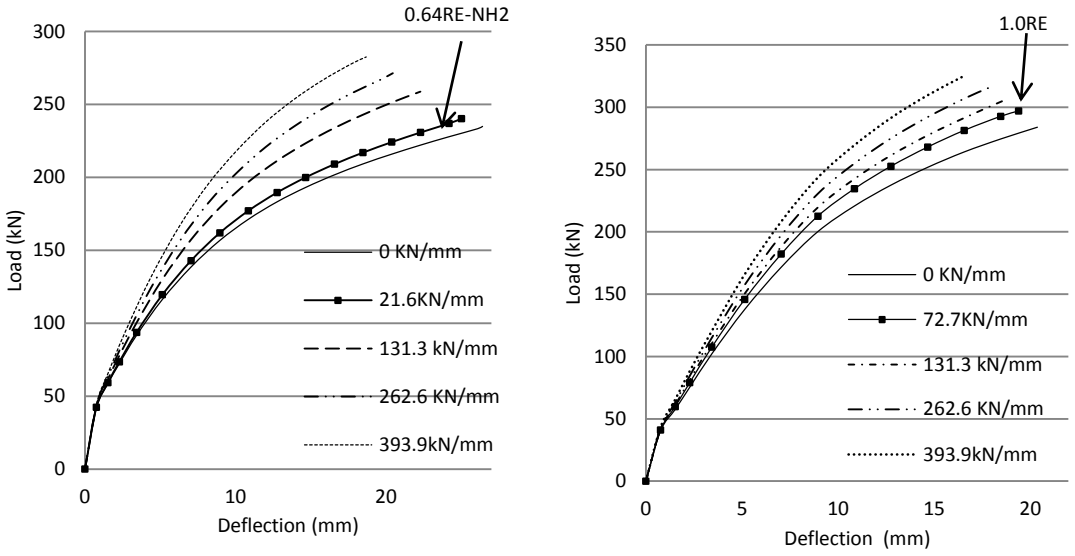

Figure 3-21 Effect of lateral restraint stiffness on load-deflection response for specimens with ρ = 0.64 and 1.0%.

The results of experiments conducted on the isolated slab-column connections without any in-plane restraints formed the basis of punching resistance defined in design codes for new constructions. However, to evaluate the existing flat plates under extreme loading events, the extra punching resistance provided by compressive membrane action can be considered. To identify the effects of compressive membrane action that an actual flat plate may encounter, numerical simulations were performed for four cases shown in Figure 3-22. Each case involved two levels of slab tensile reinforcement ratios (ρ = 0.64% and 1.0%) identical to those considered in the experiments of this study. The structures of the four cases were assumed with identical properties to those in specimens 0.64RE-NH2 and 1.0RE, including the layout of slab tensile and compressive reinforcement, material properties, column size, and slab thickness. The primary difference among the four cases was supporting condition.

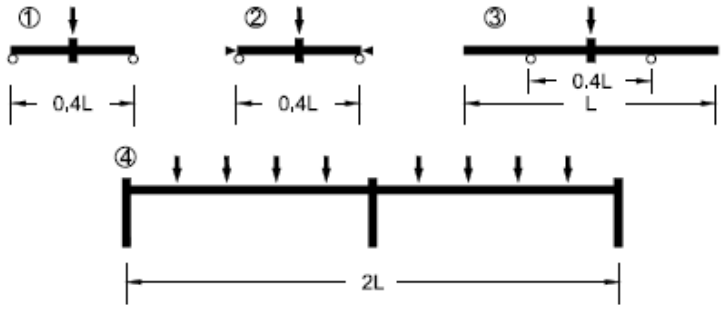

Figure 3-22 Four cases of flat-plate subassemblies subjected to gravity loading

Case 1, serving as a reference, considered isolated slab-column connections with the same dimension and support location as those of the test specimens in this study but without any lateral restraint. Case 2 duplicated Case 1 except that the slab edges were fully restrained laterally from slab expansion at the supports. Case 3, similar to the tests by Rankin and Long (1987), considered "full panel" slab-column connections with simple supports at the same locations as in Cases 1 and 2. Case 4 included four continuous slab panels simulating actual flat-plate structures. The slab span length and column height represented the prototype building described previously after scaling. In the analyses, concentrated load was applied at the center column for Cases 1 to 3, whereas uniformly distributed load was applied in Case 4.

Figure 3-23 shows the total shear transferred from slab to the center column as a function of slab rotation outside the assumed punching perimeter. For Case 3, the "full panel" slab-column connections had a loading capacity 9.1% and 4.7% greater than those in Case 1 for ρ = 0.64% and 1.0%, respectively. However, the multi-panel flat-plate structure in Case 4 demonstrated 58.4% strength increase for ρ = 0.64% and 34.5% for ρ = 1.0%. The simulated load-deformation responses for Specimens 0.64RE-NH2 and 1.0RE are also shown in Figure 3-23. It appears that "full panel" testing would result in similar restraining effects to that obtained in the experiments of this study; however neither case could build up sufficient slab in-plane

restraints that may actually exist in a flat plate. On the other hand, the punching resistance in Case 2 can be much greater than in Case 4, indicating that the tests of fully restrained slab-column connections lead to overestimated punching capacity of interior slab-column connections. It is also noted that, since compressive membrane action is more effective for slabs with lower reinforcement ratio, the failure load for the multi-panel structure (Case 4) with ρ = 0.64% was almost identical to that ρ = 1.0%.

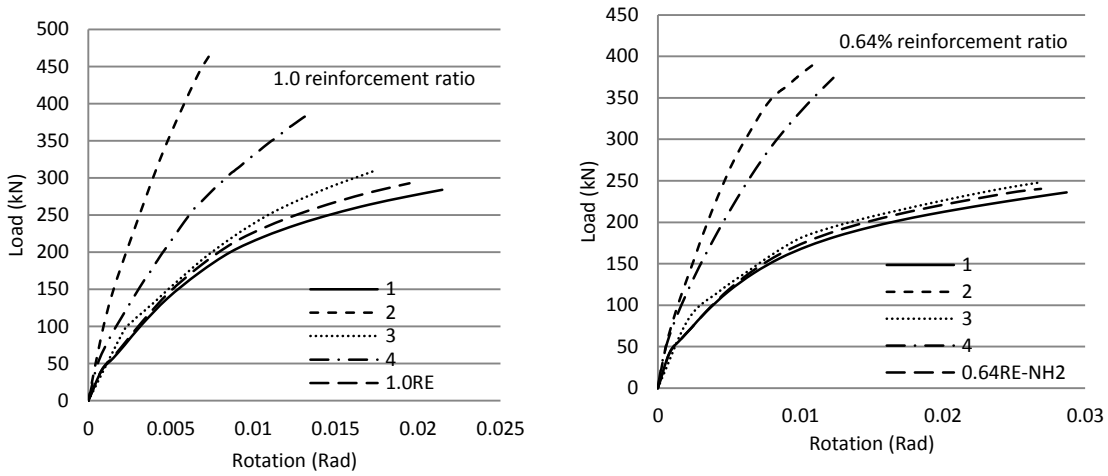

Figure 3-23 Shear force versus slab rotation response for four cases.

3.5.5 Effects of compressive membrane force on disproportionate collapse

The effects of compressive membrane action on disproportionate collapse resistance of flat plates were examined. For this purpose, numerical simulations were performed on a multi-panel substructure (Figure 3-24) scaled from the prototype building using the same factor as that used in the experiments in this study. The substructure had a 4.45 m (14.6 ft.) span in each direction. The material properties, reinforcement layout, slab thickness, and column cross section were the same as in the test specimen 1.0RE. The tension and compression reinforcement ratios were 1%

and 0.55%, respectively. No structural integrity reinforcement was assumed at slab-column connections.

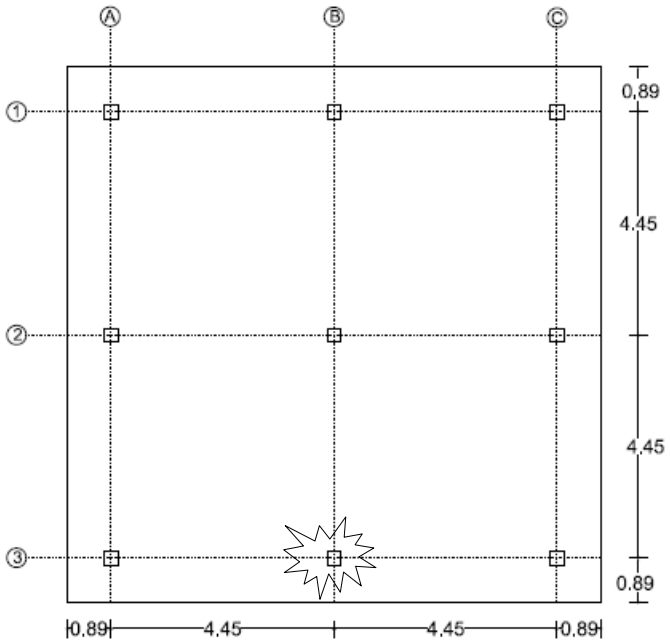

Figure 3-24 Layout of multi-panel flat-plate substructure (m).

Macro-model was developed for this substructure to examine its response after instantaneously removing column B3. The columns were fixed at their bottom ends and the slab edges were free to displace. Two connector elements were used at each side of a column. Based on the failure criterion described previously, each connector will fail in punching at a shear force of 46.25 kN if the compression membrane effect is taken into account, and fail at 35.5 kN if this effect is neglected. These values correspond to 1/8 of the loading capacity of slab-column connection considered for Cases 1 and 4 shown in Figure 3-23. The removal of column B3 will cause both increased shear and unbalanced moment transferred between slab and column at the neighboring slab-column connections. Thus, the eight connectors at a connection will not

respond evenly. Once a critical connector reaches its capacity, punching shear failure may quickly propagate to other connectors, leading to punching failure of the whole connection. The analyses started from assuming a uniformly distributed gravity load of w_d =3.36 kN/m^2 (70.2 psf). This load level was consistent with the DoD guideline (2009) and corresponded to dead load plus 50% live load when assuming an office occupancy in the prototype building. To simulate the effects of suddenly removing a column, a static analysis of the intact structure under gravity load was first conducted to determine the forces existing in the supporting column to be removed. A dynamic collapse analysis was then carried out by applying the opposite of these forces instantaneously at column B3 with a releasing time of 0.1 second.

Figure 3-26 shows slab vertical displacement profile at the peak dynamic response when a gravity load of w_d = 3.36 kN/m^2 (70.2 psf) was assumed. The maximum vertical displacement of slab at the lost column was 132 mm (5.2 in.) at time t = 0.35 sec. Based on the dynamic demands on local forces and nonlinear deformations, the connections at A3 and C3 were identified as the most vulnerable locations to punching failure. At the peak response, the shear force in the critical connectors at A3 and C3 reached 28.3 kN (6.36 kips), but didn't exceed the punching failure threshold of 35.5 kN (7.98 kips) even if the strength enhancement from compressive membrane action was neglected. Fig. 18 shows the time-history of shear force resisted by the critical connector elements. The static gravity load was then increased in the analyses to w_d = 3.83 kN/m^2 (80 psf), corresponding to dead load plus full live load. At this load level, if the punching capacity of the connectors was defined without considering any slab restraining effect, the dynamic demand at the critical connectors following the sudden removal of column B3 exceeded the punching strength of 35.5 kN (7.98 kips) and a disproportionate collapse occurred. However, if the punching strength of the connectors were defined as 46.25 kN (10.4 kips) to take into

account the compressive membrane effects, the connections would not fail in punching and thus disproportionate collapse would not happen. It was found that, only if the gravity load was increased to as much as 4.55 kN/m^2 (95 psf), the dynamic loading would fail the connectors and initiate a propagation of punching failure over the entire floor. Therefore, the numerical simulation of the multi-panel flat-plate substructure indicated that compressive membrane action can increase gravity load-carrying capacity in the disproportionate collapse scenarios by about 20%, as shown in Figure 3-26.

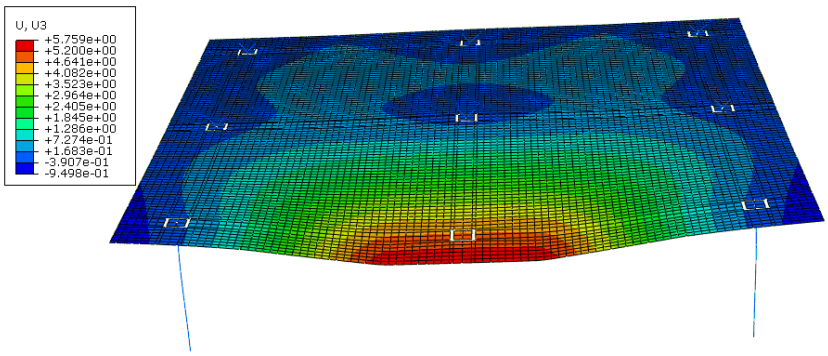

Figure 3-25 Peak response of structure considering residual post punching capacity.

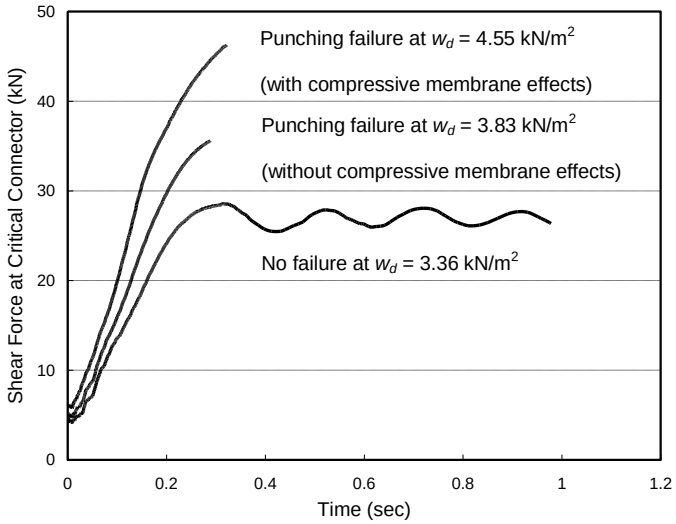

Figure 3-26 Shear force in the critical connector at column A3 under different gravity load intensities.

3.6 Conclusions

To investigate the effects of in-plane restraint on punching resistance and to identify the post-punching behavior of slab-column connections in older flat-plate buildings, a series of large-scale experiments was conducted in this study. Complementary to the experiments, numerical simulations using a macromodeling approach were carried out to further study the effects of compressive membrane action and its contribution to disproportionate collapse resistance. The following conclusions were reached from the experiments:

(1) With the lateral restraint achieved in the tests, compressive membrane actions could increase the punching capacity of slab-column connections by 9.5% and also increase their post-cracking flexural stiffness.

(2) After punching, the slab-column connections without structural integrity reinforcement could maintain only about 50% of the failure load. Moreover, this residual capacity decreased dramatically as the deformation increased. Therefore, in older flat-plate structures, the quick loss of load-carrying may inhibit their ability to resist disproportionate collapse.

(3) Anchoring the tensile reinforcement into the slab enabled the slab-column connections to obtain 80% of punching failure load as post-punching load-carrying capacity. Thus, effectively anchoring slab tensile reinforcement using hooks provides an alternative practical approach for mitigating failure propagation.

The following conclusions were reached from the numerical simulations:

(1) The macromodel employing thin shell elements and connector elements effectively simulated the behaviors of 12 unrestrained and restrained slab-column connections subjected to concentric gravity loading.

(2) The effects of compressive membrane action were a function of the level of in-plane restraints and slab reinforcement ratio. Fully restrained slab-column connections would lead to overestimated punching resistance. For a flat-plate system, the restraint associated with slab continuity could increase the static punching resistance by 34.5% and 58.4% for slabs with tensile reinforcement ratio of 1% and 0.64%, respectively.

(3) The strength enhancement contributed by compressive membrane action could significantly increase the resistance of flat-plate structures to disproportionate collapse. The analyses indicated that, for slabs with a reinforcement ratio of 1%, the compressive membrane action could increase the gravity loading capacity by 20% under dynamic loading caused by instantaneous removal of a supporting column.

CHAPTER 4 EXPERIMENTAL DYNAMIC RESPONSE OF FLAT-PLATE STRUCTURE SUBJECTED TO EXTERIOR COLUMN LOSS

4.1 Introduction

This chapter presents findings from a dynamic collapse experiment carried out on a single-story 2 by 2 bay reinforced concrete flat-plate structure representing a 9 column sub-section of a flat-plate building. A center exterior column was removed to initiate a potential collapse scenario. The load redistribution, dynamic amplification factor, and the potential of disproportionate collapse of flat-plate structures without integrity reinforcement were investigated.

4.2 Prototype Design

The initial prototype structure that the test specimen represents is described in details in section Chapter 3. The structure is an older flat-plate concrete reinforced structural design following the ACI 318-71 concrete design provisions (1971). This four floor building has a 3.05 m (10 ft) story height and four bays with an equal length of 6.10 m (20 ft). span in each direction. The slab thickness was designed as 190.5 mm (7.5 in.). The structure was designed for a 2.39 kN/m² (50 psf) live load and a superimposed 1.20 kN/m² (25 psf). dead load. Grade 413.69 N/mm² (60 ksi) reinforcing bars and a compressive strength of 27.58 N/mm² (4000 psi) concrete were assumed to be used for all the structural members. The maximum size of aggregate was assumed as 19.05 mm (0.75 in.).

The multi-panel specimen presented in this chapter representing a portion of the prototype was designed at 0.4 scale as shown in Figure 4-2. The slab thickness of scaled specimen was designed at 76mm (3in.), with Grade 413.69 N/mm² (60 ksi) reinforcing bar and concrete strength of 27.58 N/mm² (4000 psi), However, the actual cast test specimen was 89mm (3.5in)

thick, due to the difficulties to level the slab quickly in hot summer. Furthermore, the small diameter reinforcement has a yield strength of 655 N/mm² (95ksi). The concrete had a strength of 32.65 N/mm² (4735psi) concrete. Table 4-1and Table 4-2 show the original and adjusted design of prototype and scaled specimen properties, respectively. The adjusted prototype has 1.45 (373.2/255.8psf) times more flexural capacity than original prototype and 1.45 (157.9/108.4 kips) times punching shear capacity according to ACI equation. Therefore, the strength of the test specimen (with all columns intact according to ACI provisions would be 17.9 kN/m² (373 psf).

4.3 Flat Plate Model Structure Design

The story height of scaled specimen was 1.22 m (4 ft), with an 89 mm (3.5 in.) thick slab reinforced concrete slab that was supported on 152.4 mm (6 in.) square columns spaced at 2.438 m (8 ft). The column extended 152.4 mm (6 in.) above the slab. The slab had 6.35 mm (0.25 in.) cover for bottom compressive reinforcement and average 19 mm (0.75 in.) for top tensile reinforcement due to the fact that the slab was on average 12.7 mm (0.5 in.) thicker than designed. The specimen had 0.61 m (2 ft) cantilever span around three sides to simulate the exterior column strip of the peripheral columns to represent the continuity of the slab pasting the column line. The forth side had been designed as exterior side of the structure (Figure 4-1). The relationship between this test specimen and prototype structure is shown in Figure 4-2.

The specimen structure was constructed using a 6.35 mm (0.25 in.) diameter deformed reinforcing bar with yield stress 655 MPa (95 ksi), ultimate strength 737 MPa (107 ksi), and maximum elongation of 4.0% as shown in Figure 4-3. The concrete had a compressive strength of 32.7 MPa (4753 psi) and had maximum aggregate size of 10 mm (3/8 in).

Table 4-1 Original design of prototype and scaled specimen properties

	Scaled properties	Prototype properties
cover to bottom bars	7.6mm (0.3in.)	19.1mm (0.75in.)
chair height to top bars	58.4mm (2.3in.)	146mm (5.75in.)
slab depth	76.2mm (3in.)	190mm (7.5in.)
bar diameter	5.1mm (0.2in.)	12.7mm (0.5in.)
top bar spacing	50.8mm (2in.)	127mm (5in.)
bottom bar spacing	142mm (5.6in.)	355.6mm (14in.)
Yield strength	413.69 N/mm² (60 ksi.)	413.69 N/mm² (60 ksi.)
Concrete strength	27.58 N/mm² (4000 psi)	27.58 N/mm² (4000 psi)
d to top steel	61mm (2.4in.)	152mm (6in.)
d to bottom steel	61mm (2.4in.)	152mm (6in.)
reinforcement ratio negative	0.006545	0.006545
reinforcement ratio positive	0.002337	0.002337
M_u negative	11.6kN-m (102.3 kip-in)	180.5 kN-m (1598.2 kip-in)
M_u positive	4.29kN-m (38.0 kip-in)	67kN-m (593.3 kip-in)
column strip width	1219mm (48in.)	3048mm (120in.)
l_2	2438mm (96in.)	6096mm (240in.)
l_n	2286mm (90in.)	5715mm (225in.)
M_o negative	19.5kN-m (172.6 kip-in)	304kN-m (2697.4 kip-in)
M_o positive	21.7kN-m (192.3 kip-in)	339.4kN-m (3004.3 kip-in)
W_u negative	**0. 012 N/mm² (255.8 psf)**	**0. 012 N/mm² (255.8 psf)**
W_u positive	0.0136 N/mm² (284.9 psf)	0.0136 N/mm² (284.9 psf)
Punching shear capacity V_u		**482.3kN (108.4 kip)**

Table 4-2 Adjusted design of prototype and scaled specimen for exterior column removal

	Scaled properties	Prototype properties
cover to bottom bars	6.35mm (0.25in.)	15.9mm (0.625in.)
chair height to top bars	57.2mm (2.25in.)	143mm (5.625in.)
slab depth	89.0mm (3.5in.)	222.2mm (8.75in.)
bar diameter	6.35mm (0.25in.)	15.9mm (0.625in.)
top bar spacing	88.9mm (3.5in.)	222.3mm (8.75in.)
bottom bar spacing	152.4mm (6in.)	381mm (15in.)
Yield strength	413.69 N/mm² (95 ksi.)	413.69 N/mm² (95 ksi.)
Concrete strength	32.6N/mm² (4735 psi)	32.6 N/mm² (4735 psi)
d to top steel	63.5mm (2.5in.)	158mm (6.25in.)
d to bottom steel	76.2mm (3.0in.)	190.5mm (7.5in.)
reinforcement ratio negative	0.00561	0.00561
reinforcement ratio positive	0.002727	0.002727
M_u negative	16.8kN-m (149 kip-in)	263 kN-m (2332 kip-in)
M_u positive	12.2kN-m (108.3 kip-in)	191kN-m (1692 kip-in)
column strip width	1219mm (48in.)	3048mm (120in.)
l_2	2438mm (96in.)	6096mm (240in.)
l_n	2286mm (90in.)	5715mm (225in.)
M_o negative	28.4kN-m (251.9 kip-in)	444.7kN-m (3936.3 kip-in)
M_o positive	61.9kN-m (548.3 kip-in)	968kN-m (8568.5 kip-in)
W_u negative	**0. 018 N/mm² (373.2 psf)**	**0. 018 N/mm² (373.2 psf)**
W_u positive	0.039 N/mm² (812.4 psf)	0.039 N/mm² (812.4 psf)
Punching shear capacity V_u		**702.6kN (157.9 kip)**
W_u for punching		396.3
Controlling service load capacity	0. 018 N/mm² (373.2 psf)	
Dead load	6190N/ m² (129.3psf)	
Live load	5410N/ m² (113psf)	

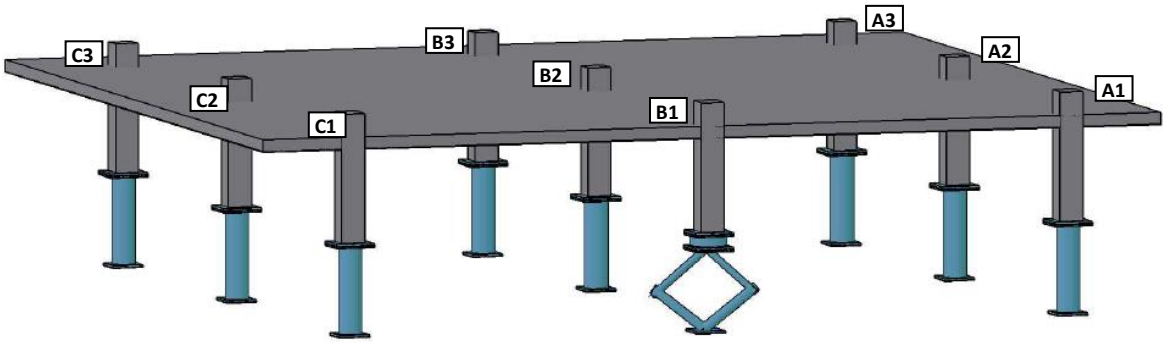

Figure 4-1 Schematic view of test model

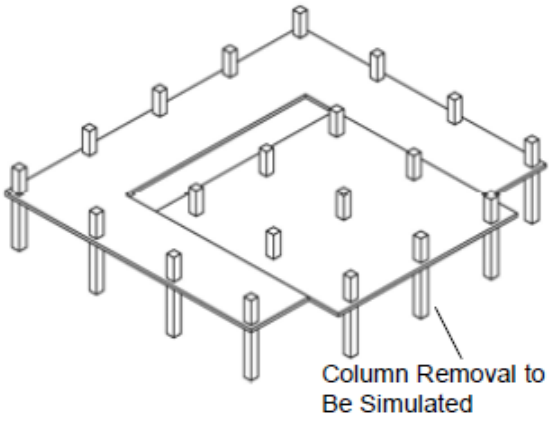

Figure 4-2 Relationship between test specimen and prototype structure

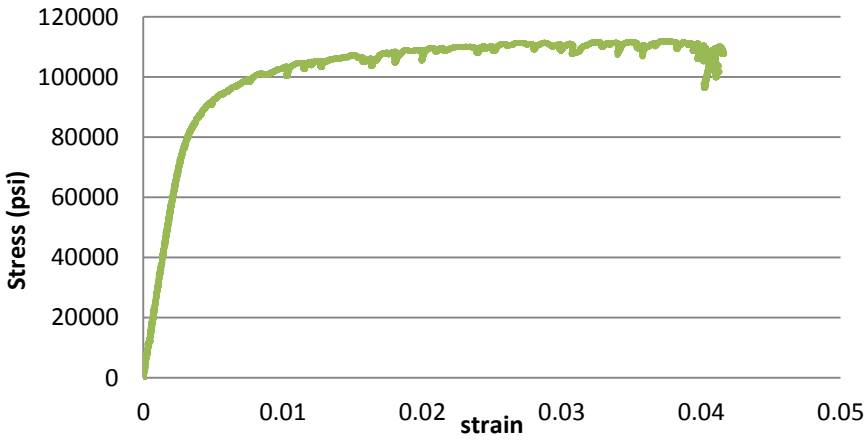

Figure 4-3 Stress-strain relationship of #2 bar

The columns of the slab were designed using a combination of steel columns and reinforced concrete columns. The 162 mm (6.38 in.) inner diameter steel tube columns with a wall thickness of 4.76 mm (0.187 in.) were fixed to strong floor and connected to concrete column using imbedded 9.5 mm (0.374 in.) diameter threaded rods as shown in Figure 4-4. The steel columns were sized so as to ensure a flexural stiffness similar to that of the concrete column. The height of the steel column was chosen to be at the location of low bending moment (midpoint of the column).

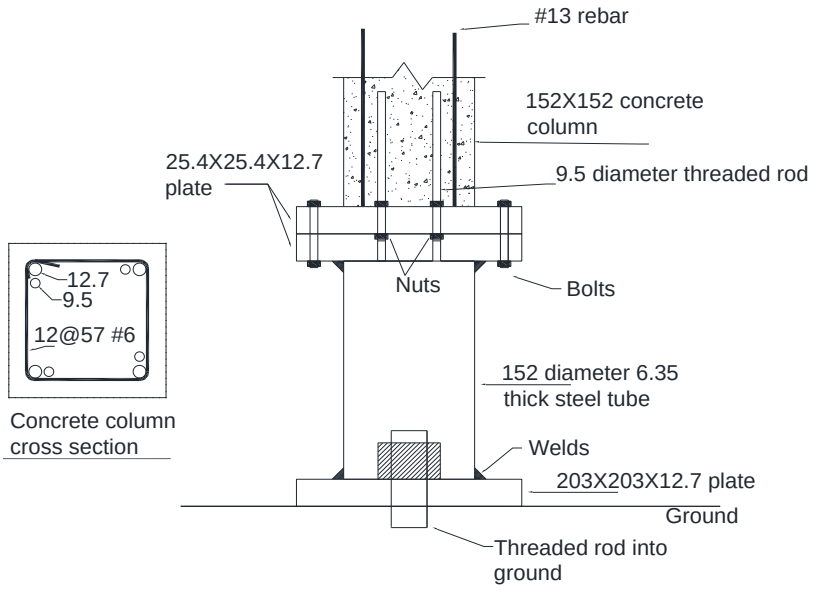

Figure 4-4 Configuration of columns (unit: mm)

Figure 4-5 shows the reinforcement layout, the right section shows the top tension reinforcement layout and the left portion illustrates the bottom compression layout. The discontinued bottom bars were anchored 30.5 mm (1.2 in) into the column to reflect the discontinuity at column line permitted by ACI318-71(1971).

As shown in Figure 4-6, the instrumentation consisted of horizontal and vertical LVDT's, concrete and steel strain gages. The measurements from LD1 and LD8 were used to determine the relative horizontal movement between columns A1 and C1. To measure the rotation of slab near the interior column B2, three vertical LVDT's (VD2, 3, 4) were situated and LD5, 6 were designed to capture the horizontal movement on column B2. LD3 and VD1 measured the lateral expansion and vertical deflection at contra-flexural point ($0.2l_n$) respectively, in order to compare that in isolated slab-column connections in this research. In addition, concrete

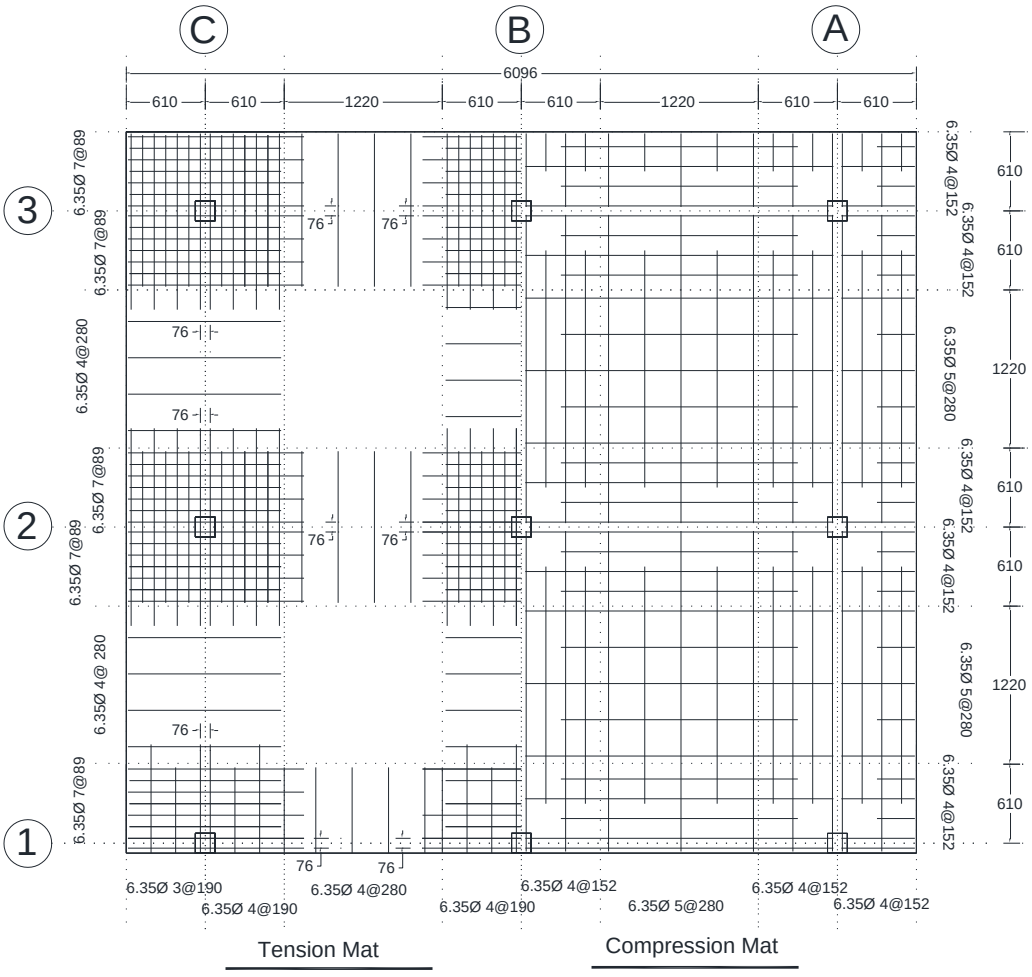

Figure 4-5 Reinforcement layout (unit: mm)

transducers were applied on both sides of slab near column A1 and B2, as indicated by the solid rectangular dots as shown in Figure 4-6. The hollow rectangular dots illustrate concrete transducers applied only on the top (tension) side of the slab. Strain gages were applied on A1, A2 and B2 steel columns to measure axial load and moment in the columns as shown in Figure 4-7.

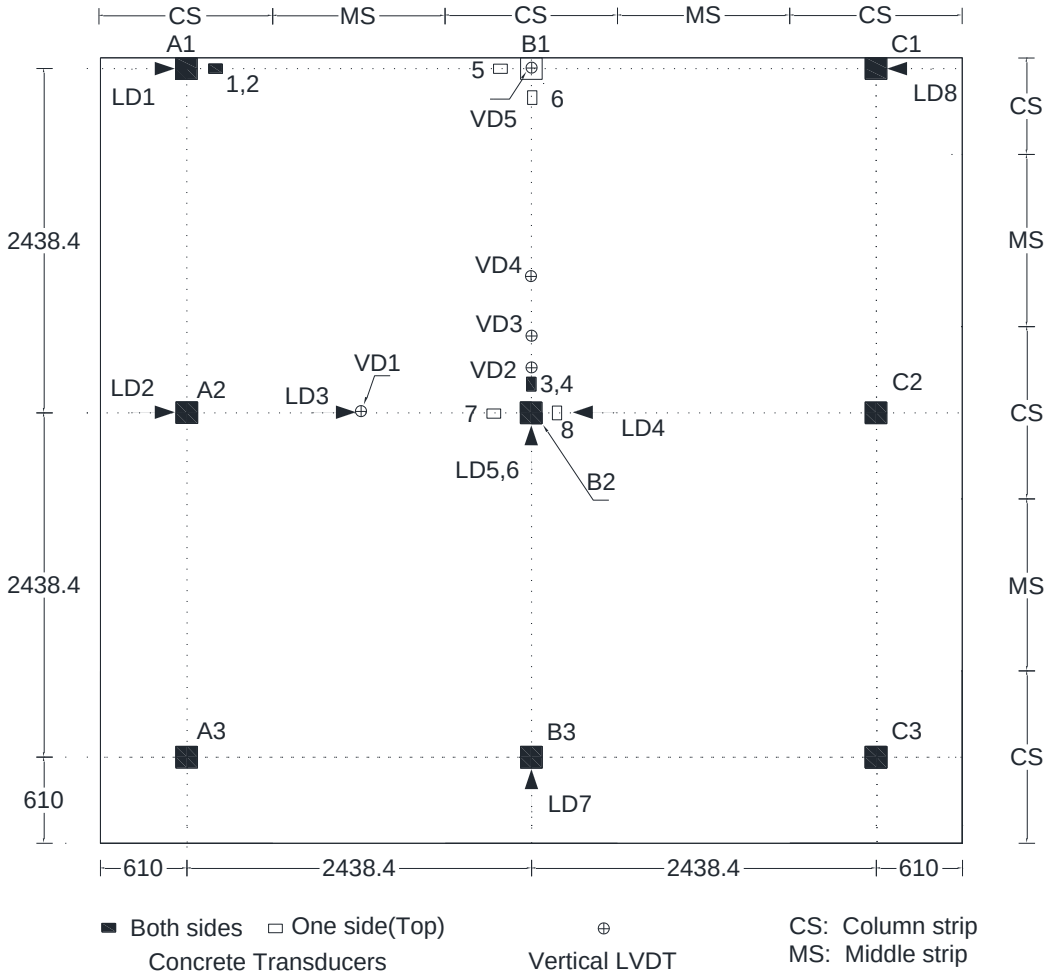

Figure 4-6 Instrumentation layout (unit: mm)

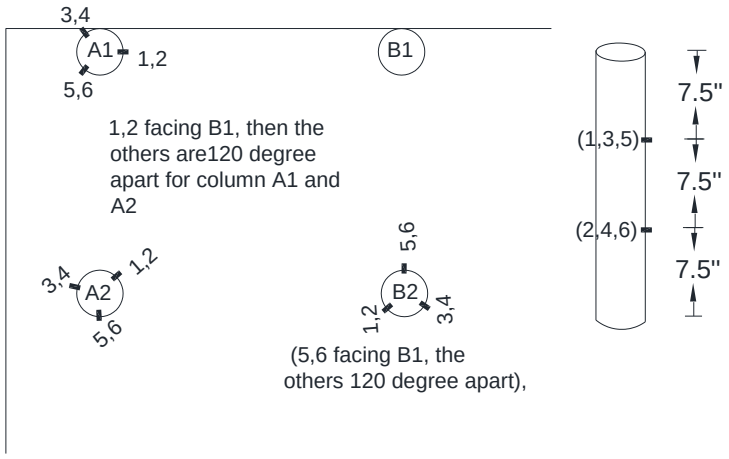

Figure 4-7 Layout of strain gages on columns

4.4 Test Procedures

The load on the outer portion of the slab was increased as shown in Figure 4-8 to simulate the proper shear condition on the columns, because the tributary shear area for columns should be $0.5l_n$, but only $0.2l_n$ was cast in the specimen. 890mm by 890mm fabric bags filled with adobe soil were used to apply a uniform superimposed dead and live load. Concrete slabs hung on the sides to apply the load on the outer portion of slab as shown in Figure 4-9.

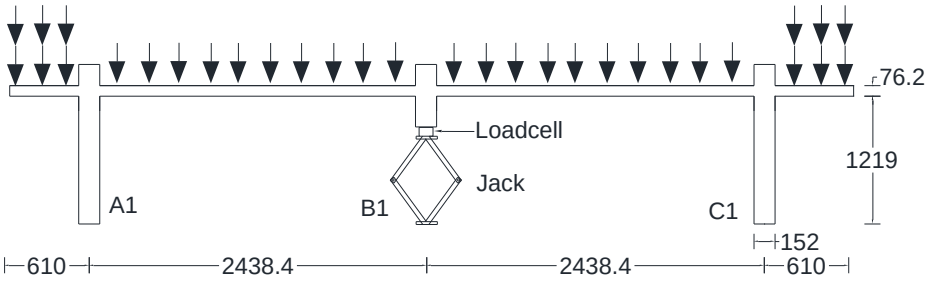

Figure 4-8 Elevation of test structure subjected to the column loss (unit: mm)

The slab was cast with a steel temporary support under the removed column B1. Prior to applying the additional dead load, the temporary support was replaced by the load releasing system. Measurements were taken to ensure that the slab was returned to its original position after replacement of column B1. The releasing system consisted of a freely collapsing scissor jack and a steel tension cable with a pneumatic quick release to enable the quick loss of column B1. A load cell was placed on the top of the jack to measure the amount of released force and the load releasing rate as shown in Figure 4-8. The data acquisition system was zeroed out after all the dead weight had been applied.

Figure 4-9 Specimen ready to test in the second drop

4.5 Test Results

4.5.1 Overall response

The loaded multi-panel specimen was tested by simulating the removal of exterior column B1 by means of the collapsing jack described earlier. The applied dead weight was 4.84 kN/m² (100 psf) in the center area and 11.37 kN/m² (237.5 psf) in the perimeter with the specimen self-weight. This load was originally thought sufficient to trigger the punching shear failure on critical columns and may initiate the disproportionate collapse in the structure. However, the specimen moved only a total of 28.9 mm (1.137 in.) at the location of the lost column (Figure 4-10) and the specimen showed little damage overall with primarily flexural cracking in the slab as shown in Figure 4-11. Due to the lack of extensive damage in the specimen under this load level, the specimen was raised to its original position at column B1, additional load added for a total of 7.18 kN/m² (150 psf) and the test performed again. Given that the load has been increased and there was damage in the initial drop, the second drop would result in a more severe response of the specimen.

However, the specimen experienced only 88.6 mm (3.49 in.) of peak deflection at the location of the lost column and some additional flexural cracking as shown in Figure 4-11(b). Again the specimen was raised to its original position and additional load added to bring the total load to 9.86 kN/m² (206 psf) on the front panel (column A1, A2, C1, C2) and 7.66 kN/m² (160 psf) on the back panel (column A2, A3, C2 and C3). During this third drop the specimen experienced disproportionate punching failure at all slab-column connections and collapsed. Therefore, the load level to fail the slab in this multi-panel column removal test was between that in drop 2 and drop 3. Table 4-4 shows the relationship between the load level applied and the design capacity for an intact structure. Based on the damage in the second drop it is estimated

that about 55% to 60% of load would fail the slab in the exterior removal case. Details of the load and reactions for each drop are given in Table 4-5. The following describes in detail the measured responses of the specimen for all three drops.

4.5.2 Load-deflection response at removed column

Load and deflection measurements were recorded at the location of the removed column. Figure 4-12 shows the time history of the deflection and axial force in the removed column B1. Negative displacements signify downward movements. The column was removed at time $t = 0$ second. For the first drop the measured axial force in column B1 before removal was 11.8 kN (2.65 kips). The load release time was approximately 0.012 sec. Unfortunately an error in the data acquisition setup caused the load versus time was to be elongated in the time domain therefore the actual load release time is unknown but shall be less than 0.012 sec. The peak deflection measured at column B1 was 28.9 mm (1.137 in.). A vibration period followed with a natural period of 0.2 sec and quickly diminished with damping ratio of 0.0575. The deflection of the slab at stead state was 28.3 mm (1.114 in.).

For the second drop, due to the pre-existing damage from the first drop, energy absorption due to cracking was not available until the deflection of second drop exceeded the maximum deflection of the first drop. This agrees with the data shown in Figure 4-12(a) that the slab experienced a free fall until the deflection reached 24 mm (0.94 in.), a value close to the maximum deflection 28.3 mm (1.14 in.) of the first drop. Then the pre-existing cracks widened and extended as the slab began to respond. The peak deflection in the second drop was 88.6 mm (3.49 in.) at 0.282 s, then the displacement decreased to 79.3 mm (3.12 in.) and a little vibration died out pretty soon after with a permanent value of 83 mm (3.27 in.). The specimen after the second drop is shown in Figure 4-13.

Table 4-3 Load calculations with initial design and adjusted design (units: kN/m² (psf))

	With initial design depth		With adjusted slab depth	
Load calculations	Prototype	scaled	Prototype	scaled
Slab depth	190.5mm (7.5in.)	76.2mm (3in.)	222.2mm (8.75in.)	89.0mm (3.5in.)
Self-weigth	**4.49 (93.75)**	**1.79 (37.5)**	**5.2 (109.3)**	**2.09 (43.75)**
Super Dead	0.95 (20)	0.95 (20)	0.95 (20)	0.95 (20)
Live load	2.4 (50)	2.4 (50)	2.4 (50)	2.4 (50)
Load for similitude		2.7(56.25)		3.14(65.62)

Table 4-4 Ratio of applied load to design capacity load (unit: kN/m² (psf))

		With initial design depth		With adjusted slab depth		applied	actual full load for test	design capacity load	Ratio
		Prototype	scaled	Prototype	scaled				
Drop1	1.0 D +0.5 L	6.64 (138.75)	6.64 (138.75)	7.39 (154.4)	7.39 (154.4)	4.83 (101)	6.94 (145)	17.86 (373.2)	0.39
Drop 2	1.2 D + 1 L	8.92 (186.5)	8.92 (186.5)	9.82 (205.3)	9.82 (205.3)	7.13 (149)	9.23 (192.8)	17.86 (373.2)	0.52
Drop3	1.4 D + 1.7 L	11.6 (244.3)	11.6 (244.3)	12.7 (266.1)	12.7 (266.1)	9.9 (206.8)	12.0 (250.5)	17.86 (373.2)	0.67
Interior column removal	1.2 D + 0.5 L	7.73 (161.5)	7.73 (161.5)	8.618 (180)	8.618 (180)	5.50 (115)	7.30 (152.5)	14.3 (299)	0.51

Table 4-5 load combinations and reactions on removed column B1

	Applied load (kN/m2)		Deflection (mm)	Reaction	
Tests	Center	Peripheral strip	Peak deflection	Residual deflection	Reaction Force on removed column B1(kN)
1	4.84	11.46	28.9	28.2	11.8
2	7.18	16.13	95.4	90	20.0
3	9.86 (front) 7.66 (back)	21.51	-	-	29.2

Figure 4-10 Specimen after first drop

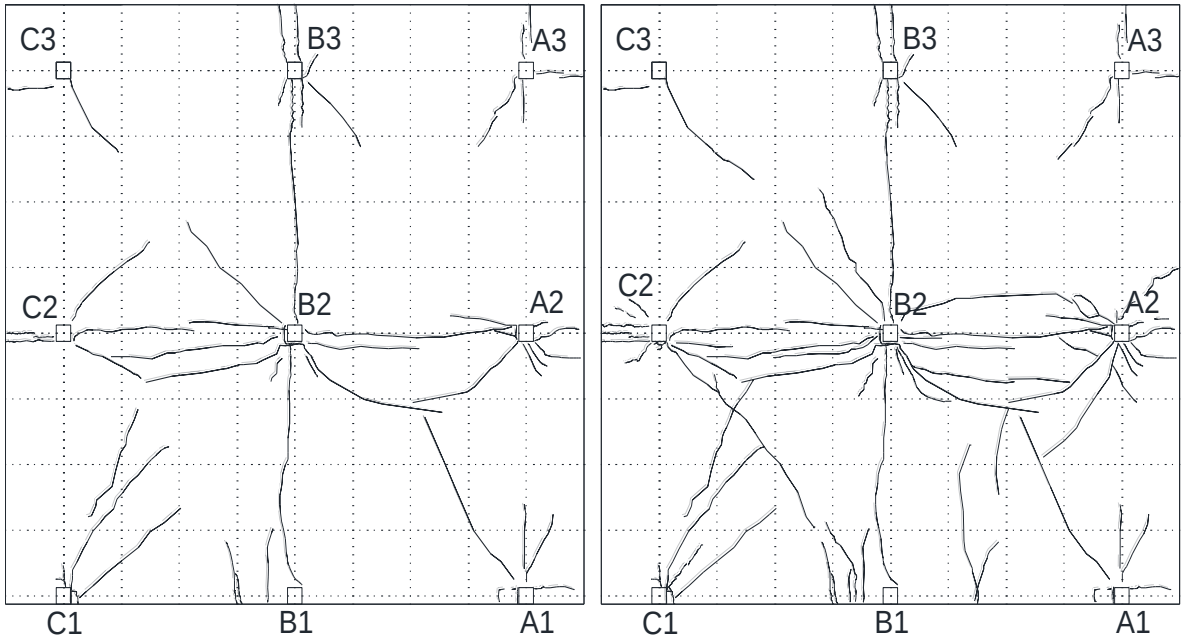

(a) First drop

(b) Second drop

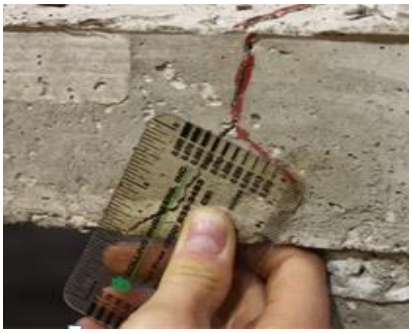

(c) Crack through cross section around column A1 after the first drop

Figure 4-11 Crack pattern on the top side

For the third drop all the columns disproportionately experienced punching failure shown in Figure 4-14. The deflection vs. time plot in Figure 4-12(a) is limited to 150 mm (5.9in.) deflection in order to clearly show the vibrations of slab caused by the first and second drops. Due to the damage accumulated from the first two drops, the slab experienced a crack reopening phase until the deflection at column B1 reached 82 mm (3.22 in.), then the stiffness of the specimen changes as the slab incurs more damage. The B1 column hit the ground at a deflection of 532 mm (20.9 in.).

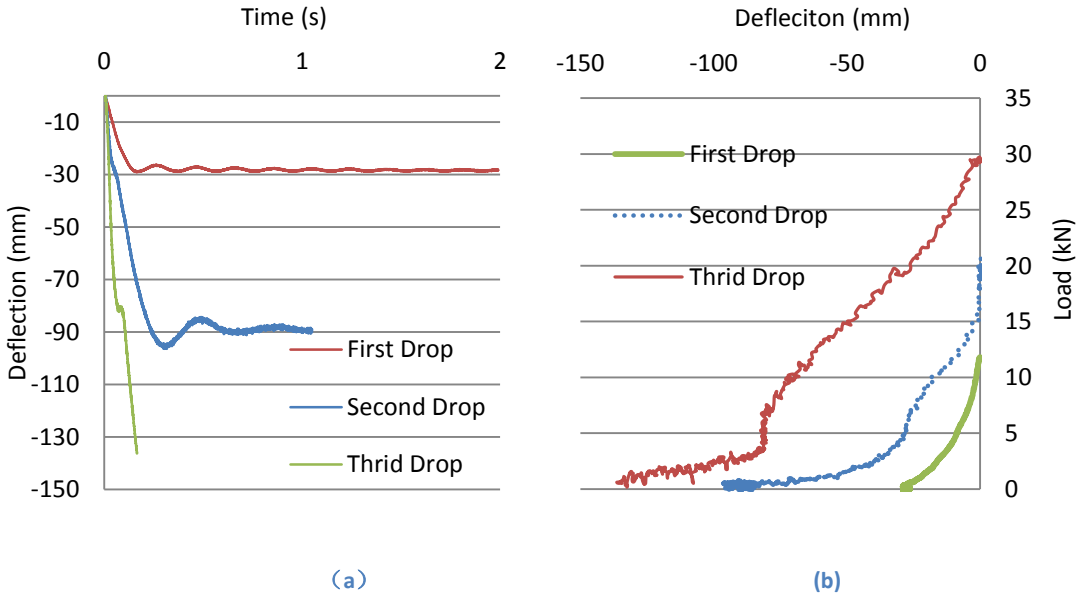

Figure 4-12 Deflection vs. load and deflection vs. time of removed column B1

Figure 4-13 Specimen after the second drop

4.5.3 Load redistribution and dynamic amplification factors

The load carried by column B1 was redistributed to the adjacent columns after removal of B1. The axial forces and bending moments in columns A1, A2 and B2 were determined by the measurements obtained from six strain gages placed in two rows on the columns (as illustrated in Figure 4-7). The axial load was calculated from the average of the six strain gage readings times an assumed Young's modulus of 200GPa (30,000ksi) and cross-sectional area of the tube section of 3.8 in^2.

The resulting load time history for the adjacent columns is given in Figure 4-15. The change in load at steady state after column B1 removal for the neighboring columns A1, A2 and B2 was 5.96 kN (1.34 kips), -3.12kN (-0.70 kips) and 9.47 kN (2.13 kips) corresponding to a load redistribution of 50%, -26.1% and 79.4%, respectively after the structure stabilized. Column A1 and B2 carried the majority of the redistributed load as they were the columns nearest to the removed column B1. The decrease in load at column A2 was due to the overall rotation of the slab.

Figure 4-14 Collapse of the specimen caused by the third drop

The moments calculated from gages on the column A1(Figure 4-7) is shown in Figure 4-16, the peak moments from the top and bottom rows of gages are 858 N·m (7.6 kip·in.) and 6485 N·m (57.4 kip·in.), therefore the shear force on column A1 was 6.64 kips (29.5kN).

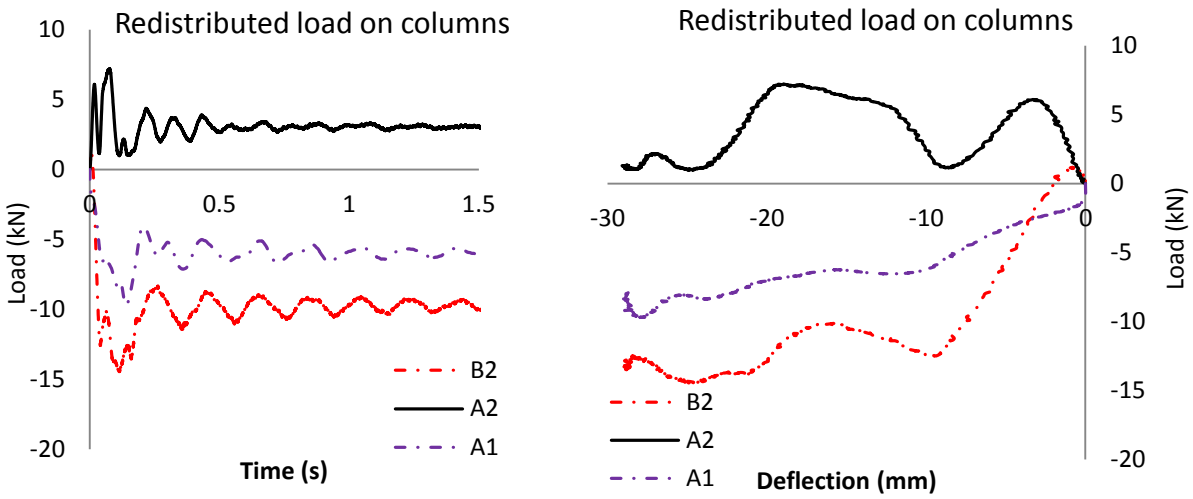

Figure 4-15 Redistributed load on columns

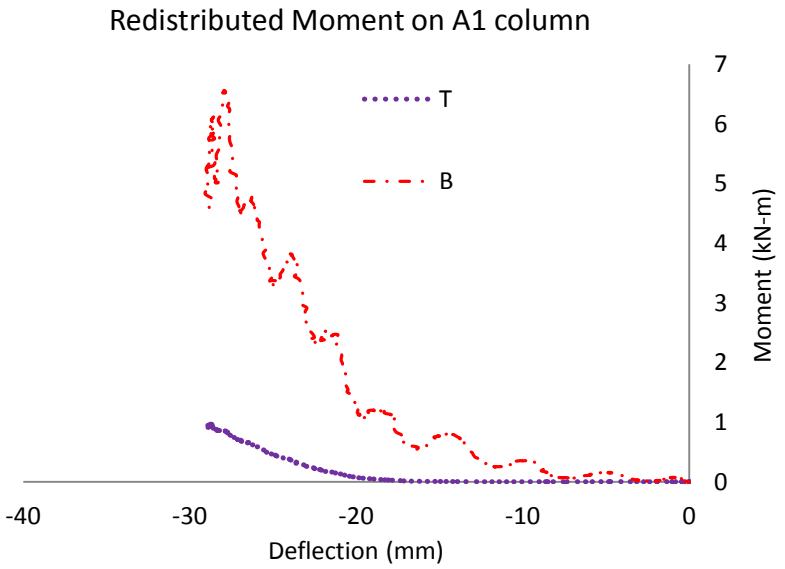

Figure 4-16 Bending moments on columns

A dynamic load amplification factor (DLAF) is defined as the ratio of peak dynamic load to the residual total load. However, the loads presented in Figure 4-15 represent only the change in load due to removal of column B1. In order to determine the load carried by each column prior to testing a FEM analysis was conducted to simulate the tests, which will be described later in Chapter 6 with details. The calculated pre-test static axial forces are presented in Table 4-6 The calculated axial fore in column B1 before its removal shows a close agreement with the load measured in this column as shown in Table 4-7. The peak measured dynamic loads redistributed to columns A1, A2 and B2 in first drop were 9.39 kN (2.11 kips), -6.85 kN (-1.54 kips) and 14.1 kN (3.16 kips) as shown in Figure 4-15. The static pre-test steady axial forces were 5.96 kN (1.34 kips), -3.12kN (-0.70 kips) and 9.47 kN (2.13 kips). If these loads are added to the load calculated prior to testing (given in Table 4-2), the ratio of the peak axial force to steady state axial force gives the DLAF values reported in Table 4-8. The maximum DLAFs among the drop tests is 1.17.

Table 4-6 Calculated column static axial force before B1 removal

	FE model (kN)			
	B1	B2	A1	A2
First drop	12.7	32.2	13.4	34.3
Second Drop	19.1	48.1	19.2	49.9

Table 4-7 Measured column axial force increase after B1 removal

	Measured reaction force (kN)			
Column	B1	B2	A1	A2
First drop	11.8	9.47	5.96	-3.12
Second Drop	20.0	11.6	7.25	-3.65

In the second drop the greater deflection of the slab and pre-existing damage from the first drop changed the amount of load redistributed to the adjacent columns. Figure 4-17 shows the load redistributed to the adjacent columns during the second drop. The change in steady state load after column B1 removal for columns A1, A2 and B2 was 7.25 kN (1.63 kips), -3.65 kN (-0.82 kips) and 11.6 kN (2.6 kips) corresponding to a load redistribution of 36%, -18% and 57.8%, respectively.

Table 4-8 Results of exterior column removal test

	static residual deflection (mm)		Redistributed static residual load (kN)					
Tests	column B1		column A1		column A2		column B2	
	Deflection	DLAF	Load	DLAF	Load	DLAF	Load	DLAF
First drop	28.3	1.021	5.96	1.17	-3.13		9.47	1.11
Second drop	83.0	1.067	2.77	1.213	2.3-4.37	1.11-1.28	5.68	1.120

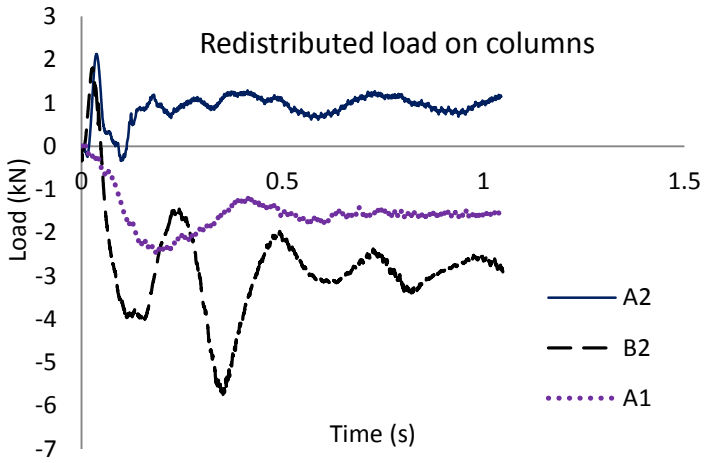

Figure 4-17 Redistributed load on columns for the second drop

Figure 4-18 shows the moments on the column in the second drop. Column A2 has higher moments than that on the column B2 due to the fact that column B2 was seriously damaged in the first drop. The shear force on column A2 was 19.18 kips while only 0.57 kips on column B2.

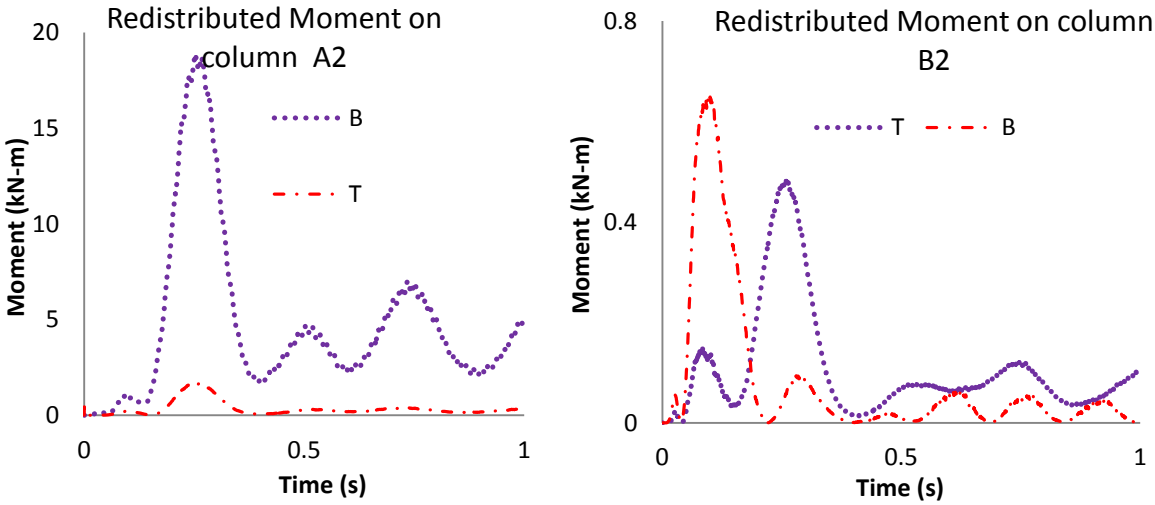

Figure 4-18 Moment on Columns in the second drop

Figure 4-19 shows the load redistribution of column A2 and B2 in the third drop. Negative values indicate increasing axial load. Column B2 did not see any increase in load due to the damage from the first two drops, the column kept losing the load to 71.2 kN (16 kips) as the column B2 punched through the slab. A2 initially saw an increase in load up to 113.9 kN (25.6 kips) then loss approximately 71.2 kN (16 kips) of load due to the punching failure of the connection.

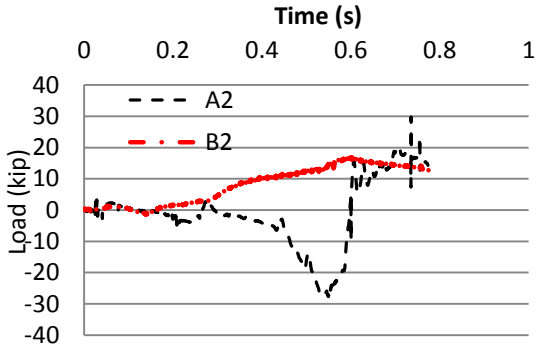

Figure 4-19 Load redistribution in the third drop

4.5.4 Horizontal (In-Plane) displacement

Horizontal deflections were measured at columns A1, C1, A2, and B3 in order to determine the horizontal movements caused by compressive and tensile membrane actions. The results for the first drop are given in Figure 4-20 where positive values indicate outward movement. The left figure in Figure 4-20 shows two stages of movement for all the columns over the test. The dashed line is the first stage of movement happened in the early time of the test, the solid line means the second stage indicated the final positions of columns after test. The legend NS and EW on the right figure of Figure 4-20 illustrate North-South movement and East-West movement, respectively, and the orientation is shown in the left figure of Figure 4-20.

The difference in movement between two columns on the same row gives the overall expansion or contraction of the slab along that column line. This information is plotted as line A1 +C1 in Figure 4-20. As can be seen in this figure initially there was a small inward movement of the columns. Because the LVDTs were connected to the column just above the slab, this small inward movement was likely due to the small flexural rotation occurring at the slab column connection. The relative movement between column A1 and C1 was inward up to 0.04 mm (0.0015 in.) at a B1 vertical deflection of 1.5 mm (0.059 in.). The movement was then changed to be outward due to the buildup of compressive membrane forces. The maximum outward movement of 1.06 mm (0.042 in.) occurred at the maximum vertical deflection of 28 mm (1.10in.) at column B1. Column A2 experienced the same trend as Column A1 though with lesser values of displacement. However, column B3 showed initial outward movement followed by inward movement. The maximum horizontal movement at contra-flexural point($0.2l_n$) around center B2 column was 0.17 mm (0.0067 in). Unfortunately the measurement at column B2 itself is unavailable.

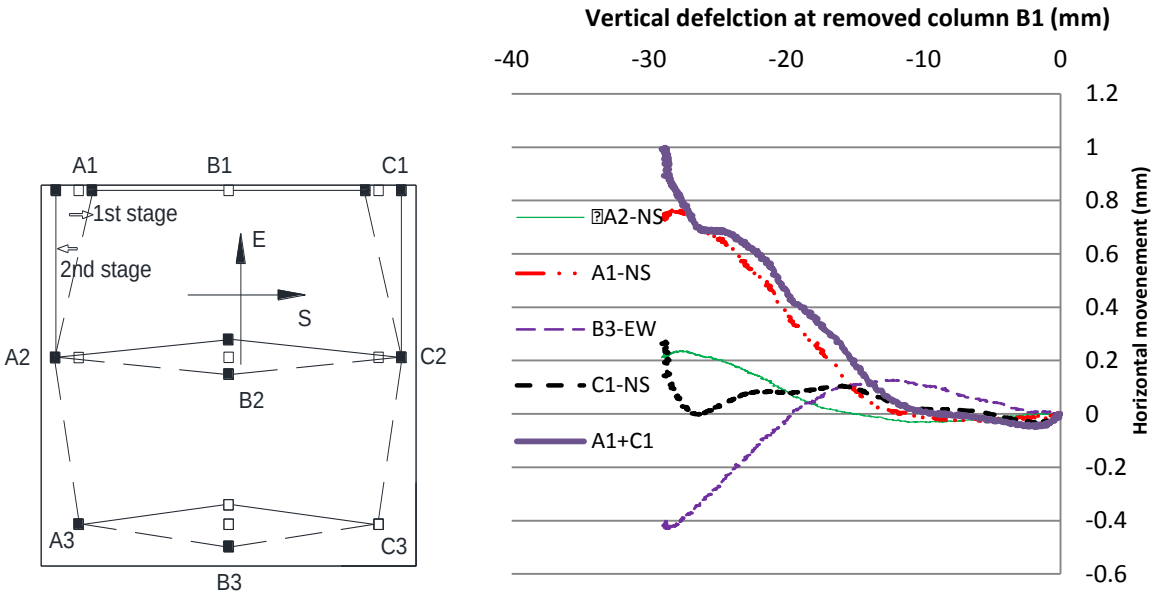

Figure 4-20 Horizontal deflection vs. vertical deflection of column B1 in first drop

The relative horizontal movements between columns A1 and C1 for all three drops are given in Figure 4-21. For the second drop, column A1 and C1 moved inward first until reached 0.25 mm (0.01 in.). Then the slab begun to move outward due to the compressive membrane action and the outward horizontal displacement between column A1 and C1 reached 1.55 mm (0.06 in.) when the vertical displacement of column B1 stablized at 79.3 mm (3.12 in.). The initial inward movement was caused by a combination of the rotation of the slab-column connection and the closing of cracks generated during the first drop. As seen in Figure 4-21, outward movement was initiated only after the vertical deflection at column B1 from the first drop (28.9mm) was exceeded.

In the third drop column A1and C1 did not move outward due to the pre-existing damage, but the greater amount of deflection achieved on removed column B1 in the third drop pulled the columns inward due to tension membrane forces. The pulling inward due to tension membrane

effects occurred at a B1 column displacement of approximately 100 mm which is close to the depth of the slab (89mm).

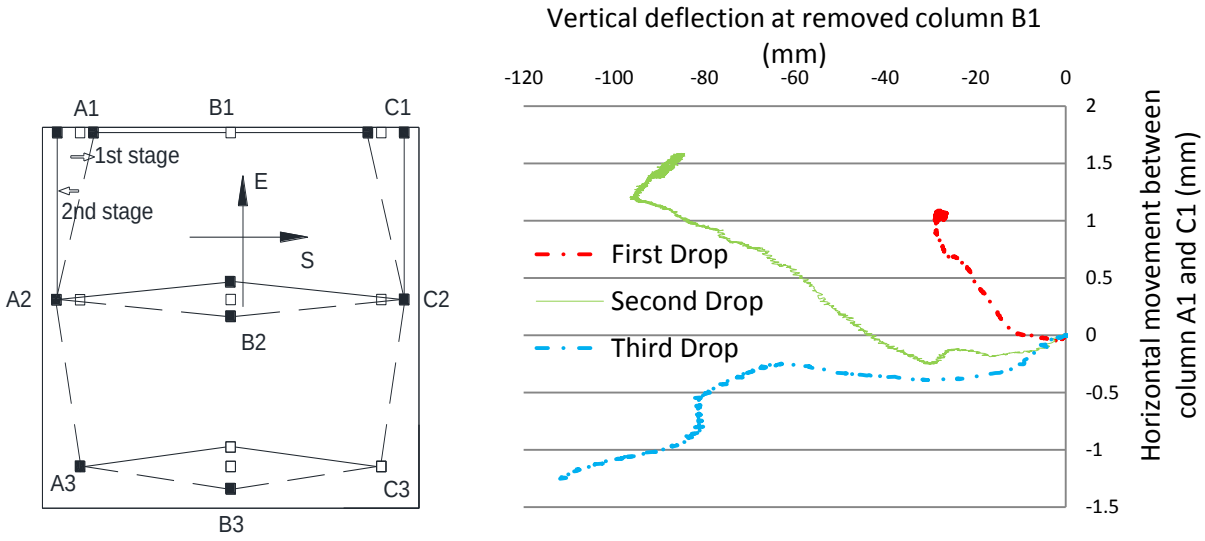

Figure 4-21 Horizontal relative movement between column A1 and C1

Figure 4-22 shows the horizontal movements of column A2 and B3 for all three drops. In the first drop column A2 expereinced a similar inward then outward movement to column A1. Column B3 experienced a initial outward then inward movement. Figure 4-22 also shows the effects of accumulated damge on in-plane deformation response of the structure. The specimen did not demonstrate in-plane deformation reponse and thus compressive membrane action was not formed until the deflection at the removed column B1 has exceeded that of the previous tests . Therefore, the preexisting damage can have a strong effect on the formation of compressive membrane action. In actual structures this damage or cracking may be present due to overloading or shrinkage cracking. Therefore the increase of punching shear capacity due to the compressvie membrane aciton in flat-slab structures may not be a reliable mechanism to help arrest disproportionate collapse in a structure with initial damage or under excessive deformation associated with large gravity loads acting on the slab.

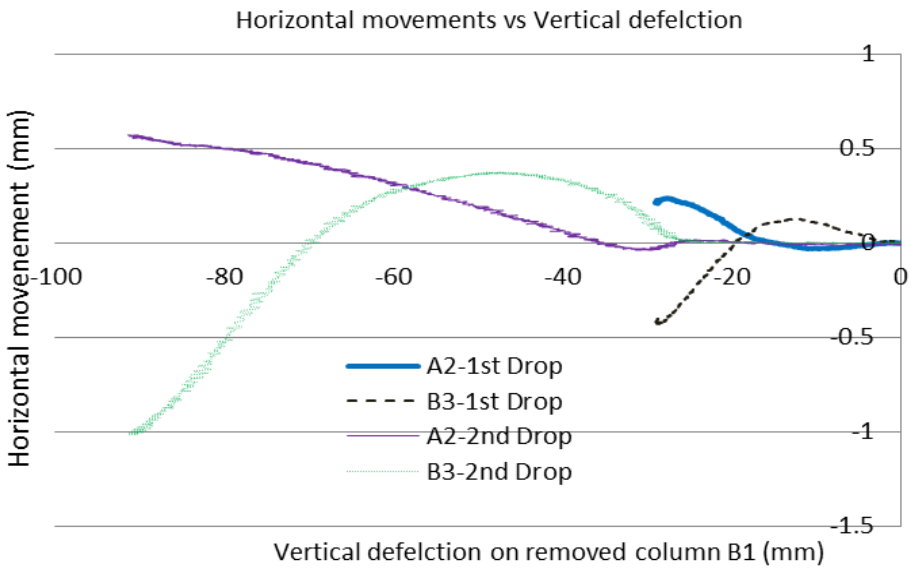

Figure 4-22 Horizontal movement of column A2 and B3

4.5.5 Rotation of slab relative to column

In order to measure the rotation of slab around center column B2, three vertical LVDTs were used to measure the vertical deflection of the slab at different distances from Column B2 as shown in Figure 4-23. The distances from the edge of center column B2 to each location were: 216 mm (5.5 in.), 564 mm (19.2 in.) (at the contra-flexural point $0.2l_n$) and 2362 mm (93 in.) right on column B1. The rotation for each location was calculated by arctangent of deflection divided by the distance from the location to the center of column. The rotations from the second drop were 0.0356, 0.0339 and 0.028 rad force three locations. In addition, two horizontal LVDTs were situated to measure the rotation of center column B2. The column rotation was 0.0023 rad and 0.00302 rad. Considering the nearest rotations as the most critical the rotation in the slab was 0.03 rad. At this rotation the connection was not yet failed (although it was likely close to failure). According to predictions of punching shear failure of the isolated slab-column connections using Muttoni's formulation (2008), once the slab rotation reaches 0.0221 rad, then

punching shear would be initiated. But this did not happen in the multi-panel case. The rotation of multi-panel slab was larger than 0.0221 rad. as stated above in the second drop, and no punching failure occurred. This was because more flexural bending in the multi-panel slab than that in isolated slabs.

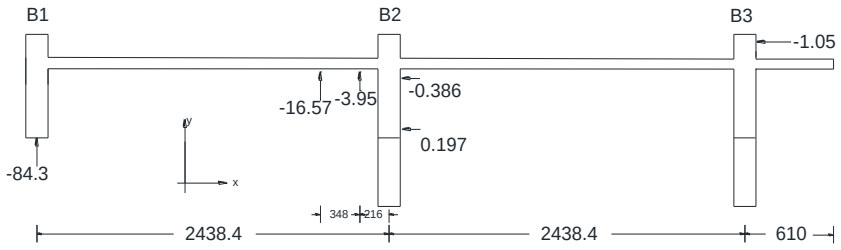

Figure 4-23 LVDT measurements for determining slab rotation relative to center column (mm)

4.5.6 Concrete and steel strains

Figure 4-24 shows the variation in the concrete strain at the top and bottom faces of slab as a function of the deflection at the removed column B1. "T" and "B" in the figure stand for top side and bottom face. All the gages in the figure were applied perpendicular to the column faces. In this figure negative values indicate compressive strains. Only "A1-T" in the figure uses the secondary axis scaled from -200 με to 150 με. The top concrete strains A1-T and B2-T were initially in tension while the bottom concrete strains at location A1-B and B2-B were in compression due to the flexural response of slab to the applied load until the deflection of removed column B1 reached 6.29 mm (0.24 in.). The concrete tensile strain at B2-T reached its maximum 231 με then started to drop down due to the formation of compressive membrane strain which cancelled out the tensile flexural strain. At the same time the concrete tensile strain at A1-T reached its peak 62 με and started to drop at the deflection of 9.8 mm (0.38 in.). This indicates that from deflection of 6.29 mm (0.24 in.) compressive membrane strain formed and

started to cancel out the tensile flexural strain. Also it's possible that the compressive membrane strain generated earlier than that, because even the top still shows tensile strain, the net axial force in the section can be in compression.

As the deflection kept increasing, the concrete tensile strain at B2-T changed into compression, and reached its maximum 590 με and dropped down to tension at the deflection of 13.9 mm (0.54 in.) while the tensile concrete strain at B1-T started to drop and reached its minimum 37με at the deflection of 19.2 mm (0.756 in.) and started to increase again due to the tensile membrane action.

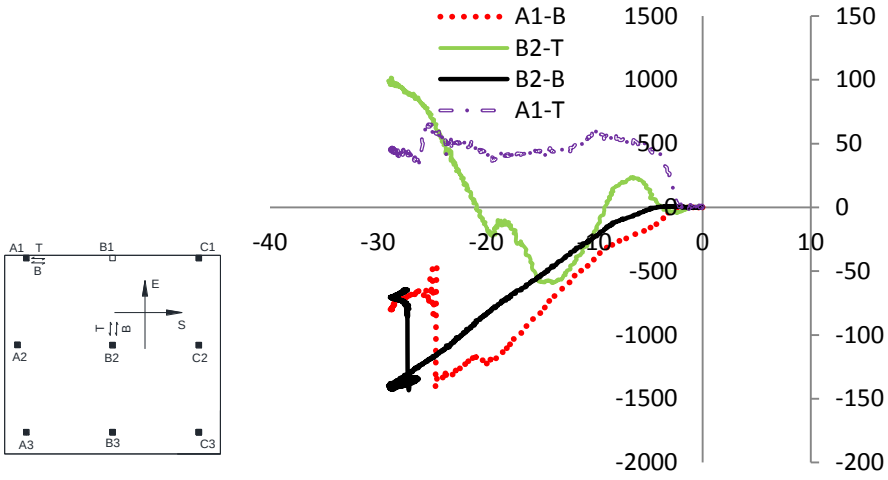

Figure 4-24 Concrete strain vs. removed column B1 deflection in the first drop

Figure 4-25 shows the variation of top concrete strains as a function of vertical deflection of removed column B1in the first drop, negative values indicate compressive strains. Concrete strains from Transducer 5 remained in compressive over the test at a magnitude of 217 με, but the value from Transducer 6 started from tensile strain and then switched to compressive strain at a magnitude of 58με due to the compressive membrane action. Transducers at location 7 and 8 were measuring the radial and tangential strains of center slab-column connection B2. Strain 7 and 8 showed the same transition from initially tensile strain to compressive strain, then the

tangential strain at location 8 changed into tension but strain at location 7 stayed in compression. Numerical analysis shows that the shear demand at location 8 was more critical to location 7 in resisting the load redistribution after the falling of column B1. Therefore tangential strain 8 turned into tensile strain up to 615 με but radial strain at location 7 stayed in compression at 60 με.

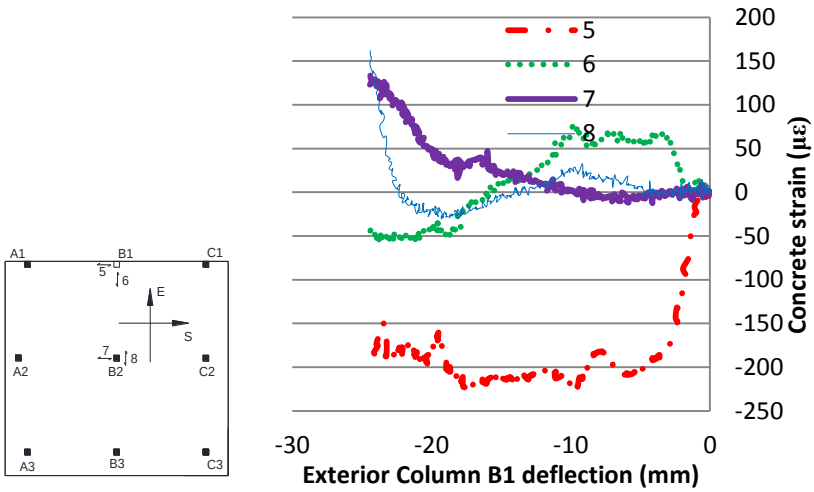

Figure 4-25 Variation of top surface concrete strains in the first drop

Figure 4-11 (b) shows the accumulated crack development after the second drop. Most of the cracks from the first drop widened and extented in the second drop. One 1 mm (0.04 in.) wide major crack formed around slab-column connection B2 and A1 each as shown in Figure 4-11 (c), causing the yielding of the tensile rebar. As shown in Figure 4-26 Location 2 and 4 are concrete compressive strain at bottom of slab and location 9 and 10 are the top tensile rebar strain, with the positive values indicating tensile strains.

The tensile rebar strain at location 10 almost linearly increased to 0.0054 and concrete compressive strain at location 4 reached 0.00225 at a deflection of 86.69 mm (3.41 in.), which indicates the slab already in a plastic deformation stage and the cross section was very near

failure. This agrees with significant cracks observed around column B2, A1 and C1. It's believed that the slab was near failure at the load level of 7.18 kN/m² (150 psf) for the second drop. The rebar tensile strain at location 10 near center column B2 is larger than that from location 9 around column A1, which indicates more load was redistributed to the center column B2 than to the exterior edge column A1.

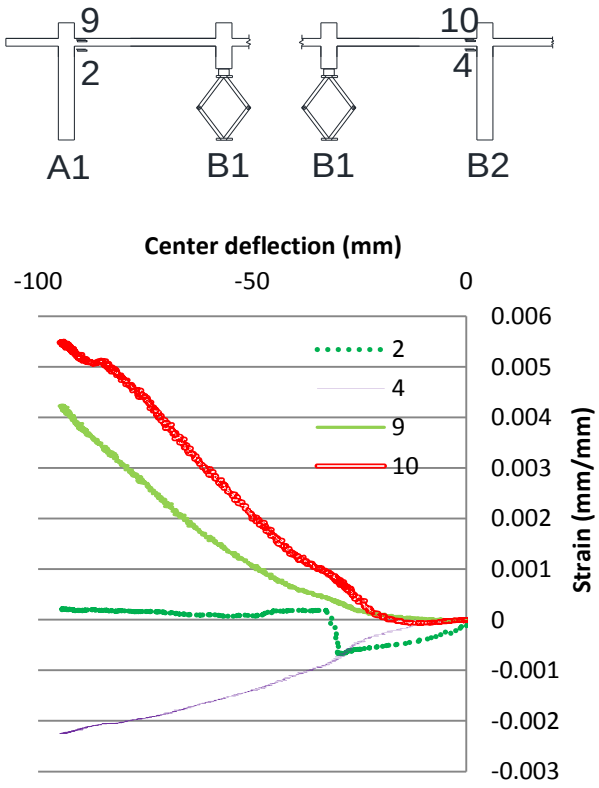

Figure 4-26 Variation of concrete and steel strains in the second column removal test

4.5.7 Strain rate effects

Dynamic loading can lead to material strength increase due to strain rate effects. Figure 4-27 shows steel and concrete strain variations over time. For the first drop test, the maximum steel strain was 0.0012 reached at 0.18 sec while the maximum concrete strain was 0.00138 at 0.158 sec, resulting in the strain rates for reinforcement and concrete in the first removal test being

0.00667/sec and 0.00873/sec, respectively. The Dynamic strength Increase Factors (DSIF) for steel and concrete at those strain rates are approximately 1.02 and 1.1, respectively based on UFC 340 (2008). Figure 4-27 also shows the maximum steel and concrete strain 0.00548 and 0.00224 in the second drop test. The corresponding strain rates for the two materials are estimated as 0.0219/sec and 0.00802/sec, respectively, which leads to the DSIFs for steel and concrete in second removal tests being equal to 1.026 and 1.1. Therefore, it would be predicted, due to the dynamic effects, steel and concrete had a 2% and 10% increase in strength, respectively.

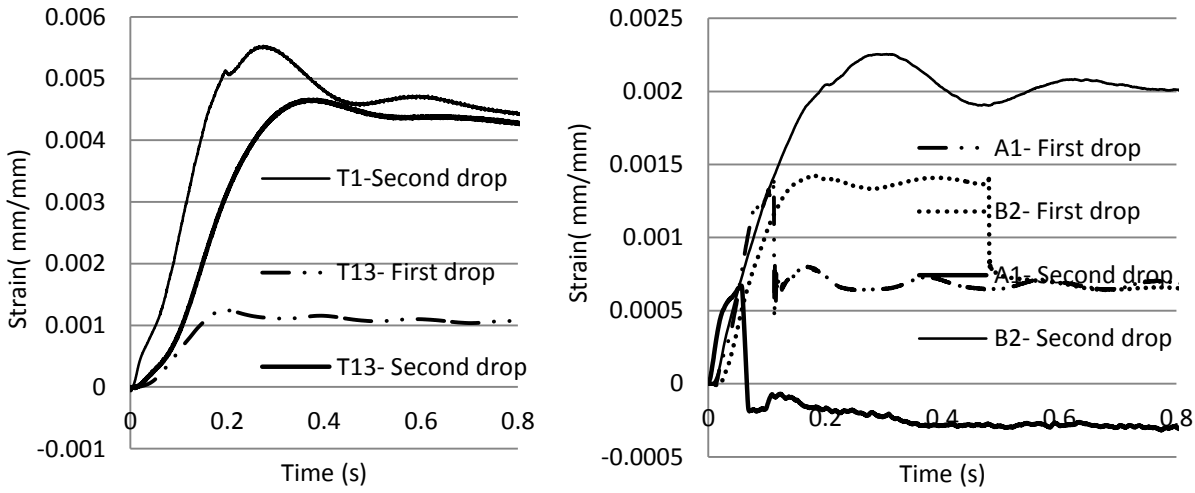

Figure 4-27 Strain rates of concrete and steel reinforcement

4.5.8. Post punching of slab

The post punching capacity of older flat plates without integrity bars consists of breaking out of concrete cover and pulling out of compressive reinforcing bars from columns. Figure 4-28 shows the top most layer of tensile bar pulled out of concrete and the top second layer of tensile bar fractured in the third drop. The post punching capacity was not able to provide an alternate load-carrying mechanism in this exterior column removal case.

Generally speaking, whether or not post punching capacity can provide an alternate loading path depends on if this capacity is capable of allowing the connection to reach a stable equilibrium structural configuration to withstand the remaining load after the load redistributed to the surrounding columns. Since post punching capacity of older flat plates without integrity bars can have approximately 50% of punching capacity in a rather small deflection as discussed in Chapter 3. Therefore, if the remaining load on columns after failure is within 50% of punching capacity, post punching capacity may provide an additional load path. However, if the load is greater like the case in the third drop, post-punching capacity may not be an alternative load carrying path.

Figure 4-28 Top Bar pulled out of concrete and fractured

4.6 Conclusions

A dynamic exterior column removal was conducted for three different load levels (three drops) on one multi-panel specimen. The main conclusions can be drawn from these drops are:

(1) Compressive membrane forces were verified in the multi-panel specimen with 1.54mm maximum outward lateral movements on columns and measured compressive strains in the concrete.

(2) Compressive membrane forces form after a column removal and gradually transition to tension membrane forces as the deflection at the removed column approaches 0.4 % of the span length (98mm/2440mm) or exceeds the slab depth (89 mm). However, preexisting damage in flat slab structures (from prior overloading or shrinkage cracking) may impede the formation of compressive membrane forces in the slab.

(3) Dynamic removal of an exterior supporting column resulted in a dynamic increase factor (increase over static redistributed loads) of approximately 1.21. Therefore, surrounding connections need to be able to carry at least 21% more than the predicted redistributed static load in a collapse analysis.

(4) The recorded rotation on the center column B2 in second drop is 36.6% more than the predicted rotation at failure by Muttoni's formulation (2008) in an isolated slab-column connection. Therefore, the rotation at failure in the multi-panel may be more than predicted.

(5) The maximum strain rates recorded in the first two drops were only 0.0219/sec and 0.00873/sec for steel and concrete. UFC 340 (2008) would predict the two materials have only a 2% and 10% strength increase due to strain rate effects, respectively. Therefore, this increase in material strength can lead to about 10% increase in the adjacent slab rotations and in the deflection on removed column..

(6) Disproportionate punching shear failures did not occur at load levels of 4.84 kN/m² (100 psf) and 7.18 kN/m² (150 psf) corresponding to approximately 40% and 52% of the design service load, although it is believed that failure was close to occurring after the second drop. Failure did occur at a level of 9.86 kN/m² (206 psf), 67% of the design service load.

CHAPTER 5 EXPERIMENTAL DYNAMIC RESPONSE OF FLAT PLATE SUB-STRUCTURE SUBJECTED TO INTERIOR COLUMN REMOVAL

5.1 Introduction

This chapter presents the results from a dynamic experimental test of a 2 bay by 2 bay flat-plate structure subjected to an interior column loss. The failure propagation over an entire flat-plate floor, load redistribution and dynamic load increase factor were studied.

5.2 Flat Plate Model Structure Design

The flat-plate structure in this chapter basically was the same as the structure presented in Chapter 4 (exterior column removal case). The difference was that the interior rather than the exterior column was removed in this test. In addition, improved concrete placement allowed for as designed slab thickness. Therefore, the slab thickness was 76 mm (3 in.) and the concrete clear cover for the top and bottom reinforcement were 6.35 mm (0.25 in.). The measured concrete strength was 30 MPa (4379 psi). The reinforcement was from the same batch as those used in the exterior column removal case and those properties can be found in Chapter 4. The schematic model of test specimen is shown in Figure 5-1.

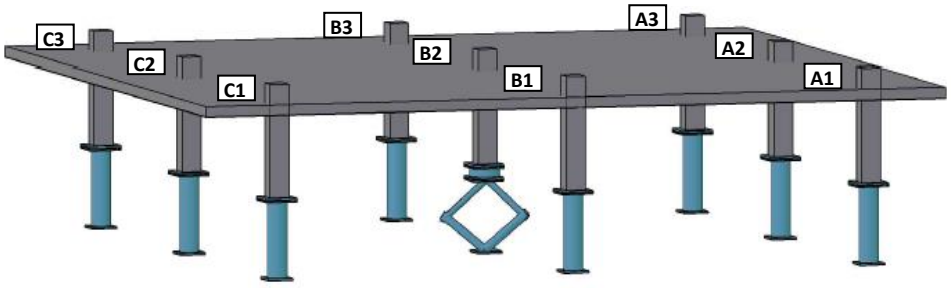

Figure 5-1 Schematic model of test Specimen

5.3 Instrumentation

The instrumentation of interior column removal test consisted of horizontal and vertical LVDTs and concrete and rebar gages. The horizontal movement of column B1, B3, C2 and A2 was measured by four LVDTs (LD1, 2, 3, 4) as shown in Figure 5-2. The rotation of slab near column B1 was determined by three vertical LVDTs (VD2, 3, 4). In addition, concrete gages (1 to 10), indicated by hollow and solid rectangular squares in the figure, were used to measure the radial and longitudinal strains on the top and bottom sides of slab-column connections. Strain gages were applied on B1, B3, and A2 steel column to measure the axial forces and moments at the columns. The arrangement of the rebar strain gages was the same as in the exterior column removal test.

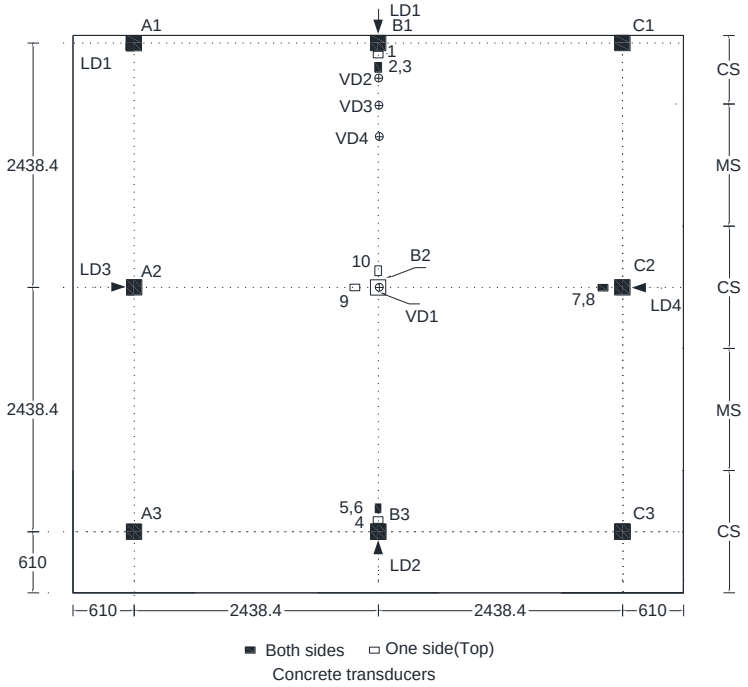

Figure 5-2 Instrumentation layout

5.4 Test Procedures

Similar to the exterior column removal case, fabric bags with adobe soil were used to apply a uniformed superimposed dead and live load. The load on the outer portion was increased in order to simulate the proper shear condition on the outer columns via hanging the concrete slabs. Based on trial analysis using modeling schemes calibrated by the exterior column removal test data, a load of 5985 N/m² (125 psf) was determined to be sufficient to barely fail the structure. Therefore, a superimposed load of 5985 N/m² (125 psf) was planned for the testing. However, during load application the cracks were seen around the slab-column connections when loading the slab, so the decision was made to reduce 10.23kN (2300 lbs) of load or 9 psf of load in the center area. Therefore the total load of 132kN (or 116psf) and 102kN (30187 lbs) were applied on the center and outer area of the slab, respectively. The specimen slab ready to be testing is shown in Figure 5-3.

The load releasing system basically was similar to the one used in exterior column removal case. The only difference was a single scissor jack was replaced by a combined double scissor jack system due to the additional static load in the center column. The data acquisition system was zeroed out after all the load had been applied just prior to the testing.

Figure 5-3 Specimen ready to be testing

5.5 Test Results

5.5.1 Overall response

The removal of column B2 was simulated, as described earlier, by releasing the pneumatic quick release. The center column B2 was removed at t=0 sec and the punching shear failure happened on four columns (A2, B1, B3 and C2) at approximately t=0.30 sec. Column A1 and C1 experienced major cracks through the cross section along with column A3 and C3 only observed fine minor cracks. The structure successfully sustained the above load through the post punching capacity. The slab after the test is shown in Figure 5-4.

Figure 5-5 shows the crack patterns on both sides of the slab, the circled cracks around the columns on the top side of slab indicate punching cones. Table 5-1 shows the adjusted design of scaled multi-panel properties.

Table 5-1 Adjusted design of prototype and scaled specimen for interior column removal

	Scaled properties	Prototype properties
cover to bottom bars	6.35mm (0.25in.)	15.9mm (0.625in.)
chair height to top bars	57.2mm (2.25in.)	143mm (5.625in.)
slab depth	76.2mm (3in.)	190.5mm (7.5in.)
bar diameter	6.35mm (0.25in.)	15.9mm (0.625in.)
top bar spacing	88.9mm (3.5in.)	222.3mm (8.75in.)
bottom bar spacing	152.4mm (6in.)	381mm (15in.)
Yield strength	413.69 N/mm² (95 ksi.)	413.69 N/mm² (95 ksi.)
Concrete strength	30.2 N/mm² (4375psi)	30.2 N/mm² (4375 psi)
d to top steel	63.5mm (2.5in.)	158mm (6.25in.)
d to bottom steel	63.5mm (2.5in.)	158mm (6.25in.)
reinorcement ratio negative	0.00561	0.00561
reinforcement ratio positive	0.003272	0.003272
M_u negative	16.8kN-m (149 kip-in)	26.1kN-m (2318 kip-in)
M_u positive	10.1kN-m (89.4 kip-in)	15.7kN-m (1396.2 kip-in)
column strip width	1219mm (48in.)	3048mm (120in.)
l_2	2438mm (96in.)	6096mm (240in.)
l_n	2286mm (90in.)	5715mm (225in.)
M_o negative	28.2kN-m (250 kip-in)	444.7kN-m (3936.3 kip-in)
M_o positive	61.9kN-m (452.4 kip-in)	968kN-m (8568.5 kip-in)
W_u negative	0.0178 N/mm² (371.0 psf)	0.0178 N/mm² (371.0 psf)
W_u positive	0.032 N/mm² (670.3 psf)	0.039 N/mm² (670.3 psf)
Punching shear capacity V_u		531.3kN (119.4kip)
W_u for punching		299.8
Controlling service load capacity	0. 018 N/mm² (373.2 psf)	
Dead load	5446N/ m² (113.75psf)	
Live load	3959N/ m² (82.7psf)	

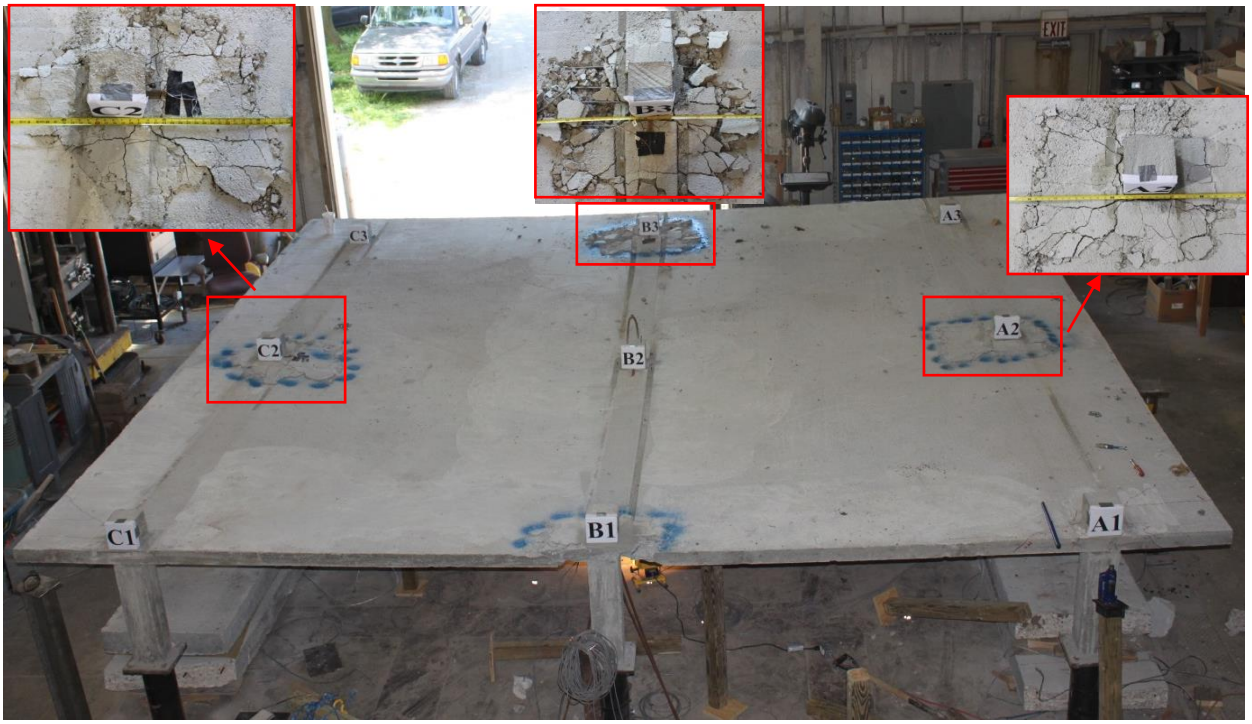

Figure 5-4 Slab after the test

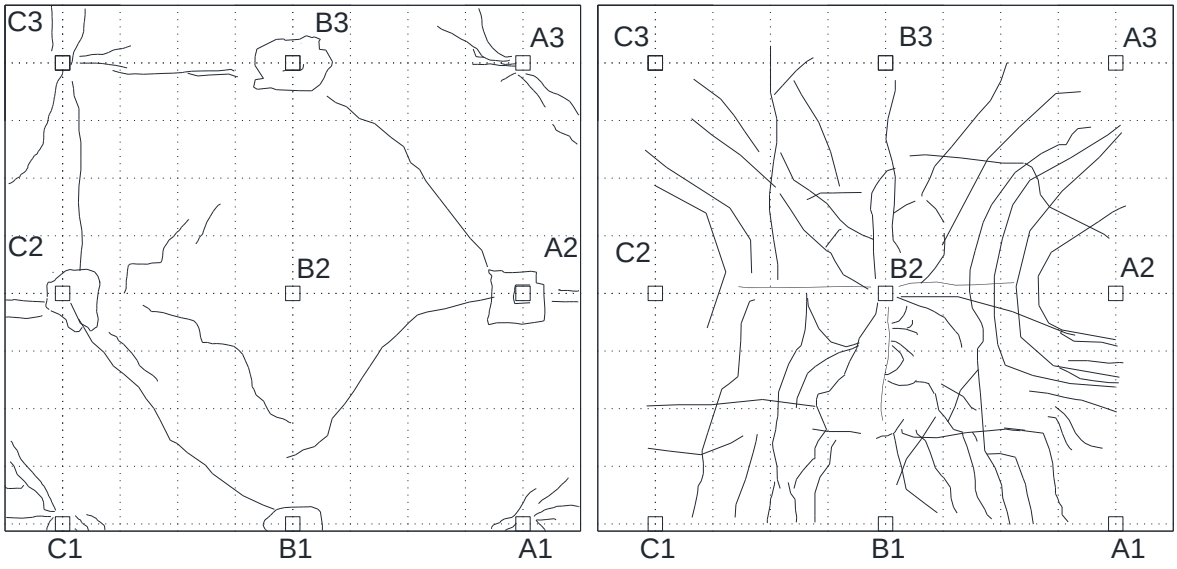

(a) the top side (b) the bottom side

Figure 5-5 Crack patterns on both sides of the slab.

Since the punching shear failure happened at 116 psf in this interior column removal test or, about 54% of service load failed as Table 4-4 indicates, the multi-panel slab is vulnerable to the disproportionate collapse in interior column removal case.

5.5.2 Load-deflection response at removed column

Figure 5-6 shows the time history of vertical displacement of removed column B2. The punching failure happened at columns A2, B1, B3 and C2 when the deflection of removed center column B2 reached approximately 123mm at 0.30 sec, Load was sustained in columns A2, B1, B3, and C2 through post-punching capacity, Column B2 eventually reached a peak deflection of 155.8 mm within 0.55 sec, followed by a vibration period. The load releasing time for interior column removal was approximately 0.0074 sec. The load releasing rate before 0.003 sec was relatively slow as shown in Figure 5-7. This was due to the time required to open the pneumatic quick release. Then after the quick release was completely opened, the load releasing rate was almost linear after that as shown in Figure 5-7.

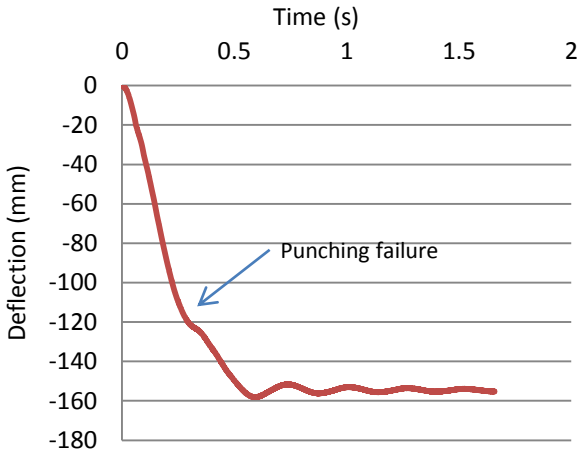

Figure 5-6 Deflection vs. time response at removed center column B2

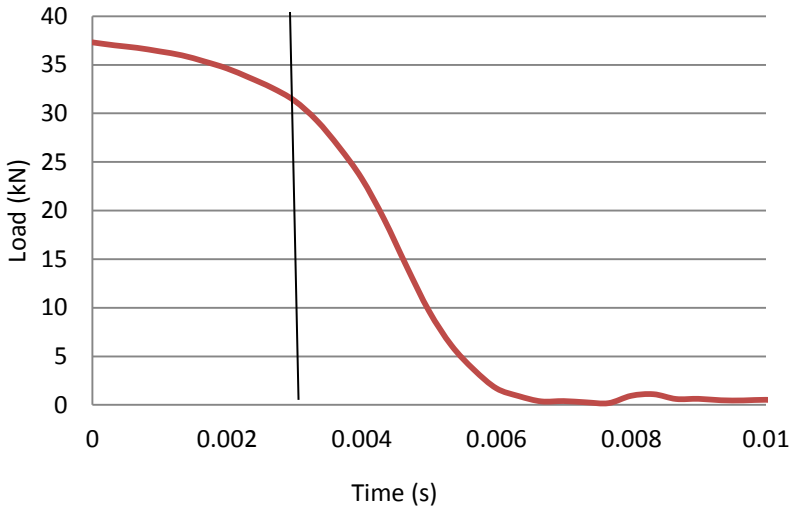

Figure 5-7 Load vs. time response at removed column B2

5.5.3 Load Redistribution

The load carried by column B2 was redistributed to the adjacent column after removal of column B2. The axial force and moment in column A2, B1and B3 were measured by six strain gages placed in two rows on the columns. The resulting load time history for the adjacent columns is given in Figure 5-8 (compressive load in the column is negative). The first increase in compressive load in the figure was due to the load redistribution after the removal of column B2. The peak measured dynamic loads redistributed to column A2, B1 and B3 were 19.53, 14.37 and 16.68 kN (4.39, 3.23 and 3.75kips respectively). Each column reached the peak compressive load points at different times. Figure 5-8 indicates column B1 experienced punching shear failure first, followed by column B3 and A2. The loss of compressive load shown in Figure 5-8 was due to the punching failure of columns. Note, that since the gages were zeroed after the dead weight was applied but before testing, the positive load shown in Figure 5-8 is not actually tension. The actual load in the columns would be the combination of the static load prior to testing (Table 5-2) and the load shown in Figure 5-8.

After punching shear failure the compressive load in the columns again increased due to the change of the load carrying mechanism of slab-column connection from pre-punching into post-punching phase. The residual load after column B1 removal for columns A2, B1 and B3 was 5.96 kN (1.34 kips), 5.96 kN (1.34 kips) and 4.49 kN (1.0 1kips) corresponding to load redistribution of 15.7%, 15.7% and 11.9%, respectively, after the structure stabilized.

Because the columns experienced punching shear failure a true dynamic load redistribution value (DLAF) cannot be determined. However, if assuming that the residual load measured after punching will be less than the residual load that would have occurred if punching did not happen and maximum DLAF can be determined. For the interior column removal case the maximum DLAF is 1.27.

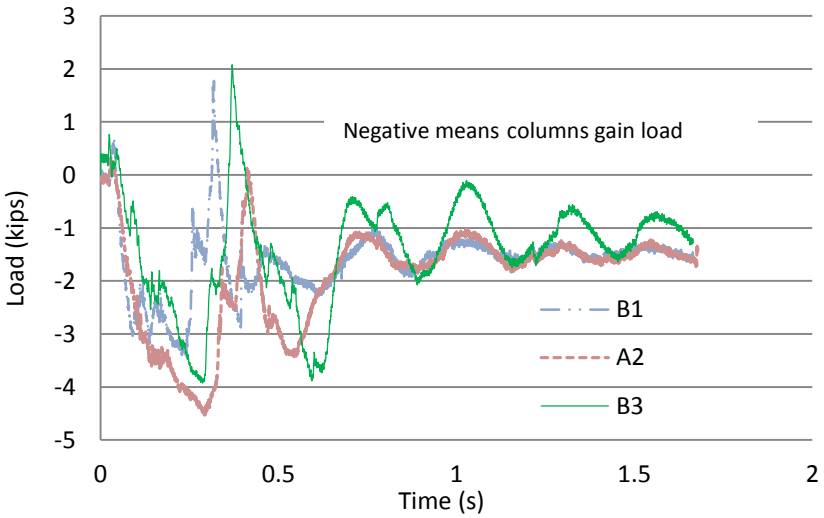

Figure 5-8 Time history of axial load on adjacent columns

Table 5-2 Load response on columns before and after testing

	Static load from simulation	Peak dynamic load from test	Residual load from test	DIF
B1	24.3kN (5.45kip)	14.6kN (3.28kip)	6.45kN (1.45kip)	1.27
B3	50.7kN(11.4kip)	17.1kN (3.84kip)	4.67kN (1.05kip)	1.22
A2	50.7kN (11.4kip)	19.5kN (4.39kip)	6.9kN (1.56kip)	1.22

5.5.4 Horizontal (In-Plane) displacement

Horizontal deflecitons were recorded on columns A2, C2, B1 and B3 in order to determine the horizontal movements from compressive membrane and tensile membrane actions. Figure 5-9 shows the movement of each column. Positive value means outward movement. All the columns showed initially inward movement until the deflection of removed column reached about 24.2 mm (0.95 in.) as seen in the exterior column removal test. Then the movement columns C2 and B3 turnned to outward up to 0.005 mm (0.0002 in.) and 0.25 mm (0.001 in.), respectively due to compressive membrane action. Eventually, the large deflection achieved on removed column B2 resulted in tensile membrane action that pulled the column A2, C2 and B3 inward up to 2.8 mm (0.11 in.) on average. This change in behavior occurred at a B2 column deflection of approximately 69 mm which is similar to the depth of the slab 76mm. The behavior of column B1 is an exception, experienced much larger outward and inward movement as indicated by Figure 5-9. due to the fact that B1 is an exterior column with less restraint from surrounding slab and columns.

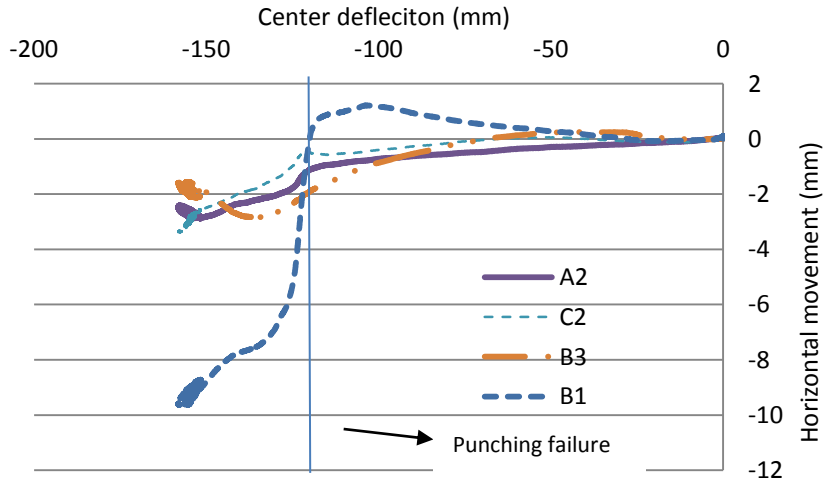

Figure 5-9 Horizontal movement on column A2, C2 and B3

The difference of the horizontal deflection of two columns in a column line shows the overall expansions or contraction along that column line. As seen in Figure 5-10, the relative movement between B1, B3 and A2, C2 moved inward first due to the initial bending of the columns until the vertical deflection of center column reached 22.5 mm (0.88 in.). The overall expansion between B1 and B3 was larger than that along A2 and C2. Since the LVDTs were located to columns just above the slab, the larger combined "B1+B3" horizontal movement value may indicates that more flexural bending occurred along B1, B3 column line. Then the slab moved outward due to the formation of compressive membrane force until the vertical deflection of center column B2 reached 99.2 mm (3.9 in.). However, for combined movement "A2+C2" , no compressive membrane action was observered from Figure 5-10. After that the compressive membrane action changed into tension membrane phase until punching failure happened on adjacent columns at vertical deflection of center column 118 mm (4.64 in.). For this test punching shear failure of the adjacent columns did not occur during the compressive membrane phase, but occurred after the tension membrane force is formed. This would indicate that compressive membrane forces were not avaiable to improve the punching shear capacity of the connections.

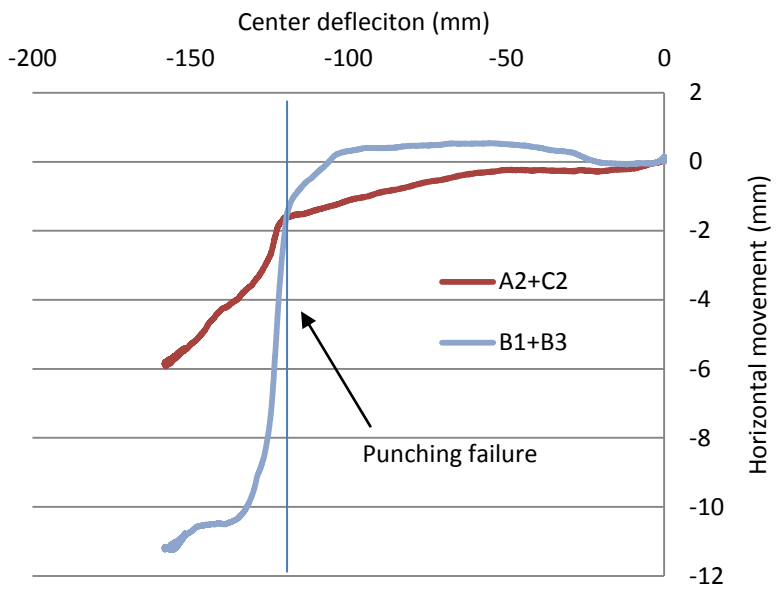

Figure 5-10 Overall movement of columns along the column line

Figure 5-11 shows the three horizontal measurements on column B1 used to find the rotation of the column during the test. B1-T was 6.35 mm (0.25 in.) above the slab, B1-M and B1-B were 216 mm (8.5 in.) and 533 mm (21 in.) below B1-T, respectively. As the figure indicates B1-T moved inward first while B1-M and B1-B move outward, this inward movement actually is the result of a combination movement due to rotation caused by flexural bending of slab and outward movement due to the formation of compressive membrane action. Three LVDTs reached their maximum outward movements at a center column deflection of 100.6 mm (3.96 in). This point of transition from compressive membrane to tensile membrane occurred at a similar level of center column deflection as seen in the other deflection measurements. The tensile membrane action pulled the column inward until a maximum deflection of 9.5mm. The B1 column showed an average rotation from the three measurements of 0.0004rad at punching shear failure of that column, and 0.0063rad at the end of the test.

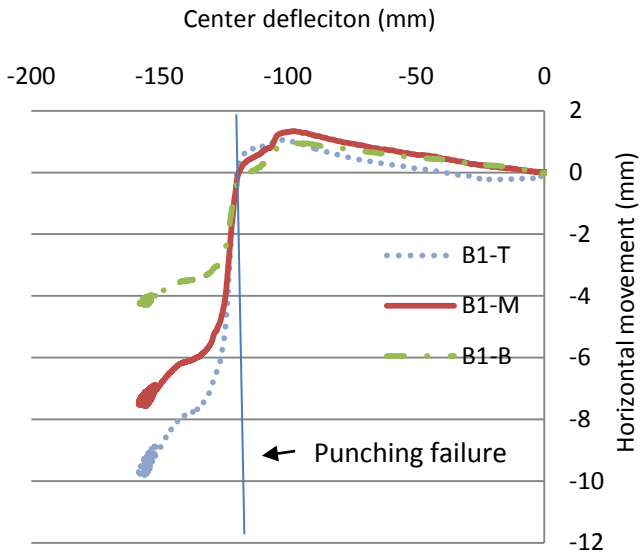

Figure 5-11 Horizontal movement at three locations of column B1

5.5.5 Rotation measurement

The rotation measurement of the slab around column B1 consisted of three vertical LVDTs as shown in Figure 5-12, B1-V1 was located 70 mm (2.75 in.) away from the column face, B1-V2 and B1-V3 were 95.25 mm(3.75 in.) and 280 mm(11 in.) away from B1-V1, respectively. Before punching shear failure happened in B1 column, B1-V1, B1-V2 and B1-V3 moved almost linearly to 4.49 mm, 8.45 mm and 16.3 mm, respectively until B1-V3 went out of range. The slab rotations at these three locations are 0.065rad, 0.051rad and 0.0365rad before punching failure. Because the rotation nearest the column most directly affects punching shear capacity, the rotation measured from B1-V1 minus the measured column rotation gives a rotation of 0.0646rad on the interior face of the B1 slab column connection.

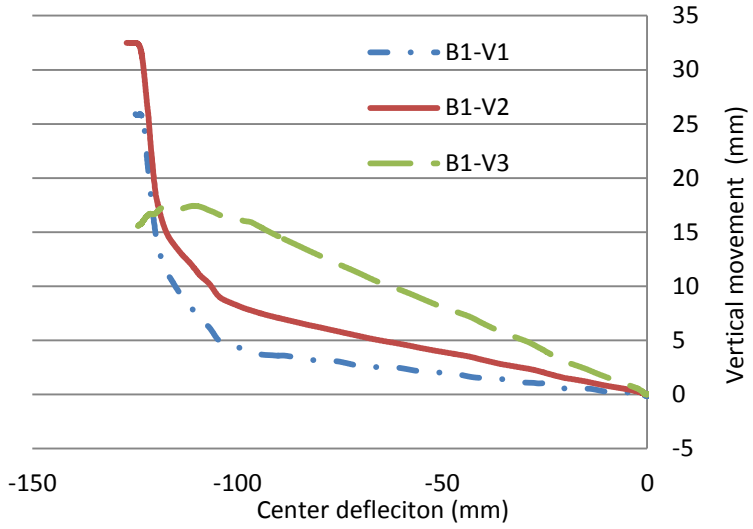

Figure 5-12 Vertical deflection measurement on B1 column before punching failure

5.5.6 Concrete and steel strain

Measurements from the concrete and steel strain gages follow the trends found by the loads and found in the exterior column removal test. The top concrete gages showed strain in the top surface of the concrete due to flexural bending around the column as shown in Figure 5-13. Gage B3-T-PER showed tensile strain throughout the test while the other gages showed initial compressive strains. Gage B1-T-PAR was placed parallel to the column and showed compressive strains throughout. At approximately a center column deflection of 80 mm cracks in the concrete caused the top gages to break.

All the concrete bottom gages showed the same trend of first compression strain due to bending and compressive membrane action and then increasing to tension due to the formation of tensile membrane action, as seen in Figure 5-14. The change from compression into tension occurred at approximately 100 mm (3.4 in.) center column displacement as seen in the previous data. The radial strain on column B3 and C2 (B3-B-PER and C2-B-PER) showed the same

magnitude at 0.00085 mm/mm and the transverse strain (B3-B-PAR) of concrete was around 0.002 mm/mm before punching shear happened.

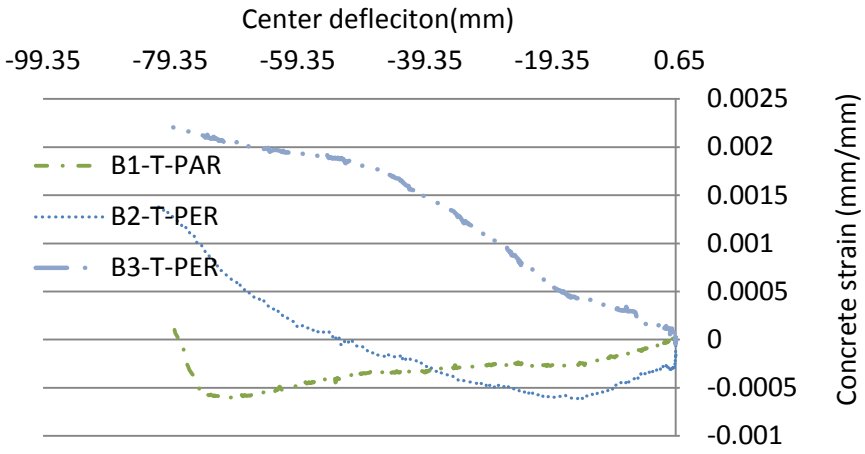

Figure 5-13 Top concrete strain vs. center deflection

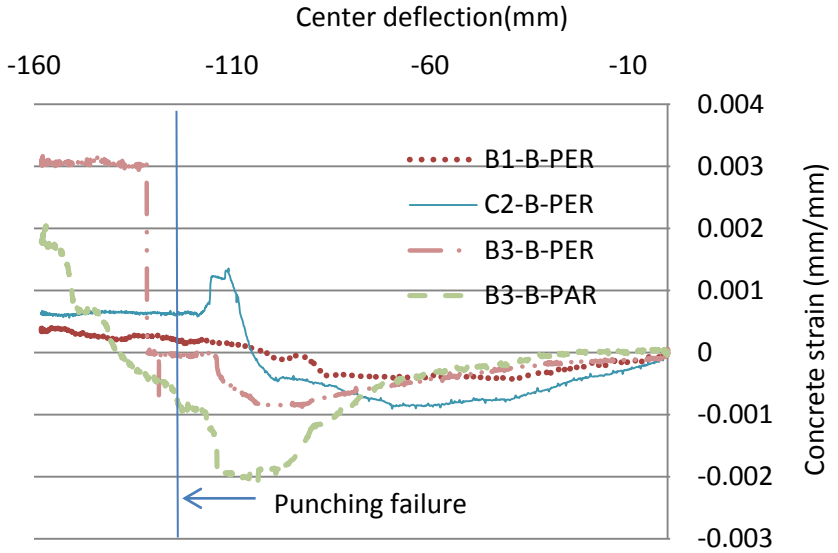

Figure 5-14 Bottom concrete strain vs. center deflection

5.5.7 Strain rate effects

The dynamic loading of the specimen can lead to material strength increase due to strain rate effects. Figure 5-15 shows steel and concrete strain variations over time for a few sample gages. The maximum steel strain was 0.0076 and reached that strain at 0.55 sec while the maximum concrete strain was 0.002 at 0.19 sec, resulting in the strain rates for reinforcement and concrete in the exterior column removal test being 0.0138/sec and 0.011/sec, respectively. The Dynamic Strength Increase Factors (DSIF) for steel and concrete at those strain rates are approximately 1.07 and 1.1, respectively, based on UFC 340 (2008). Therefore, it would be predicted that steel and concrete have a 7% and 10% increase in strength, respectively, due to the dynamic effects.

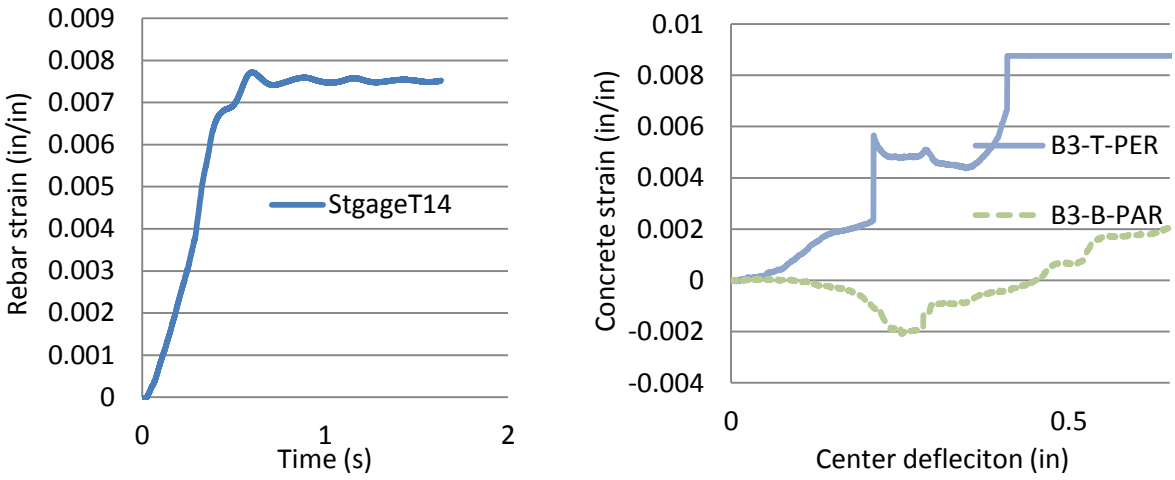

Figure 5-15 Rebar and concrete strain vs. Time

5.5.8 Post punching capacity

The post punching capacity, consisting of breaking out of concrete cover and pulling out of reinforcing bars, is generally thought to be structurally unstable if the bottom bars are

discontinuous. Experimental results from the isolated tests showed that this load carrying mechanism can only carry about 50% of the punching load in small deflections, then load carrying capacity drops dramatically nearly to zero as deflection increases. However, this multi-panel test results showed that post-punching capacity can play an important role in stopping collapse of a structure.

Figure 5-16 shows the failure patterns and punching cones of slab-column connection C2, A2 and B3 and Figure 5-19 shows the pulling out of the bottom bar from column B1. As can be seen in the figure, concrete top cover broke off and the top bars began to be pulled out of the concrete. Due to the placement of the dead weights on the top of the slab some of these bars were restrained from pulling out completely as seen in Figure 5-17 around column B1. However, as can be seen in Figure 5-18 the spalling of the concrete stopped well short of the dead weight locations, therefore dead weight did not affect the pull out resistance of the top bars in most locations. Although, the post-punching capacity was enhanced in some locations this is expected to be as typical in real structures where items (non-structural walls, book cases, etc) may be placed around the columns.

5.5.9 Isolated slab-column connections

Slab-column connection A2, B1, B3 and C2 failed while A3 and C3 saw only minor cracks in the test. Therefore, the decision was made to cut out and test isolated slab-column connection A3 and C3 as shown in Figure 5-20 to investigate the punching capacity of the slab-column connection in the static loading.

Figure 5-16 Post punching capacity of slab-column connections

Figure 5-17 Bars restrained from pulling out by dead weight bags

Figure 5-18 Spalling of the concrete stopped well short of the dead weight locations

Figure 5-19 Pulling out of the bottom bar from column B1

Figure 5-20 Column A3 isolated slab-column connection

The test set up of the isolated slab-column connection basically was the same as the unrestrained test presented in Chapter 3. The slab-column connection was simple supported by eight supports as shown in Figure 5-21.

Figure 5-22 shows the load vs. deflection of slab –column connection A3 and C3. Both connections showed about the same initial stiffness. Since the slab-column connections were initially damaged after the column removal test, the initial cracking response is not shown. The punching capacity for isolated slab-column connections A3 and C3 around 84.55kN (19kips) at the deflection of 10.9 mm (0.43in). However, Table 6-1 shows the maximum reaction load on the columns at punching was only 70.3kN (15.79kips), 16.9% less than the tested capacity. The reduction in capacity is due to the unbalanced moment in collapse scenario reducing the punching capacity of slab-column connections.

Figure 5-21 Test set up of isolated slab-column connection C3

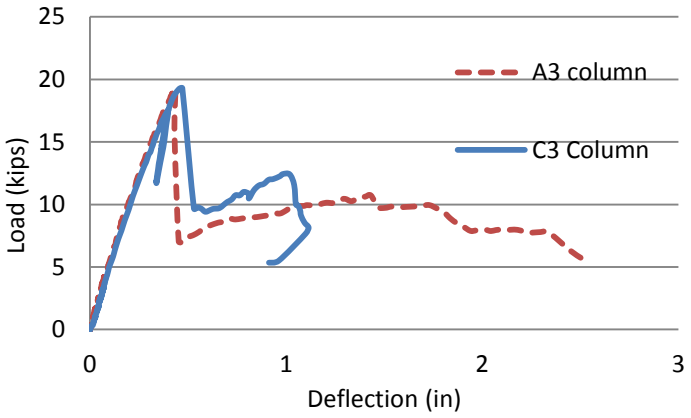

Figure 5-22 Load vs. deflection of column A3 and C3

5.6 Conclusions

For one multi-panel slab subjected to an interior column removal, the slab successfully sustained the applied load after the removal by the post punching capacity. The main conclusions from this test are:

(1) The punching failure happened on the exterior column B1first among all the critical columns in the interior column removal test. This indicates exterior columns could be the most vulnerable ones in an interior column removal case due to lack restraint from the surrounding slabs.

(2) For the specimen tested, punching shear failure did not occur in the compressive membrane phase, but occurred in the tensile membrane phase (at a removed column deflection of 120mm). Therefore under excessive deformation associated with large gravity loads acting on the slab, strength enhancement through compressive membrane action may not be applicable in a column removal scenario.

(3) Punching shear failure occurred at a load level of approximately 51% of the design serice load capacity. Therefore, flat plate structures may be vulnerable to disproportionate collapse.

(4) Punching shear failure occurred on 4 of the surrounding conneciton, but not the other 4 connection. The four connection that did exhibit punching shear failure showed continuted load carrying capacity after failure. Therefore, this multi-panel test result showed that post-punching capacity can play an important role in stopping collaspe of a flat-plate structure.

(5) Dynamic removal of an interior supporting column resulted in a dynamic increase factor (increase over static redistributed loads) of approximately 1.27. This factor is in agreement with the one found in exterior column removal test (1.21). Therefore, surrounding connections need to be able to carry at least 30% more than the predicted redistributed static load in a collapse analysis.

(6) Similar to the exterior column removal results, the maximum strain rates recorded were 0.0138/sec and 0.011/sec for steel and concrete. UFC 340 (2008) would predict the two materials have only a 7% and 10% strength increase due to strain rate effects, respectively. Therefore, this increase in material strength can lead to about 10% increase in the adjacent slab rotations and in the deflection on removed column.

(7) The punching resistance of connections in this column removal test was about 17% less than that from isolated simple supported slab-column connection testing due to unbalanced moments and rotations on the connection in the removal test.

CHAPTER 6 COMPUTER MODELING OF EXTERIOR AND INTERIOR COLUMN REMOVAL

6.1 Introduction

This chapter presents the numerical simulation of exterior and interior column removal tests presented in Chapter 4 and 5. The general commercial software ABAQUS package was used in this analysis. The properties of models are the same as the ones in isolated tests. The element type, material properties modeling, geometry and loading of analytical model are discussed in more details in this chapter. The simulation results were compared with the test results.

6.2 Material Models

6.2.1 Concrete in compression

The concrete compressive strength is usually obtained by concrete cylinder testing. The stress-strain curve relationship suggested by (Hognestad, 1951) is widely used, the model with a uniaxial compressive properties and concrete tension stiffening is presented in Figure 6-1.

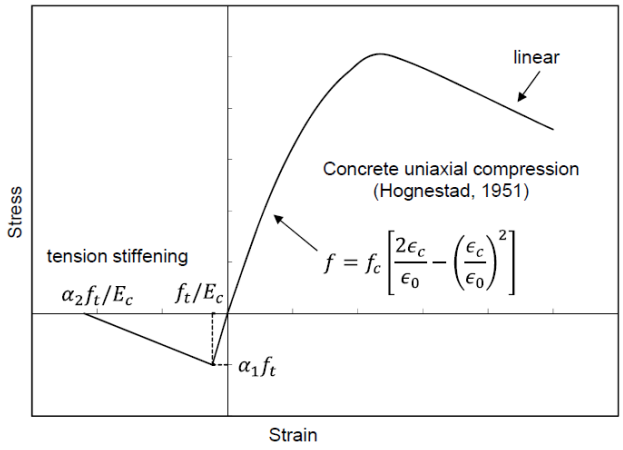

Figure 6-1 Modeling of uniaxial stress-strain relationship of concrete (Hognestad, 1951)

The concrete damaged plasticity has been used to simulate the concrete properties.

This plasticity model is developed with the damaged variables that account for the stiffness degradation associated with concrete cracking and crushing with the following formula.

$$\sigma_{ij} = (1 - d)D^{e}_{ijkl}(\varepsilon_{ij} - \varepsilon^{p}_{ij})$$

Where σ_{ij} is the stress tensor, ε_{ij} and ε^{p}_{ij} are the total strain tensor and plastic strain tensor, D^{e}_{ijkl} is the initial elasticity matrix and d is the damage variable, which ranges from zero (undamaged material) to one (fully damaged material). The advantages of concrete damaged plasticity over concrete smeared cracking are as follows:

1) Concrete damaged plasticity model was developed to provide a general capability for the analysis of concrete structures under cyclic and/or dynamic loading. It's able to implement rate-sensitivity analysis under fast loading. 2) Concrete damaged plasticity model is applicable of both implicit and explicit algorithms. And the explicit algorithm is a powerful tool to overcome divergence problem in a dynamic analysis. Therefore, the concrete damaged plasticity was used in disproportionate collapse analyses in the current study.

6.2.2 Concrete in tension

For reinforced concrete the tension stiffening describes the decrease in tensile force after cracking, Tension stiffening used in this study took the form of a linear post- failure stress-strain relationship shown in Figure 6-2., where σ^{u}_{t} denotes the uniaxial tensile strength of concrete, E_o Young's modulus of concrete, and ε_u the tensile strain at which stress is reduced to zero

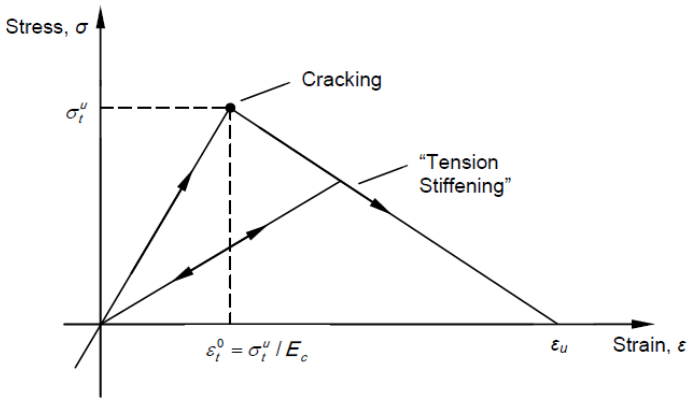

Figure 6-2 Modeling of concrete tension softening model of concrete

6.2.3 Reinforcement Steel

Slab flexural reinforcement is modeled as uniaxial material, a bilinear stress-strain relationship is assumed for reinforcing bar by specifying yield stress f_y, yield strain ε_y, and ultimate stress f_u and ultimate strain ε_u from rebar testing. The slab flexural reinforcement was modeled by a rebar layer. Through this option, the equivalent "smeared" orthotropic steel layers were generated according to the actual bar area, spacing, orientation, and location along the slab depth. Totally four layers of reinforcement, two in each direction, to model the top and bottom mats of rebar.

6.3 The Finite Element Model

6.3.1 Macromodel

The slab-column joint region is modeled by rigid shell elements. Consistent with ACI 318-14 (2014) provisions for two-way shear, a punching perimeter was assumed at half slab effective depth away from slab-column joint. Thin shell elements is used to simulate the slab outside of the punching perimeter and are defined with rebar layers and nonlinear material

properties. Due to the high-computational cost of solid element, a shell element was used to model the reinforced concrete slab, S4R: A 4-node doubly curved general propose shell S4R with reduced integration and finite membrane strains was used for the simulation.

The small portion of slab between joint and punching perimeter is simulated by two connector beam elements on each side of a joint. The connectors transfer forces associated with six degrees of freedom from slab to column, in which primary bending moment and torsion were defined with nonlinear behaviors and shear with linear behavior. More detail can be found in the paper (Liu et al. 2014).

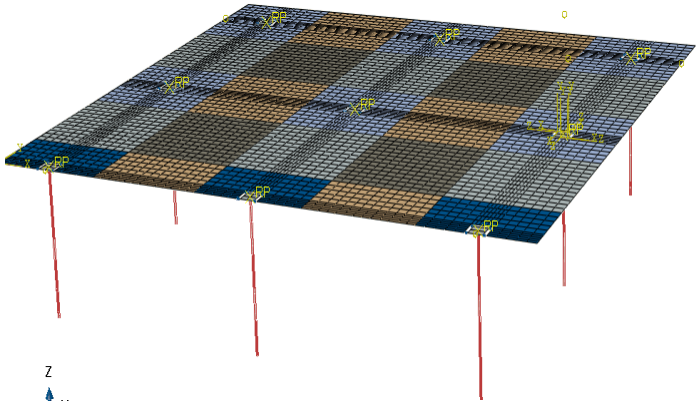

Figure 6-3 FE model of the specimens

6.3.2 Simulation procedure

To simulate the effects of sudden loss of the supporting columns in two tests (exterior and interior column removal), the recorded reaction forces from the test existing at this column before the removal was statically applied on column A1 while maintaining the gravity loads, then dynamic analysis is carried out by releasing the reaction forces at a rate recorded from the tests.

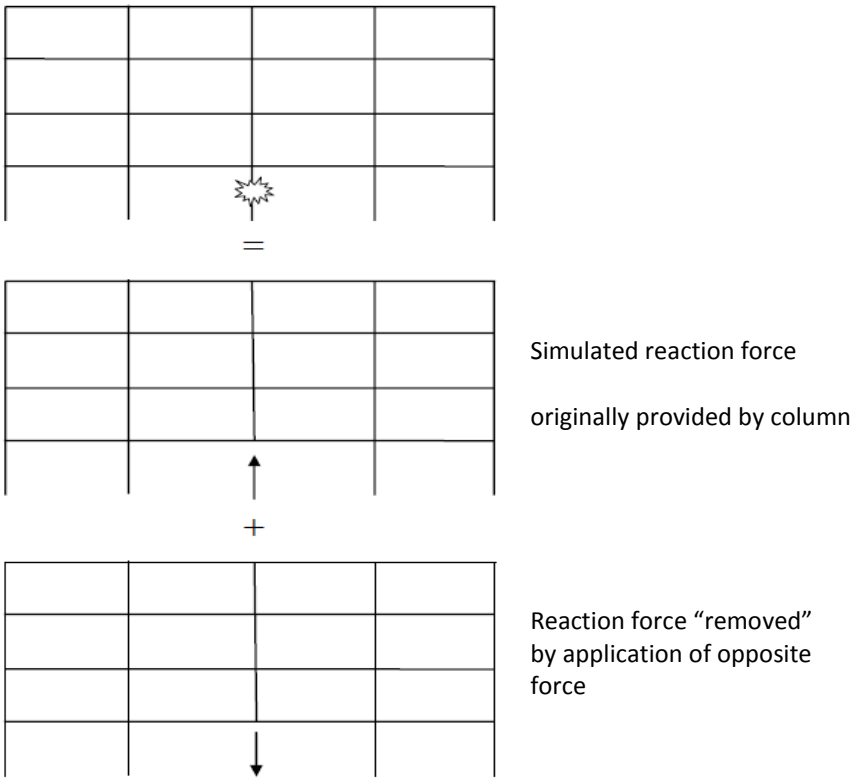

Figure 6-4 Simulation procedures

6.4 Exterior Column Removal Simulation

The first drop of exterior column removal test was simulated by the FE model. The overall simulated response of the specimen was then compared with the test results.

6.4.1 Load and deflection response

Figure 6-5 shows the deflection contour of the slab at the peak deflection and the comparison between test and simulation results is shown in Figure 6-6. The FE model was able to predict 29.3 mm (1.15 in.) of deflection in 0.1sec at column B1 while the deflection from the test was 28.9 mm (1.137 in.) in 0.14sec. As it can be seen in Figure 6-6, the slope matched well until the deflection reached about 18mm (0.71in.) then the result from the test showed a little

stiffness deterioration while it did not show in the FE simulation results, This is because the computer model cannot track the stiffness deterioration of slab due to the cracking and tension softening of concrete accurately.

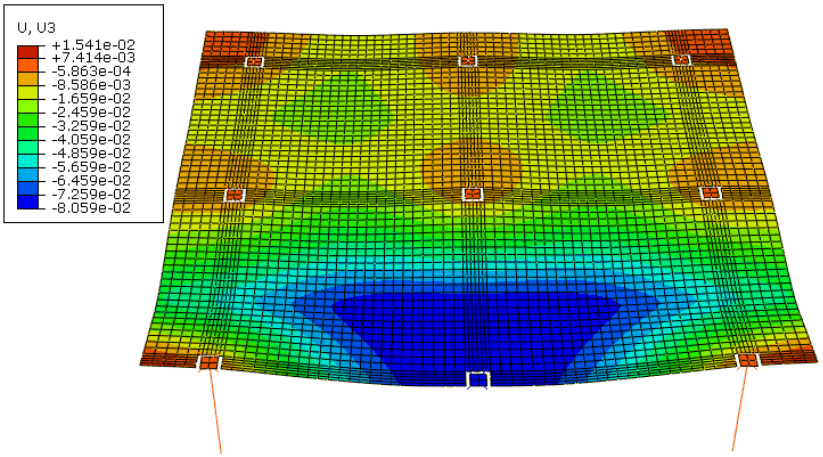

Figure 6-5 Deflection contour of the slab at the peak deflection (unit: ft)

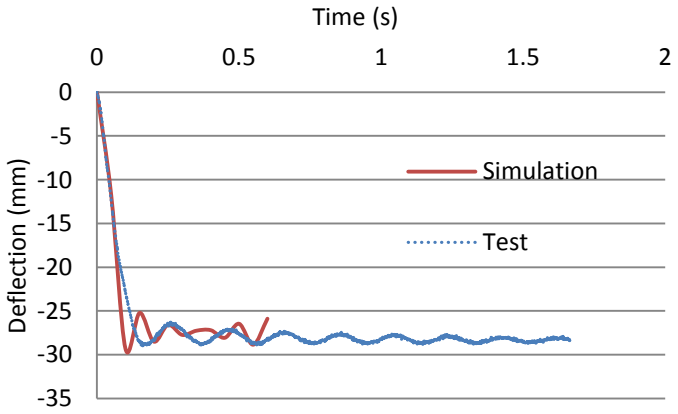

Figure 6-6 Comparison of deflections between simulation and test in the first drop

The comparison of deflections for the second drop test is shown in Figure 6-7. Even though the concrete plastic damage model used for this simulation is able to account for the cracking of concrete by inputting concrete compression and tension damage parameters, the model was unable to track the deterioration of slab stiffness due to the accumulated damage of

cracking from the first drop. The peak deflection 96 mm (3.78in.) from simulation was 6.78% more than that from the test result.

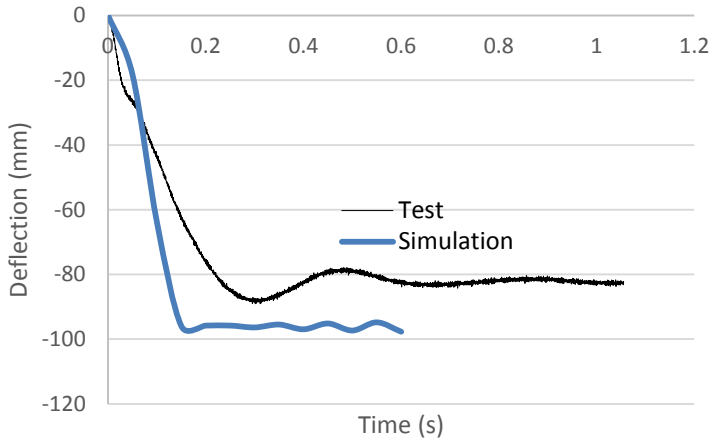

Figure 6-7 Comparison of deflection in the second drop for the exterior column removal.

6.4.2 The axial load in columns

Figure 6-8 and Figure 6-9 provide redistributed load on columns from test and FE simulation results for the first drop test, respectively. The simulation results have a good agreement with the redistributed peak loads in the columns right after the removal of exterior column, however, the calculated irregular vibration mode of slab from FE model leads to errors.

The simulation results also confirm the loss of load on column A2, because the whole slab panel (Column A1, A2, B2 and B1) was bending along the column line A1 and B2 when the column B1 was falling due to the removal of support, so the slab panel around column A2 had a tendency to rotate upward showing a loss of 3.87 kN (0.87 kips) in the simulation and 5.29 kN (1.19 kips) in the test at the peak point. Table 6-1 gives the peak redistributed loads on the columns for both the test and simulation. In general there was a 23.8% error on average between the test and simulation results.

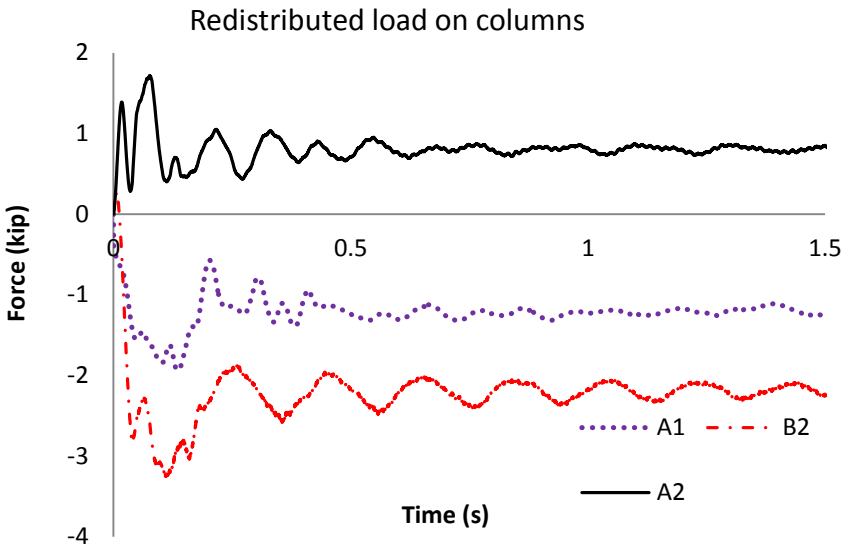

Figure 6-8 Redistributed load on columns in the first drop test from test results

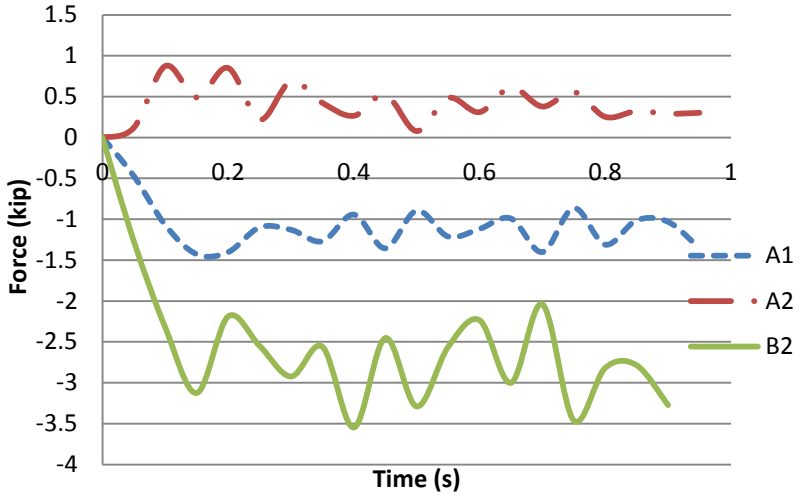

Figure 6-9 Redistributed load on columns in the first drop test from FE simulation

Table 6-1 Redistributed peak load on columns

	First drop			Second drop		
Tests	column A1	column A2	column B2	column A1	column A2	column B2
Simulation	-1.4	0.87	-3.125	-2.15	1.6	-2.96
test	-1.85	1.19	-3.10	-2.31	1.87	-3.74
Error	24.3%	26.8%	0.8%	6.9%	14.4%	20.8%

Figure 6-10 shows redistributed load on columns in the second drop from test and simulation results, respectively. The change in steady state load after column B1 removal for columns A1, A2 and B2 was 7.25 kN (1.63 kips), -3.65 kN (-0.82 kips) and 11.6 kN (2.6 kips) from the test results while it was 6.85 kN (1.54 kips), 4.85kN (-1.09 kips), 11.3 kN (2.56kips) from simulation results, respectively. Therefore FE model can predict the load redistribution well with a 23.8% of difference from test.

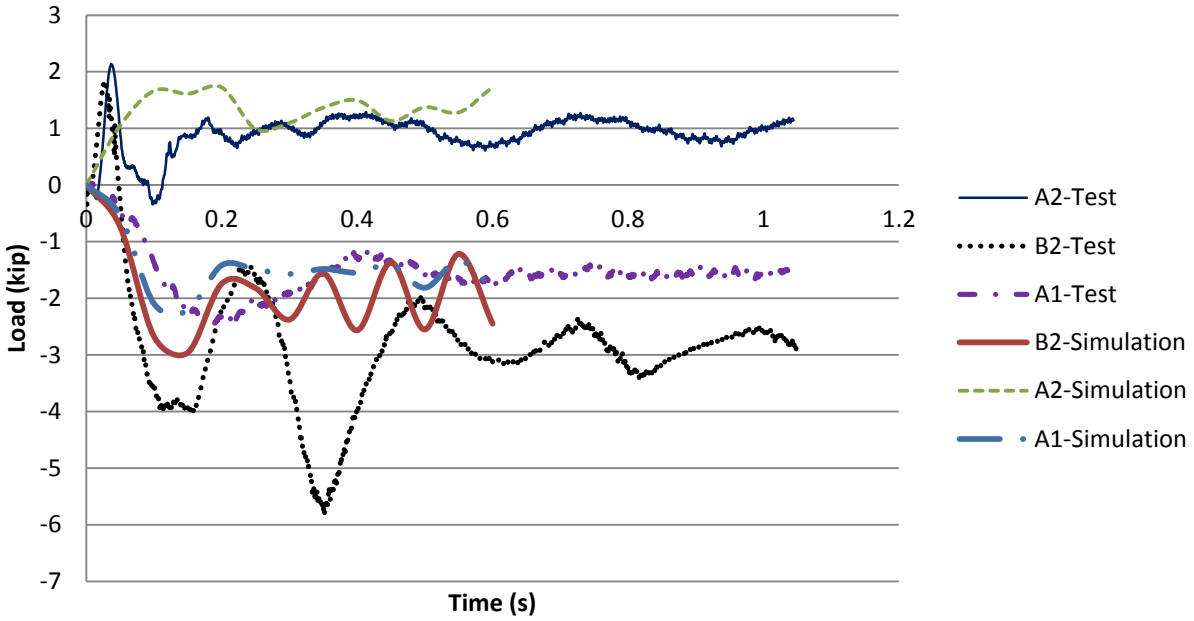

Figure 6-10 Redistributed load on columns in the second drop from test results

6.4.3 Rotation of slab

Figure 6-11 and Figure 6-12 provide the contour of slab rotation around two axes. Column A1 and C1 have the maximum rotation 0.01985 rad around axis-1 after the removal of column B1 and center column B2 has a rotation of 0.01842 rad. In addition, the rotation of A2 and C2 are much smaller. Column A1 and C1 have the maximum rotation 0.01533 rad around axis-2 but this rotation is too small to fail the slab-column connection.

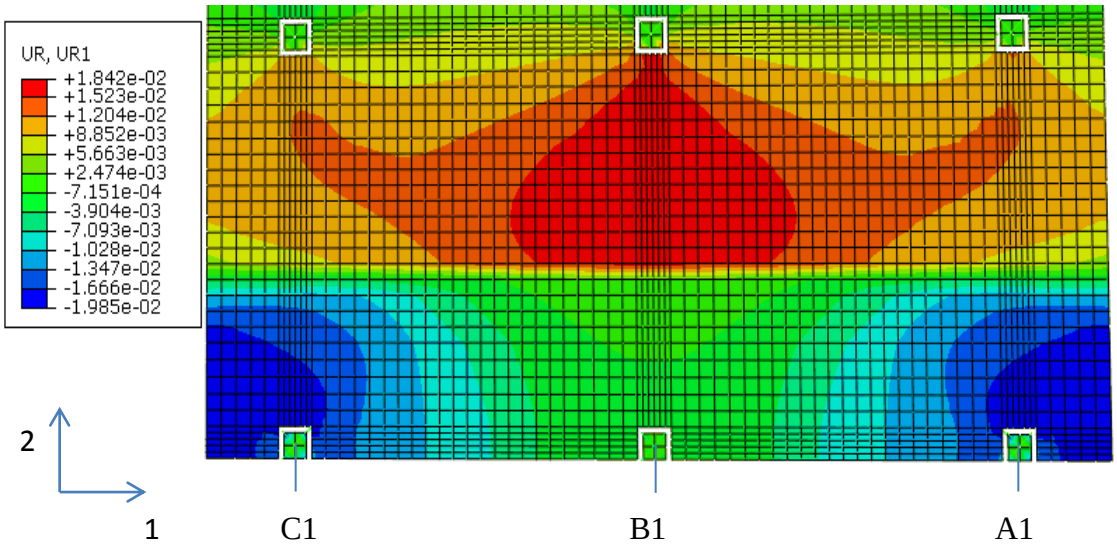

Figure 6-11 Slab rotation around axis-1 (unit: rad)

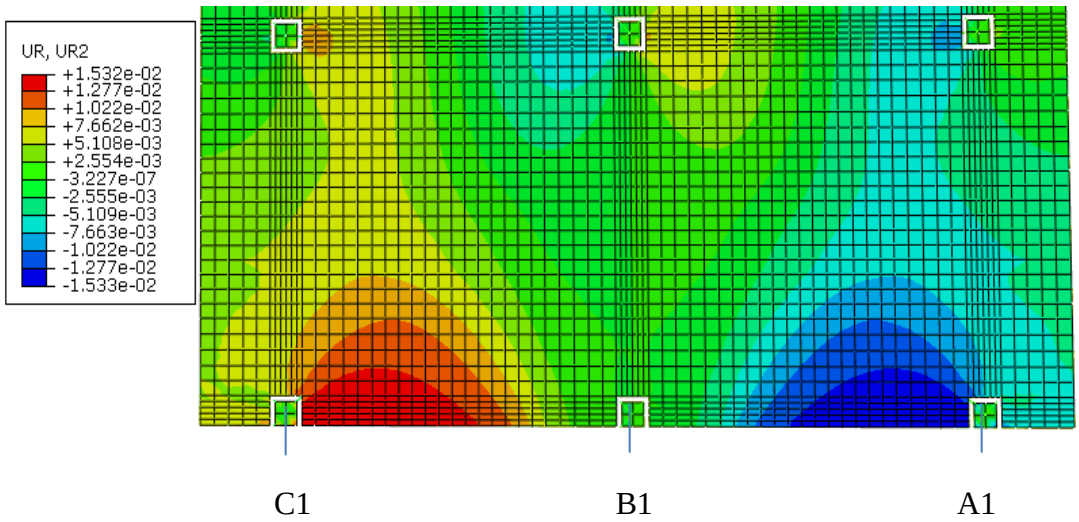

Figure 6-12 Slab rotation around axial-2 (unit: rad)

6.5 Interior Column Removal Simulation

6.5.1 Load and deflection response

The predicted deflection vs. time relationship is shown in Figure 6-13. As can be seen in the figure the deflection curve from experiment is cut off at the punching failure point due to the fact that the FE model is only able to predict the behavior prior to punching failure. The

simulation resulted did reflect the behavior of the slab after the removal of center column B2. The difference in slopes between the test and predicted results is due to the different slab stiffness mainly decided by the concrete stiffness. However, tracking the concrete stiffness is a challenge with FE method. In addition, as stated in Chapter 5 the cracks were seen when doing the application of dead load, making it even more difficult to predict the concrete initial stiffness prior to the testing.

The predicted peak deflection at removed column is 101mm (3.98 in), which is 18.5 % less than the deflection from test result124 mm (4.88 in.). Figure 6-14 shows the deflection contour around center column B2. As it can be seen the contour is unevenly distributed along the column line A2–C2. The slab is not symmetric along the axis and the exterior columns have less restraint from the surrounding slabs, therefore the exterior columns experienced more rotation as will be later.

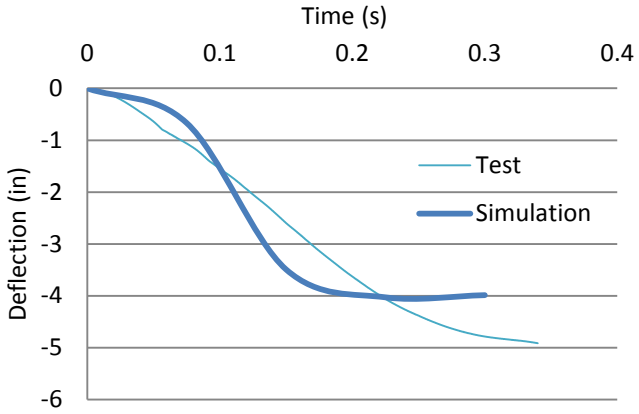

Figure 6-13 Simulation of deflection before punching failure

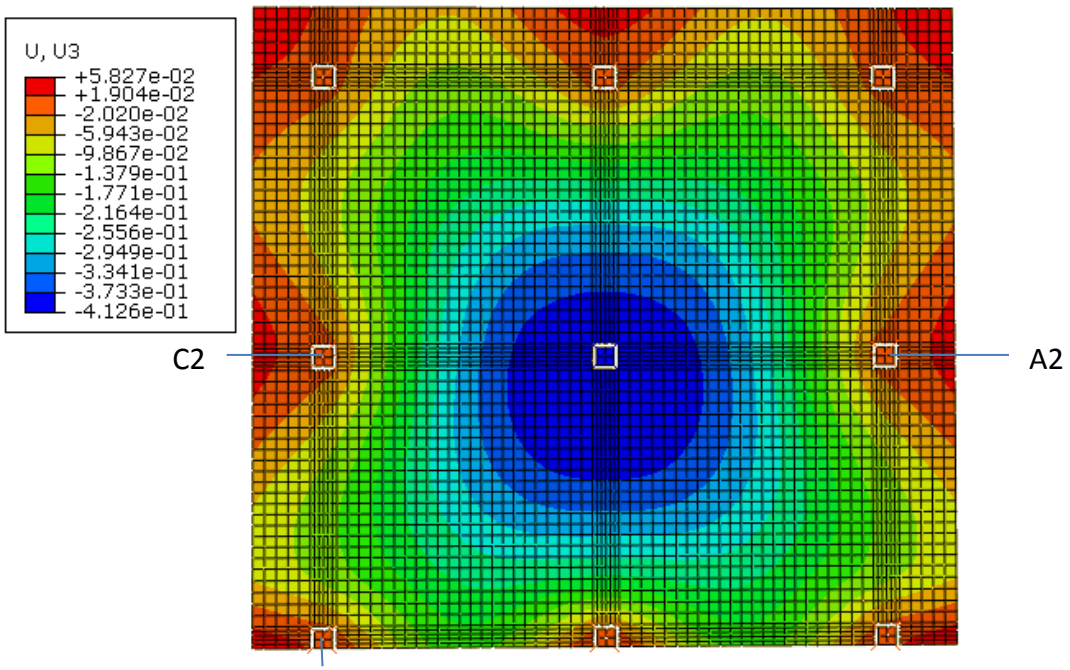

Figure 6-14 Vertical deflection of slab subjected to removal of center column B2 (unit : ft)

6.5.2 Compressive membrane force

Figure 6-15 and Figure 6-16 show the slab in-plane force at two directions at the peak deflection. The negative value means concrete in compression. After the removal of column B2, the slab in the vicinity of connection B2 is subjected to tension while most areas near to the other columns is under compression. It can be found from Figure 6-15 and Figure 6-16 that the in-plane tension membrane force along column line B1 and B3 is larger than that along the column line A2 and C2. This shows tension membrane force along column B1 an B3 is the main load carrying mechanism, therefore, B1 and B3 are damaged more seriously over the removal test as has been discussed in Chapter 5.

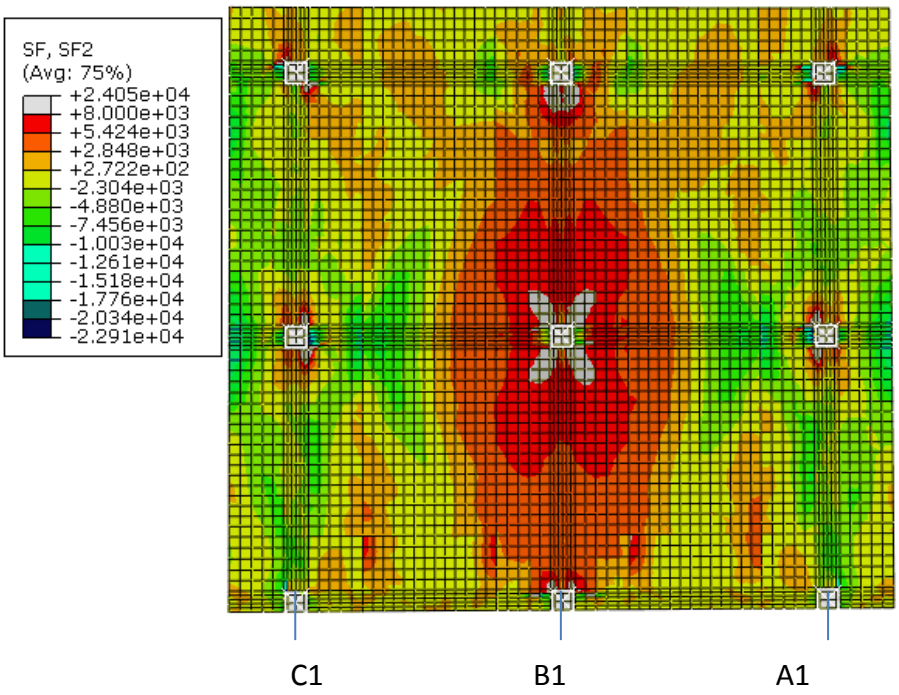

Figure 6-15 Slab in-plane force at direction 2 at the peak deflection

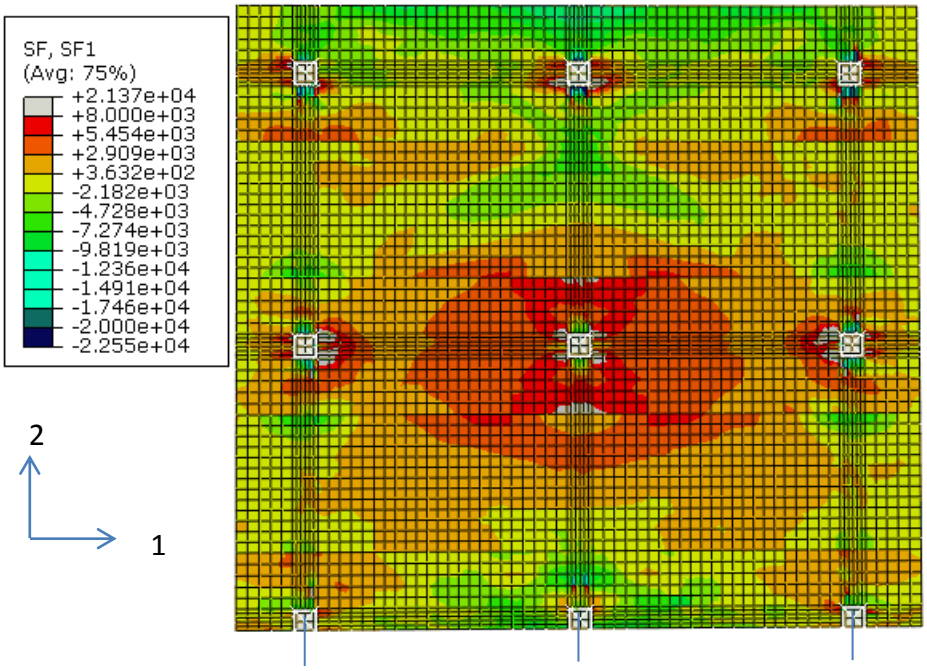

Figure 6-16 Slab in plane force at direction 1 at the peak deflection

6.5.3 Axial load on columns

Figure 6- 17 shows the axial load on columns before and after the column removal. Since column A2 and B3 have the same load tributary area, the overall load response of two columns are similar as can be seen in the figure. Column B1 has about half the load response as column A2 and B3 due to its being an exterior column.

The maximum load on the columns after the removal of column is around 16 kips, however, the punching failure threshold of this size of slab-column connection without lateral restraint should be 19 kips as discussed in Chapter 5. The failure did happen on those column over the test due to two reasons: (1) punching failure is localized failure, once one area failed because of unbalance moment or rotation then the failure will propagate around the connection causing the failure of the whole connection, therefore, failure is controlled by the single connector in the model, not by total load response on columns. (2) Rotation of slab is critical to the punching failure. It needs to reach a threshold, then punching failure can happen.

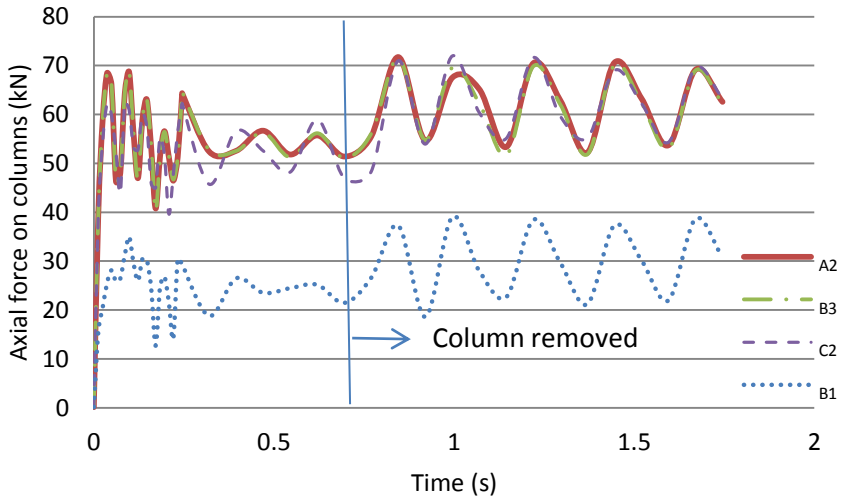

Figure 6- 17 Axial load on columns

6.5.4 Strain rate effects

The effects of strain rate on material properties are not considered in the DoD guideline (2009) and were neglected in almost all past studies. The test results in Chapter 4 and 5 show the recorded strain rates would predict 7-10% of steel strength increase and about 10% of concrete strength increase according to UFC 340 (2010).

Figure 6-18 shows the effects of strain rates on the deflection of removed column B2. Since with increased strain rates the material strength increases and the slab is stiffer indicated by the slightly different slopes in two curves. The column deflection is 10.3% less with strain rate effects than that without strain rate effects.

Figure 6-19 and Figure 6- 20 show the effects of strain rate on the slab rotations. The initial points of curves in the figure are the rotation due to the static loading prior to the testing. As can be seen in the figure slab rotation around column B1 is almost twice as much as that around column B3 due to the fact that column B1 is an exterior column and has much less restraint from the surrounding structural members. In addition, the rotations of slab around both columns reduced by 10% due to the strain rate effects.

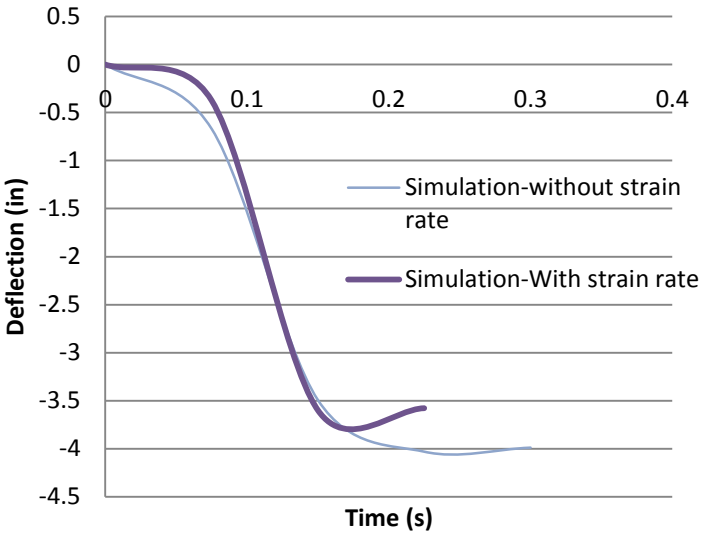

Figure 6-18 Strain rate effects on deflection of removed column B2

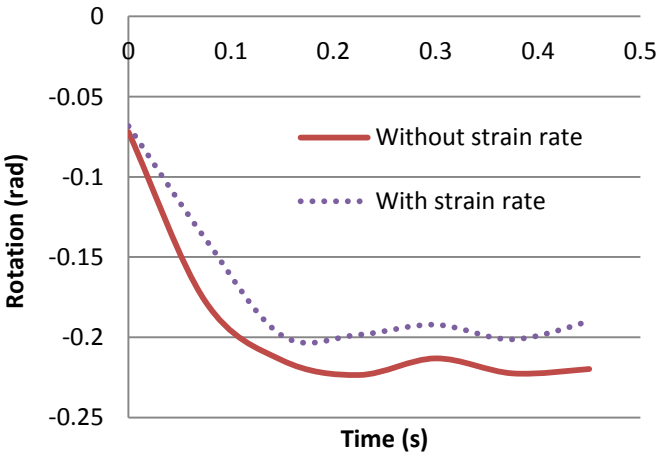

Figure 6-19 strain effect on the slab local rotation near column B1

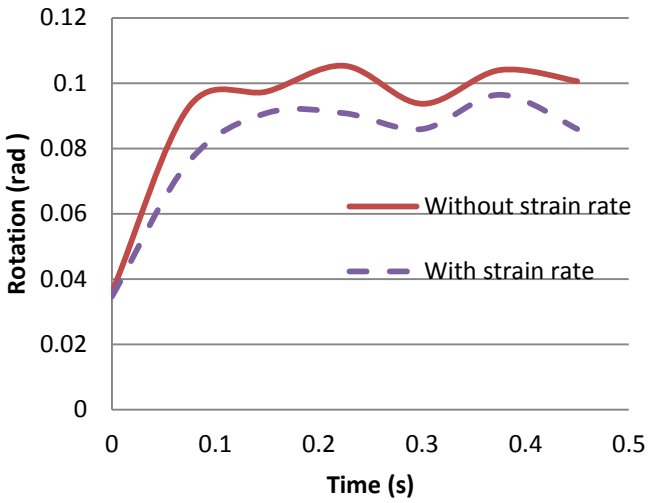

Figure 6- 20 Strain effect on the slab local rotation near column B3

6.6 Conclusion

The FE model results were compared with the test results for exterior and interior removal cases in term of deflections of removal the columns, the redistributed load on columns and rotation of slab. The model generally can simulate the behavior of slabs subjected to column removal. The main conclusions for this chapter are:

(1) 10% increase in material strength can lead to about 10% increase in slab rotation and deflection on removed column.

(2) For interior column removal case the in-plane stress of slab around removed column is in tension but compressive membrane force is dominant force in the slab around the adjacent columns.

(3) The FE model generally can capture the behavior of slab in the column removal case with less than 28% of difference overall.

CHAPTER 7 SUMMARY AND CONCLUSIONS

7.1 Summary

The overall goal of this research is to evaluate the potential of dynamic disproportionate collapse in older reinforced concrete flat-plate structures subjected to a sudden loss of a supporting column. The main objectives of this research include:

(1) Evaluate effects of in-plane lateral restraint and reinforcement ratio on slab loading-carrying capacity and deformation capacity.

(2) Study the post-punching behavior, especially the capacity of developing tensile membrane action, of slab column connections with discontinuous slab bottom compressive reinforcing bars through columns.

(3) Evaluate potential of disproportionate collapse of flat-plate structures subjected to large deformations due to the loss of a supporting column.

(4) Provide experimental data for characterizing failure propagation over entire structure and for developing and validating analytical models.

In order to accomplish the research objects a series of experimental tests and analyses were conducted. The research consisted of six isolated slab-column connection tests, one exterior multi-panel column removal test, one interior multi-panel column removal test, and a computer model to predict punching shear failure in flat-plate structures. The main conclusions from each are summarized below.

7.2 Results from tests and simulations

7.2.1 Isolated slab-column connection test

The six isolated slab-column connection tests provided insight on the effects of in-plane restraint on punching resistance and identified the post-punching behavior of slab-column connections in older flat-plate buildings. In addition, numerical simulations using a macromodeling approach were carried out to further study the effects of compressive membrane action and its contribution to disproportionate collapse resistance. The following conclusions were reached from the experiments:

(1) With the lateral restraint achieved in the tests, compressive membrane actions was found to increase the punching capacity of slab-column connections by 9.5%.

(2) After punching, the slab-column connections without structural integrity reinforcement could maintain only about 50% of the failure load. Moreover, this residual capacity decreased dramatically as the deformation increased.

(3) Anchoring the tensile reinforcement into the slab enabled the slab-column connections to obtain 80% of punching failure load as post-punching load-carrying capacity. Thus, effectively anchoring slab tensile reinforcement using hooks provides an alternative practical approach for mitigating failure propagation.

The following conclusions were reached from the numerical simulations:

(4) The macromodel employing thin shell elements and connector elements effectively simulated the behaviors of both 12 unrestrained and restrained slab-column connections subjected to concentric gravity loading.

(5) The effects of compressive membrane action were a function of the level of in-plane restraints and slab reinforcement ratio. Fully restrained slab-column connections

would lead to overestimated punching resistance. For a flat-plate system, the restraint associated with slab continuity could increase the static punching resistance by 34.5% and 58.4% for slabs with tensile reinforcement ratio of 1% and 0.64%, respectively.

(6) The strength enhancement contributed by compressive membrane action could significantly increase the resistance of flat-plate structures to disproportionate collapse. The analyses indicated that, for slabs with a reinforcement ratio of 1%, the compressive membrane action could increase the gravity loading capacity by 20% under dynamic loading caused by instantaneous removal of a supporting column.

7.2.2 Exterior column removal test

Dynamic testing of a multi-panel slab specimen simulated the loss of a supporting exterior column to determine the potential of disproportionate collapse of flat- plate structures without integrity reinforcement. Three drop tests were conducted at different load levels in specimen. The load redistribution, dynamic amplification factor, and potential for progression punching shear failure were analyzed.

The main conclusions are:

(1) Compressive membrane forces were verified in the multi-panel specimen with 1.54 mm (0.059in.) maximum outward lateral movements on columns and measured compressive strains in the concrete.

(2) Compressive membrane forces form after a column removal and gradually transition to tension membrane forces after the deflection at the removed column approaches 4% of the span length (98mm/2440mm) or exceeds the slab depth (89mm). However, preexisting damage in flat slab structures (from prior overloading or shrinkage cracking) may impede the formation of compressive membrane forces in the slab.

(3) Dynamic removal of an exterior supporting column resulted in a dynamic increase factor (increase over static redistributed loads) of approximately 1.21. Therefore, surrounding connections need to be able to carry at least 21% more than the predicted redistributed static load in a collapse analysis.

(4) The recorded rotation on the center column B2 in second drop is 36.6% more than the predicted rotation at failure by Muttoni's formulation (2008) in an isolated slab-column connection. Therefore, the rotation at failure in the multi-panel may be more than predicted.

(5) The maximum strain rates recorded in the first two drops were only 0.0219/sec and 0.00873/sec for steel and concrete. UFC 340 (2008) would predict the two materials have only a 2% and 10% strength increase due to strain rate effects, respectively. Therefore, this increase in material strength can lead to about 10% increase in the adjacent slab rotations an in the deflection on removed column.

(6) Disproportionate punching shear failures did not occur at load levels of 4.84 kN/m² (100 psf) and 7.18 kN/m² (150 psf) corresponding to approximately 40% and 52% of the design service load, although it is believed that failure was close to occurring after the second drop. Failure did occur at a level of 9.86 kN/m² (206 psf), 67% of the design service load.

7.2.3 Interior column removal test

For the interior column removal case a multi-panel specimen was also tested. The possibility of post punching capacity to arrest disproportionate collapse and progression of punching failure over an entire slab was studied. The main conclusions from this test are:

(1) The punching failure happened on the exterior column B1first among all the critical columns in the interior column removal test. This indicates exterior columns could be the most vulnerable ones in an exterior column removal case due to lack restraint from the surrounding slabs.

(2) For the specimen tested, punching shear failure did not occur in the compressive membrane phase, but occurred in the tensile membrane phase (at a removed column deflection of 120mm). Therefore, under excessive deformation associated with large gravity loads acting on the slab, strength enhancement through compressive membrane action may not be applicable in a column removal scenario.

(3) Punching shear failure occurred at a load level of approximately 51% of the design serice load capacity. Therefore, flat plate structures may be vulnerable to disproportionate collapse.

(4) Punching shear failure occurred on 4 of the surrounding conneciton, but not the other 4 connection. The four connection that did exhibit punching shear failure showed continuted load carryin capacity after failure. Therefore, this multi-panel test result showed that post-punching capacity can play an important role in stopping collaspe of a flat-plate structure.

(5) Dynamic removal of an interior supporting column resulted in a dynamic increase factor (increase over static redistributed loads) of approximately 1.27. This factor is in agreement with the one found in exterior column removal test (1.21). Therefore, surrounding connections need to be able to carry at least 30% more than the predicted redistributed static load in a collapse analysis.

(6) Similar to the exterior column removal results, the maximum strain rates recorded were 0.0138/sec and 0.011/sec for steel and concrete. UFC 340 (2008) would predict the two materials have only a 7% and 10% strength increase due to strain rate effects, respectively. Therefore, this increase in material strength can lead to about 10% increase in the adjacent slab rotations and in the deflection on removed column.

(7) The punching resistance of connections in this column removal test was about 17% less than that from isolated simple supported slab-column connection testing due to unbalanced moments and rotations on the connection in the removal test.

7.2.4 Computer simulations

A FEM computer model was calibrated by the test results and used to analyze failure propagation in flat-plate structures. The main conclusions from the analyses are:

(1) 10% increase in material strength can lead to about 10% increase in slab rotation and deflection on removed column.

(2) For interior column removal case the in-plane stress of slab around removed column is in tension but compressive membrane force is dominant force in the slab around the adjacent columns.

(3) The FE model generally can capture the behavior of slab in the column removal case with less than 28% of difference overall.

7.3 Conclusions

Based on all the six isolated tests, two multi-panel column removal tests and computer simulations, the main conclusion can be summarized as below:

(1) The effects of compressive membrane action on punching capacity are a function of the level of in-plane restraints and slab reinforcement ratio. Theoretically for a flat-plate

system, the lateral restraint stiffness associated with slab continuity could increase the static punching resistance by 34.5% and 58.4% for slabs with tensile reinforcement ratio of 1% and 0.64%, respectively. However, compressive membrane forces that form after a column removal gradually transition to tension membrane forces at deflections that exceed the slab depth and preexisting damage in flat slab structures (from prior overloading or shrinkage cracking) may impede the formation of compressive membrane forces in the slab. Because punching shear failure generally occurs at much greater removed column deflections there may be little to no compressive membrane enhancement of a slab column connection in a disproportionate collapse analysis.

(2) Based on strain rates measured during the multi-panel tests, strength increase factors for steel and concrete in the test are approximately 1.07 and 1.1, respectively. This increase in material strength can lead to about 10% increase in the adjacent slab rotations and in the deflection on removed column.

(3) Dynamic removal of an exterior supporting column resulted in a dynamic increase factor (increase over static redistributed loads) of approximately 1.3. Therefore, surrounding connections need to be able to carry at least 30% more than the predicted redistributed static load in a collapse analysis.

(4) Post-punching capacity can be effective way of arresting the disproportionate collapse of flat plate structures and was able to stop the collapse of the exterior multi-panel column removal test. Post punching capacity is enhanced if the top reinforcement is anchored into the slab.

(5) The FEM computer model was able to predict the punching behavior of the isolated connection tests and was able to predict the response and failure load of the multi-panel column removal tests.

(6) Punching shear failure occurred in both multi-panel tests around 51% of the design service load capacity. Therefore, flat plate structures may be vulnerable o disproportionate collapse.

7.4 Future Research

(1) The older flat plate structures have certain percentage of post punching capacity. The proposed computer model needs to be updated so that it's able to predict the post punching capacity in older and new flat plate structures and be able to analyze if that capacity is sufficient to arrest collapse of the structure.

(2) The effects of lateral restraint to punching capacity can be more quantitatively studied with different slab thickness, reinforcement ratio, etc.

(3) The multi-panel specimen tested was only 0.4 scale. Size effects on behavior of slab-column connection and multi-panel slab from prototype to the test specimen is unknown. More work needs to be done in specimens closer to full scale.

(4) Because this research has shown that flat plate structures are vulnerable to disproportionate collapse, mitigation methods need to be developed that can efficiently enhance the collapse resistance of these structures.

APPENDIXES

Reinforcement detailing for two-way slab (Figure reproduced from (ACI 318-1971))

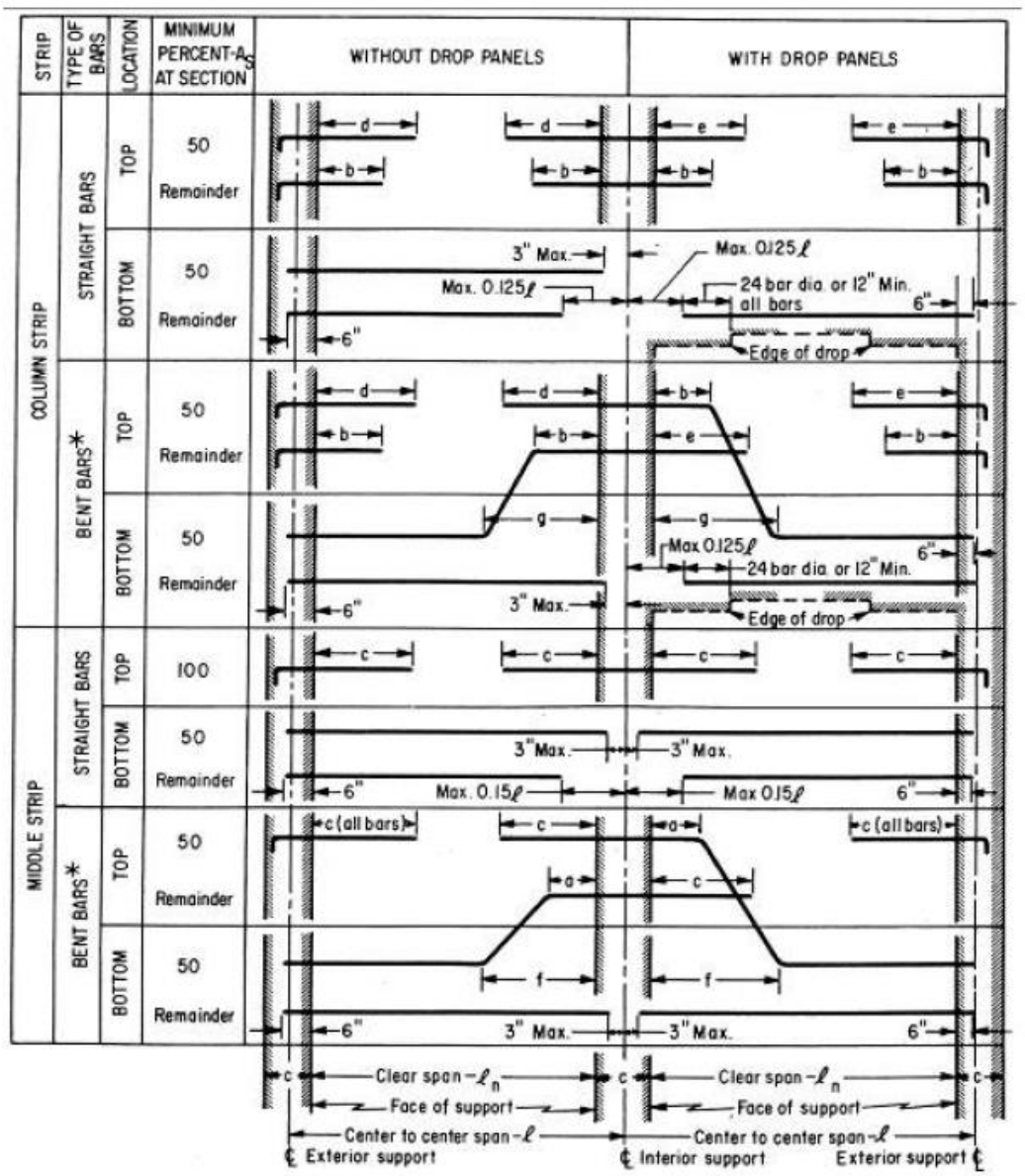

* Bent bars at exterior supports may be used if a general analysis is made

	BAR LENGTH FROM FACE OF SUPPORT						
	MINIMUM LENGTH					MAXIMUM LENGTH	
MARK	a	b	c	d	e	f	g
LENGTH	$0.14\ell_n$	$0.20\ell_n$	$0.22\ell_n$	$0.30\ell_n$	$0.33\ell_n$	$0.20\ell_n$	$0.24\ell_n$

Fig. 13.5.6—Minimum length of slab reinforcement, slabs without beams
(See Section 12.2.1 regarding extending reinforcing into supports)

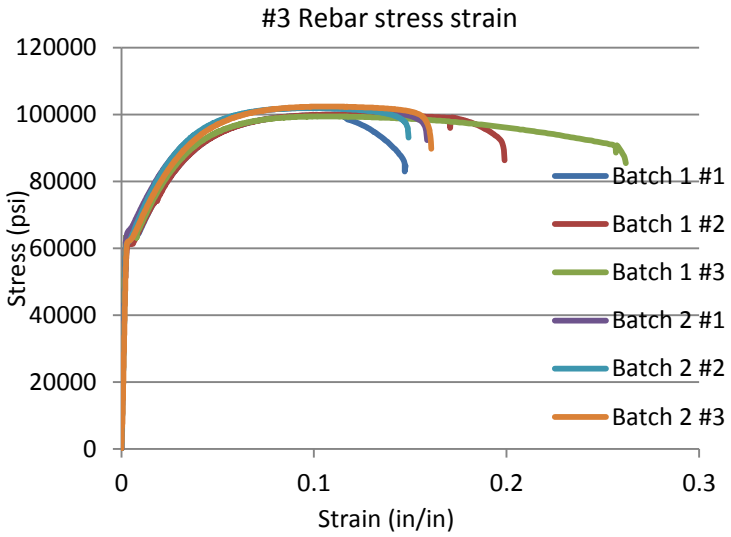

Figure 1 Stress – Strain plots recorded using an MTS machine during the tensile testing of the #3 rebar samples.

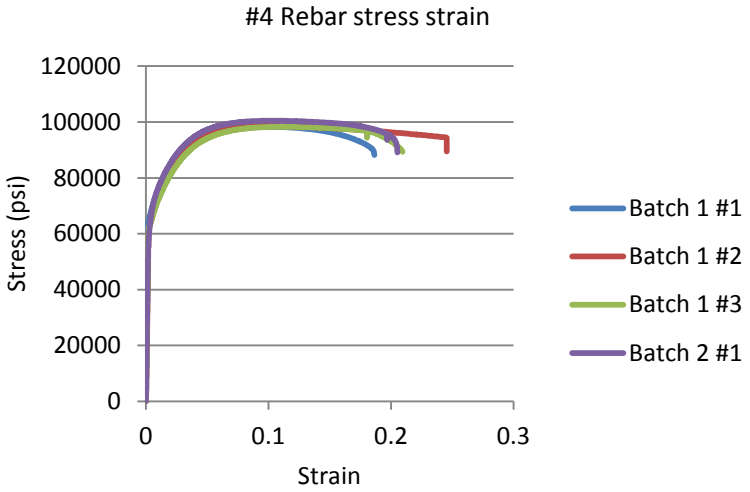

Figure 2 Stress – Strain plots recorded using an MTS machine during the tensile testing of the #4 rebar samples.

Table 1Summary of concrete compressive strengths for each of the four slab specimens (psi)

Slab Specimen	1.0RE	1.0UN	0.64UN	0.64RE	0.64RE-NH	0.64RE-NH2
Cylinder #1 f_c	4944	4476	4793	6450	4534.6	5510
Cylinder #2 f_c	5327	4410	4631	6412	4285.0	5289
Cylinder #3 f_c	5302	4981	4449	6481	4341.2	5302
Cylinder #4 f_c	5723	5042	4748	6332	3859.9	5330
Cylinder #5 f_c	5384	4922	4789	-	-	-
Cylinder #6 f_c	5007	5221	4818	-	-	-
Average f_c	5281	4842	4705	6418	4255	5358

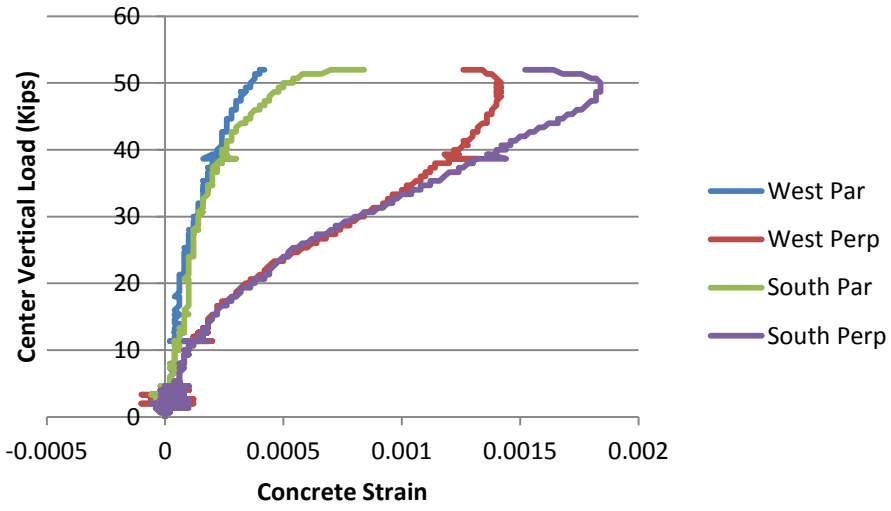

0.64UN

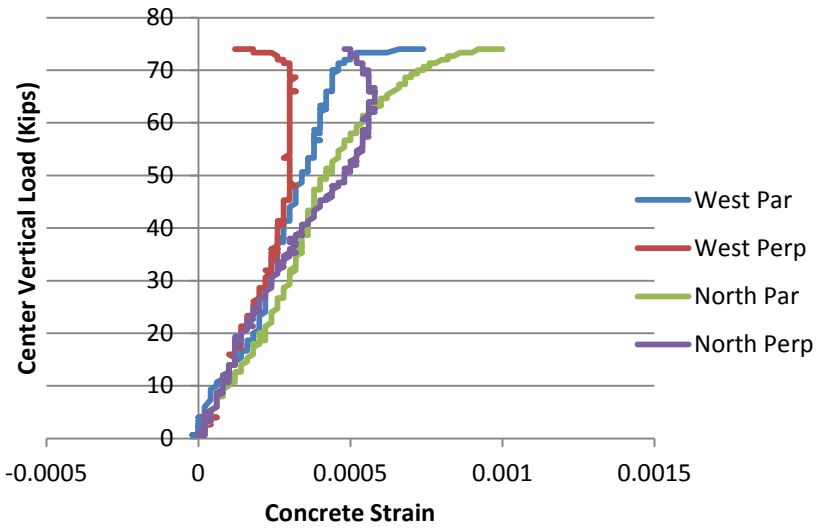
Center Vertical Load (Kips)
80
70
60
50
40
30
20
10
0
-0.0005
0
0.0005
0.001
0.0015
Concrete Strain
West Par
West Perp
North Par
North Perp

1.0RE

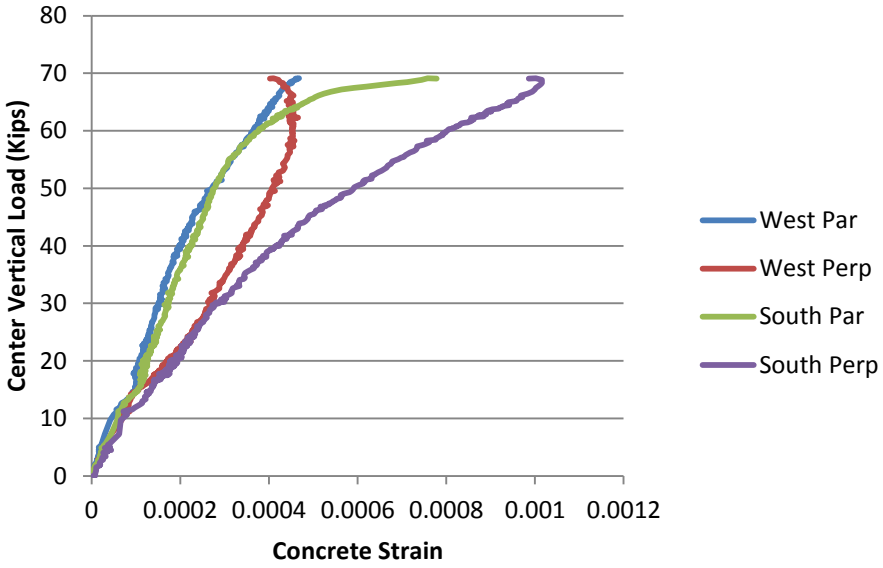
Center Vertical Load (Kips)
80
70
60
50
40
30
20
10
0
0
0.0002
0.0004
0.0006
0.0008
0.001
0.0012
Concrete Strain
West Par
West Perp
South Par
South Perp

1.0UN

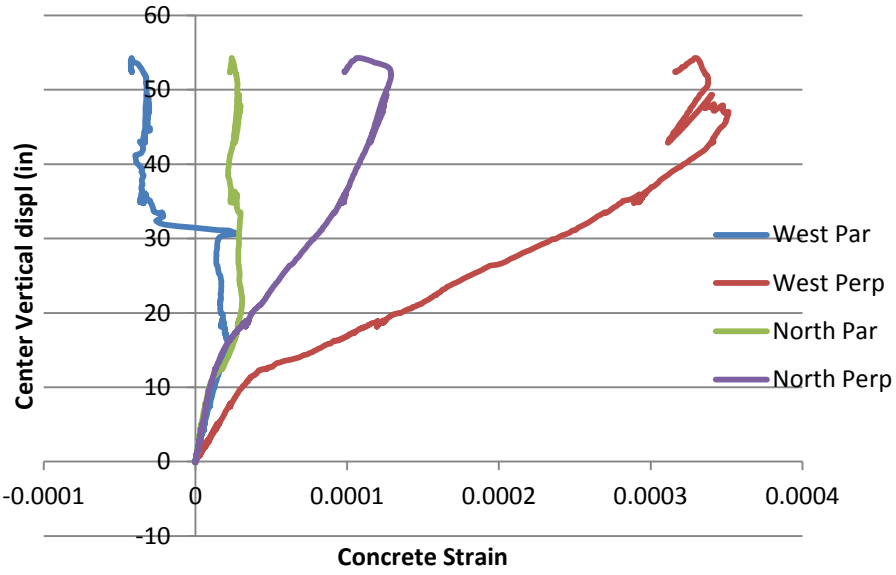
60
50
40
30
20
10
0
-10
-0.0001
0
0.0001
0.0002
0.0003
0.0004
Center Vertical displ (in)
Concrete Strain
West Par
West Perp
North Par
North Perp

0.64UN-NH

REFERENCE

ACI Committee 318, “Building Code Requirements for Reinforced Concrete (ACI318-89) and Commentary (318R-89),’’ American Concrete Institute, Farmington Hills, MI, 1989.

American Society of Civil Engineers(ASCE).(2005). “ Minimum Design Loads for Buildings and other Structures (SEI/ASCE 7/05).” Reston Va., USA.

ACI Committee 318. (2014). “Building code requirements for reinforced concrete (ACI318-05).” American Concrete Institute.

ACI Committee 318. (1971). Building Code Requirements for Reinforced Concrete and Commentary (ACI 318-71). American Concrete Institute, Farmington Hills, MI, 1971.

Abaqus (2011). Abaqus., Abaqus Analysis User’s Manual.

Alam, A.K.M.J., Amanat, K.M., and Seraj, S. M. (2009). “Experimental investigation of edge restraint on punching shear behavior of RC slabs.” Civil & Structural Engineering, Vol.2, No. 1, Feb 2009, 35-46.

Broms, C,E., “Punching of Flat Plates-A Question of Concrete Properties in Biaxial Compression and Size Effect,” ACI Structural Journal, V.87, No.3, May-June 1990, pp.292-304.

Broms, C.E.(1990a), “Punching of flat plates- A Question of Concrete Properties in Biaxial Compression and Size Effect”, ACI Structural Journal, V.87, No.3, pp. 292-304.

Carl Erik Broms (2009). “ Design method for imposed rotations of interior slab-column connections.”ACI Structural Journal, V.106, No.5.

DoD UFC 4-023-03, "Design of Building to Resist Disproportionate Collapse," Unified Facility Criteria, United States Department of Defense, Washington, DC, 2005.

Dat, Xuan Pham., Hai TK. Experimental Study of Beam-Slab Sub Structures subjected to a penultimate-internal column loss. Eng Struct (2013).

Eurocode Eurocode 2: Design of concrete structures- Part 1-1: General rules and rules for buildings, European Committee for Standardization (CEN), Brussels, December, 2004.

Ghali, A., Elmasri, M. Z., and Dilger, W. (1976). "Punching of Flat Plates under Static and Dynamic Forces." ACI Journal Proceedings, 73 (10), 566-572.

GSA, "Disproportionate Collapse Analysis and Design Guidelines for New federal Office Buildings and Major Modernization of projects," United States General Service Administration, Washington, DC,2003.

Guice, L. K. and Rhomberg, E. J. (1988). "Membrane Action in Partially Restrained Slabs," ACI Structural Journal, 85 (4), 365-373.

Habibi, F., Redl, E, Egberts, M., Cook, W., and Mitchell, D. (2012) "Assessment of CSA A23.3 Structural Integrity Requirements for Two-Way Slabs", Can. J. Civ. Eng., 39: 351-361.

Habibi, F., M., Cook, W., and Mitchell, D. (2014) "Predicting Post-Punching Shear Response of Slab-Column Connections", ACI Structural Journal., 11(1): 123-134.

Hawkins, N. M. and Mitchell, D. (1979). "Disproportionate Collapse of Flat Plate Structures," ACI

Journal Proceedings, 76 (7), 775-808.

Kinnunen,S., and Nylander ,H. (1960). Punching of Concrete Slabs without Shear Reinforcement, Meddelande No.158, Transactions of the Royal Institute of Technology, Stockholm, Sweden.

Liu, J., Tian,Y., and Orton,S. (2013). "Vulnerability of disproportionate collapse in older flat plate buildings subjected to sudden removal of a bearing column." Proceedings of the 2013 Structures Congress, ASCE, 2814-2823.

Leibenberg,A.C." Arch action in concrete slabs", Pretoria, SA, National Building Research Institute Bulletin No.40, CSIR Research Report NO. 234,1966.

Lubliner,J., Oliver, J., Oller, S. and Onate, E.(1989). A plastic- Damage Model for Concrete. International Journal of Solids Structures, 25(3), 299-329.

Lee, J and Fenves, G.L. (1998). Plastic-Damge Model for Cyclic Loading of Concrete Structures. ASCE Journal of Engineering Mechanics, 124(8), 892-900

Muttoni, A & Schwarts, J 1991, Behavior of beams and punching in slabs without shear reinforcement', IABSE Colloquium, vol.62,pp. 703-708.

Muttoni A., 2008, Punching shear strength of reinforced concrete slabs without transverse reinforcement, ACI Structural Journal, V.105, No 4, pp. 440-450.

M.E. Criswell. (1974) Static And Dynamic Response of Reinforced Concrete Slab-Column Connections. ACI Special Publication.

Muttoni, A. (2008). Punching Shear Strength of Reinforced Concrete Slabs without Transverse Reinforcement. ACI Structural Journal, 105(4), 440-450.

Mitchell, D. and Cook, W. D. (1984). "Preventing disproportionate collapse of slab structures" Journal of Structure Engineering, 23(07).

Mirzaei Y. (2010). " Post-Punching Behavior of Reinforced Concrete Slabs." EPFL, Lausanne, Switzerland, Ph.d Thesis.

Ockelston, A.J. (1955). Loads tests on a three-story reinforced concrete building in Johannesburg. The Structural Engineer, 33(10).

Osama A. Mohamed., (2006) "Disproportionate Collapse of Structures: Annotated

Bibliography and Comparison of Codes and Standards.", Journal of Performance of Constructed Facilities ASCE.,2006.

Orton, S., Tian, Y. Peng, Z., Henquient, C.(2014), "Effects of In-plane Restraint and Post-punching Capacity on Load-carrying Capacity of Slab-Column Connections against Disproportionate Collapse," ASCE/SEI Structural Congress.

Park, R., and Gamble, W.L. (2000). Reinforced Concrete Slabs (Second edition). New York: John Wiley and Sons Inc.

Rankin, G.I.B., and Long, A.E.(1987). " Predicting of enhanced punching strength of interior slab-column connections". Proc.Instn CIV.Engrs, Part1,1987,82,Dec.,1165-1186

Rankin, G.I.B., Niblock. R.A, Skates.A.S and Long, A.E.(1991). "Compressive membrane action strength enhancement in uniformly loaded, laterally restrained slabs." The Structural Engineering. volume 69/NO.16/20.

Ruiz, M., Mirzaei, Y., Muttoni, A., (2013) "Post-Pinching Behavior of Flat Slabs", ACI Structural Journal, 110(5): 801-811.

Salim, W. and Sebastian, W.M. (2003). "Punching shear failure in reinforced concrete slabs with compressive membrane action.'' ACI Structural Journal, 100(4), 471-479.

Sasani, M., Bazan, M., Sagiroglu, S., (2007), "Experimental and Analytical Disproportionate Collapse

Evaluation of Actual Reinforced Concrete Structures," ACI Structural Journal, 104(6), Nov.-Dec. 2007, pp. 731-739.

Tian, Y., Su, Y. (2011) "Dynamic Response of Reinforced Concrete Beams Following Instantaneous Removal of a Bearing Column" International Journal of Concrete Structures and Materials, Vol 5, No. 1, pp. 19-28.

Vecchio, F. J., & Tang, K. (1990). Membrane action in reinforced concrete slabs. Canadian Journal of Civil Engineering, 17(5), 686-697.

Wei-Jian Yi; Fan-Zhen Zhang; and Sashi K. Kunnath. (2014) "Disproportionate Collapse Performance of RC Flat Plate Frame Structures". J. Struct. Eng. 2014.140.

Xiao, Y., Zhao, Y.B., Li, F.W., Kunnath, S., Lew, H.S. (2013). "Collapse Test of a 3-story Half-scale RC frame structure" Proceedings of the 2013 Structures Congress, ASCE.

Yi, W. J., He, Q. F., Xiao, Y., Kunnath, S. K., (2008), "Experimental Study on Disproportionate Collapse-Resistant Behavior of Reinforced Concrete Frame Structures," ACI Structural Journal, 105(4), July-August 2008, pp. 433-439.

VITA

The author Zhonghua Peng was born in Jianli County, Hubei Province, China in 1987. He attended Jiangxi Science & Technology Normal University, Nanchang, China from September 2005 to July 2009 and received Bachelor of Science in Civil Engineering. He then continued graduate school at Beijing Jiaotong University, Beijing, China in September 2009 and graduated with his Master of Science degree in December 2011. He began work toward his ph.D in Structural Engineering at the University of Missouri-Columbia, Missouri, USA in January 2012 and will graduate with his ph.D in Civil Engineering in July 2015 and will be a structural engineer in GMS, NY, USA.